Bursting and Synchronization in Noisy Oscillatory Systems

Chunming Zheng

Universitäts-Dissertation

zur Erlangung des akademischen Grades
"doctor rerum naturalium"
(Dr. rer. nat.)
in der Wissenschaftsdisziplin Theoretische Physik

eingereicht an der

Mathematisch-Naturwissenschaftlichen Fakultät

in der Arbeitsgruppe

Statistische Physik und Chaostheorie

am

Institut für Physik und Astronomie
Universität Potsdam

Hauptbetreuer   Professor Dr. Arkady Pikovsky
und 1. Gutachter: Universität Potsdam

2. Gutachter: Professor Dr. Benjamin Lindner
                       Humboldt-Universität zu Berlin

3. Gutachter: Professor Dr. Eckehard Schöll
                       Technische Universität Berlin

Abstract

Noise is ubiquitous in nature and usually results in rich dynamics in stochastic systems such as oscillatory systems, which exist in such various fields as physics, biology and complex networks. The correlation and synchronization of two or many oscillators are widely studied topics in recent years.

In this thesis, we mainly investigate two problems, i.e., the stochastic bursting phenomenon in noisy excitable systems and synchronization in a three-dimensional Kuramoto model with noise. Stochastic bursting here refers to a sequence of coherent spike train, where each spike has random number of followers due to the combined effects of both time delay and noise. Synchronization, as a universal phenomenon in nonlinear dynamical systems, is well illustrated in the Kuramoto model, a prominent model in the description of collective motion.

In the first part of this thesis, an idealized point process, valid if the characteristic timescales in the problem are well separated, is used to describe statistical properties such as the power spectral density and the interspike interval distribution. We show how the main parameters of the point process, the spontaneous excitation rate, and the probability to induce a spike during the delay action can be calculated from the solutions of a stationary and a forced Fokker-Planck equation. We extend it to the delay-coupled case and derive analytically the statistics of the spikes in each neuron, the pairwise correlations between any two neurons, and the spectrum of the total output from the network.

In the second part, we investigate the three-dimensional noisy Kuramoto model, which can be used to describe the synchronization in a swarming model with helical trajectory. In the case without natural frequency, the Kuramoto model can be connected with the Vicsek model, which is widely studied in collective motion and swarming of active matter. We analyze the linear stability of the incoherent state and derive the critical coupling strength above which the incoherent state loses stability. In the limit of no natural frequency, an exact self-consistent equation of the mean field is derived and extended straightforward to any high-dimensional case.

Zusammenfassung

Rauschen ist in der Natur allgegenwärtig und führt zu einer reichen Dynamik in stochastischen Systemen von gekoppelten Oszillatoren, die in so unterschiedlichen Bereichen wie Physik, Biologie und in komplexen Netzwerken existieren. Korrelation und Synchronisation von zwei oder vielen Oszillatoren ist in den letzten Jahren ein aktives Forschungsfeld.

In dieser Arbeit untersuchen wir hauptsächlich zwei Probleme, d.h. das stochastische Burst-Phänomen in verrauschten anregbaren Systemen und die Synchronisation in einem dreidimensionalen Kuramoto-Modell mit Rauschen. Stochastisches Bursting bezieht sich hier auf eine Folge von kohärenten Spike-Zügen, bei denen jeder Spike aufgrund der kombinierten Effekte von Zeitverzögerung und Rauschen eine zufällige Anzahl von Folge Spikes aufweist. Die Synchronisation als universelles Phänomen in nichtlinearen dynamischen Systemen kann anhand des Kuramoto-Modells, einem grundlegenden Modell bei der gekoppelter Oszillatoren und kollektiver Bewegung, gut demonstriert und analysiert werden.

Im ersten Teil dieser Arbeit wird ein idealisierter Punktprozess betrachtet, der gültig ist, wenn die charakteristischen Zeitskalen im Problem gut voneinander getrennt sind, um statistische Eigenschaften wie die spektrale Leistungsdichte und die Intervallverteilung zwischen Neuronen Impulsen zu beschreiben. Wir zeigen, wie die Hauptparameter des Punktprozesses, die spontane Anregungsrate und die Wahrscheinlichkeit, während der Verzögerungsaktion einen Impuls zu induzieren, aus den Lösungen einer stationären und einer getriebenen Fokker-Planck-Gleichung berechnet werden können. Wir erweitern dieses Ergebnis auf den verzögerungsgekoppelten Fall und leiten analytisch die Statistiken der Impulse in jedem Neuron, die paarweisen Korrelationen zwischen zwei beliebigen Neuronen und das Spektrum der Zeitreihe alle Impulse aus dem Netzwerk ab.

Im zweiten Teil untersuchen wir das dreidimensionale verrauschte Kuramoto-Modell, mit dem die Synchronisation eines Schwarmmodells mit schraubenförmigen Flugbahnen beschrieben werden kann. Im Fall ohne Eigenfrequenz jedes Teilchensist das System äquivalent zum Vicsek Modell, welches in der Beschreibung der kollektiven Bewegung von Schwärmen und aktiver Materie eine breite Anwendung findet. Wir analysieren die lineare Stabilität des inkohärenten Zustands und leiten die kritische Kopplungsstärke ab, oberhalb derer der inkohärente Zustand an Stabilität verliert. Im Fall ohne Eigenfrequenz wird eine exakte selbstkonsistente Gleichung für das mittlere Feld abgeleitet und direkt für höherdimensionale Bewegungen verallgemeinert.

Contents

Chapter 1

Introduction

In nature, basically all processes are noisy, by which we mean stochastic fluctuations are ubiquitous and inevitable in various systems, e.g., cells, neurons, organs etc in biology [Lin+04; Tsi14; Bre14]. While noise is a factor that is supposed to be reduced in processes like signal processing, it can play a constructing role in providing energy in non-equilibrium systems, in neuronal communication and synchronization of oscillators. Three prominent examples are: (a), *stochastic resonance* [BSV81; Gam+98], which refers to the frequency in the noise resonating with that of the signal to amplify the original signal; (b), *coherence resonance* [Gan+93; PK97], which represents maximization of coherence of the noise-induced oscillations in various excitable systems [Lin+04]; (c), the individual noise in an ensemble of coupled oscillators prevents the system from synchronization [Pik+03; Ace+05], in other words, the oscillators need larger coupling strength to synchronize than that in the deterministic case.

Noisy systems can be described by stochastic ordinary differential equations (SODE) since their dynamics generally belongs to the class of Brownian motion, although the size of them doesn't have to be the same as the pollen of the plant Clarkia pulchella first studied by the botanist Robert Brown.

In this thesis, two main topics are concerned, i.e., the *stochastic bursting* phenomenon both in a single excitable, noisy system (Chap. 2) in networks (Chap. 3,4), and the synchronization in a three-dimensional noisy Kuramoto model (Chap. 5). The organization of this thesis is as follows:

Chap. 1 serves as an introduction of the basic two noisy models of oscillating dynamics, i.e., noisy excitable model and noisy 2D Kuramoto model. As the minimal model of an excitable system, the noisy version of the active rotator or the so-called theta neuron is introduced in terms of the Langevin equation and the Fokker-Planck equation. Since our main interest lies in the statistics of the spike trains induced by the noisy excitable unit, we adopt the point process to depict the spikes and introduce the basic measure of them, i.e., interspike interval distribution (ISI) and power spectrum. Moreover, since our second main part in this thesis is about 3D Kuramoto model, thus a basic description of the 2D version is given, in terms of the stationary solution by the self-consistent method and linear stability analysis of the incoherent state.

In Chap. 2, we investigate the combined effect of time delay and noise in a single excitable unit, where a novel coherent spiking pattern which we call *Stochastic bursting* is observed. We use a point process of leader-follower relationship to represent the spike train and derive the ISI distribution and power spectral density analytically. Moreover, a numerical method by the Fokker-Planck equation is used to confirm the probability we obtain by simulating the corresponding Langevin equation. The results in this chapter are based on the publication in [ZP18].

Chap. 3 and Chap. 4 are extensions to the delay-coupled case, i.e., the unidirectional delay-coupled case and a chain of three units.

In Chap. 3 we derive a general result for N unidirectionally delay-coupled units in terms of ISI distribution and power spectral density, for each unit in the networks. The correlations and thus cross-spectrum between any two units in the networks are also derived, by the point process with a lead-follower relationship. The results in this chapter are reported in [ZP19].

In Chap. 4, we use a tree lattice to investigate the statistics of the spike train in a chain of three units and obtain a good approximation of the correlation between any two units in the chain. Based on the results in the above chapters, we can conclude that the stochastic bursting is a phenomenon that occurs commonly in excitable systems with both time-delay feedback and noise. The results in this chapter are reported in [ZPnu].

In Chap. 5, we propose a noisy version of a three-dimensional Kuramoto model, which can be used to describe the dynamics of a multi-agent system in a noisy 3D environment. Each agent is rotating and diffusing on a unit sphere and subject to a common mean field. In the case without natural frequency, the model is connected to another famous model in collective motion, i.e., the Vicsek model. For general frequency distribution both in direction and amplitude, the linear stability of the incoherent state is analyzed and the critical coupling strength for the incoherent state to lose stability is obtained. Due to the influence of noise, the phase transition of the order parameter is continuous instead of discontinuous in the deterministic case. Moreover, the 3D noisy Kuramoto model is used to describe the synchronization of the swarming motion with helical trajectory. The results in this chapter are based on the publication in [ZTP20].

A collaboration work on the Kuramoto model subject to common noise [Gon+19] is not presented in this thesis.

1.1 Noisy excitable system

1.1.1 Type I excitable system: Theta neuron

The excitable system refers to a unit, e.g., a neuron or oscillator, which is in the resting state, being a fixed point in equilibrium or small-amplitude oscillations, but has the potential to be excited to generate a large amplitude excursion, i.e., firing for neurons. The excitation sources can be a constant force, periodic stimulation or random noise, which is the factor we consider throughout the thesis. According to the bifurcation from the resting state to the firing state, the excitability is usually classified into 2 categories: type I and type II excitability [Hod48; Izh00]. Type I neurons, e.g., theta neuron, Morris–Lecar model etc undergo a saddle-node bifurcation and form a limit cycle to fire, while type II neurons, e.g., FitzHugh–Nagumo model, undergo a Hopf bifurcation to induce oscillations of large amplitude. In this thesis, we mainly focus on a theta-neuron like model, which is also called active rotor model with noise as described by

$$\dot{\theta} = a + \cos\theta + \xi(t), \tag{1.1}$$

where θ is the phase of the oscillator with period 2π, a is a bias and $\xi(t)$ is Gaussian white noise with $< \xi(t) >= 0$, and $< \xi(t)\xi(t - t') >= 2D\delta(t - t')$. D is the noise intensity, which is zero in the deterministic case. when a is smaller than 1, the phase has two fixed points , one stable and the other unstable, as shown in Fig. (1.1). The stable fixed point is $\theta_s = \arccos(-a)$ and the unstable fixed point is $\theta_u = 2\pi - \arccos(-a)$. On the other hand, when a is larger than 1, the system is oscillating periodically.
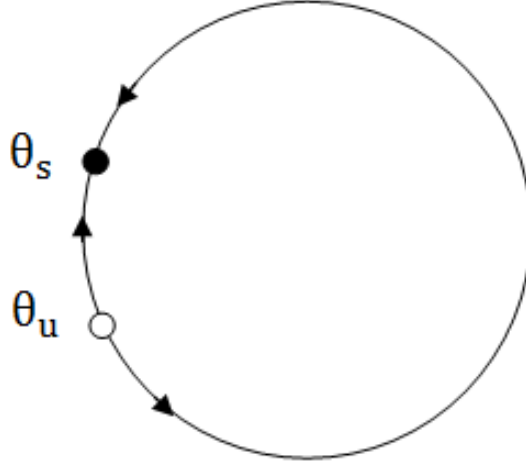
FIGURE 1.1: Schematic illustration of the oscillator described by Eq. (1.1) in the deterministic case, where θ_s is the stable fixed point and θ_u is the unstable fixed point.

In the noisy environment, the oscillator will be randomly kicked, leading to the transition from resting state to firing state and back and forth. The Fokker-Planck equation [Ris96] is to describe the probability density of the phase, i.e.,

$$\begin{aligned}
\frac{\partial P(\theta, t)}{\partial t} &= -\frac{\partial}{\partial \theta} J \\
&= -\frac{\partial}{\partial \theta}(a + \cos\theta)P(\theta, t) + D\frac{\partial^2}{\partial \theta^2}P(\theta, t),
\end{aligned} \tag{1.2}$$

where J is the probability current (or flux) and it is a constant in the stationary state. The stationary solution of Eq. (1.2) with periodic boundary condition $P(\theta) = P(\theta + 2\pi)$ is

$$P_{st}(\theta) = C\int_{\theta}^{\theta + 2\pi} \frac{d\psi}{D} e^{-\int_{\theta}^{\psi} \frac{a + \cos\varphi}{D} d\varphi}, \tag{1.3}$$

where C is the normalization constant to ensure $\int_0^{2\pi} P_{st}(\theta)d\theta = 1$ [SP10]. When the noise intensity is small, the phase will mostly be in the vicinity of θ_s as shown in Fig. 1.1 and occasionally go across θ_u and perform one excursion back to θ_s. The phase increasing a 2π period is called a spike, the rate of which is equal to the probability current of Eq. (1.2) [Ris96], i.e.,

$$\lambda = J = C\left(1 - e^{-\int_0^{2\pi} \frac{a + \cos\theta}{D} d\theta}\right). \tag{1.4}$$

1.1.2 Point process description

A spike train is a temporal sequence of action potential, which plays an important role in the communication between cells and neurons. In mathematics, spike trains are encoded point processes, which are widely used to model physical processes that can be represented as a stochastic set of events in time or space. The events are ideally represented by series of δ functions

$$\varsigma(t) = \sum_j \delta(t - t_j), \tag{1.5}$$
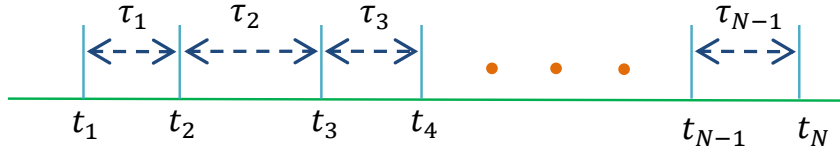
FIGURE 1.2: Schematic representation of a spike train, where t_i is the time at which the ith spike occurs and τ_i is the i-th interspike interval.

where t_j is the recorded time at which the event occurs. The average firing rate (or spiking rate) depicts the average frequency action potentials fired during a time period T, i.e.,

$$< r(t) >= \lim_{T \to \infty} \frac{N}{T} = \lim_{T \to \infty} \frac{\int_0^T \varsigma(t)dt}{T}, \tag{1.6}$$

where N is the number of spikes generated within the duration T.

Interspike interval distribution

The interspike interval (ISI) is the time between two subsequent spikes. Measurement of ISI distribution $\rho(\tau)$ is a usual way to study the neuronal activity in a stationary sense, and thus the mean interval is straightforward, i.e.,

$$< \tau >= \int_0^\infty \rho(\tau)\tau d\tau, \tag{1.7}$$

which gives an alternative description of the mean firing rate, i.e.,

$$< r(t) >= \frac{1}{< \tau >} = \frac{1}{\int_0^\infty \rho(\tau)\tau d\tau}. \tag{1.8}$$

The ISI distribution can also be interpreted as the conditional probability density

$$\rho(\tau) = P(t + \tau | t), \tag{1.9}$$

where the probability density $P(t'|t)$ multiplied by a small interval Δt gives the probability to observe a spike in the interval $[t', t' + \Delta t]$, given a spike at time t. The cumulative version of the ISI distribution is

$$Q(\tau) = \int_0^\tau P(t + s | t)ds, \tag{1.10}$$

which describes the probability that there is at least one spiking event within the duration $[t, t + \tau]$. Since $P(t + s | t) = P(s)$ in the stationary state, Eq. (1.10) can be simplified to

$$Q(\tau) = \int_0^\tau P(s)ds. \tag{1.11}$$

Survival function

Given the probability density $P(t + \tau | t)$ as above, the probability of the neuron not to fire within the duration $[t, t + \tau]$ is

$$S(\tau) = 1 - \int_0^\tau P(s)ds. \tag{1.12}$$

Let us consider a simple and commonly used model, i.e., the homogeneous Poisson process, in which the spiking rate is constant, and hence the probability to have n spikes during the interval $[0, \tau]$ is

$$P(n \text{ spikes in} \quad \tau) = \frac{e^{-r\tau}(r\tau)^n}{n!}. \tag{1.13}$$

Thus the survival function in this case is exponential, i.e.,

$$S(\tau) = e^{-r\tau}, \tag{1.14}$$

and the ISI distribution is

$$P(\tau) = re^{-r\tau}. \tag{1.15}$$

Autocorrelation and power spectrum

The autocorrelation function reveals how every two spikes correlate with each other, as defined by

$$C(s) = \langle (X(t) - \langle X(t) \rangle)(X(t+s) - \langle X(t) \rangle) \rangle, \tag{1.16}$$

where $\langle \cdot \rangle$ denotes the average over all spikes in multiple realizations of the experimental condition. which is a function only with respect to the interval s in the stationary state. The autocorrelation function $C(s)$ is intemately related to the ISI distribution $P(s)$. For $s > 0$, the autocorrelation function $C^+(s)$ for $s > 0$ can be interpreted in terms of ISI distribution $P(\tau)$ as follows:

$$
\begin{aligned}
C^+(s) &= P(s) + \int_0^\infty P(s_1)P(s - s_1)ds_1 \\
&\quad + \int_0^\infty \int_0^\infty P(s_1)P(s_2)P(s - s_1 - s_2)ds_1 ds_2 + \cdots \\
&= P(s) + \int_0^\infty P(s_1)C^+(s - s_1)ds_1.
\end{aligned}
\tag{1.17}
$$

For $s < 0$, due to the symmetry, we have $C^-(s) = C^+(-s)$. Together with the delta peak of the autocorrelation at $s = 0$, we finally obtain

$$
\begin{aligned}
C(s) &= r[C^+(s) + C^-(s) + \delta(s)] \\
&= r[C^+(s) + C^+(-s) + \delta(s)]
\end{aligned}
\tag{1.18}
$$

Applying the Fourier transform to Eq. (1.18), we obtain

$$\hat{C}(\omega) = r\text{Re}\left[\frac{1 + \hat{P}(\omega)}{1 - \hat{P}(\omega)}\right], \tag{1.19}$$

where $\hat{C}(\omega)$ and $\hat{P}(\omega)$ are the Fourier transform of the functions $C(s)$ and $P(s)$ respectively. Noteworthy, here $\omega \neq 0$ ensures the extraction of the mean value of $X(t)$, as defined in Eq. 1.16. Eq. (1.19) is a standard solution of the stationary renewal process.

An alternative interpretation of correlation function is to consider it as a first order statistics instead of second order. The conditional probability density $P(t, t + \Delta t; t + s, t + s + \Delta t)$ denotes the probablity that there is a spike in the small interval $[t + s, t + s + \Delta t]$, given that there is a spike in the former or later (depending on sign

of s) small interval $[t, t + \Delta t]$. Thus the correlation function can be represented as

$$C(s) = \frac{1}{T} \int_0^T dt \lim_{\Delta t \to 0} \frac{P(t, t + \Delta t; t + s, t + s + \Delta t)}{\Delta t^2}, \quad (1.20)$$

where T is the time window in which the spike trains occur.

According to the Wiener-Khinchin theorem, the power spectral density is the Fourier transform of the autocorrelation function, as demonstrated by the following equalities:

$$\begin{aligned}
S(\omega) &= \int_{-\infty}^{\infty} C(s) e^{-i\omega s} ds \\
&= \lim_{T \to \infty} \frac{1}{T} \int_{-T/2}^{T/2} X(t) \int_{-\infty}^{\infty} X(t+s) e^{-i\omega s} ds\, dt \\
&= \lim_{T \to \infty} \frac{1}{T} \int_{-T/2}^{T/2} X(t) e^{i\omega t} dt \int_{-\infty}^{\infty} X(s') e^{-i\omega s'} ds' \\
&= \lim_{T \to \infty} \frac{1}{T} \left| \int_{-T/2}^{T/2} X(t) e^{-i\omega t} dt \right|^2.
\end{aligned} \quad (1.21)$$

The autocorrelation function quantifys the temporal structure within the spike train in a single neuron. Here, the interpretation of a second-order statistics, i.e., the correlation function, via a first-order statistics, i.e., the mean value of the joint events, shows advantage also in cross-correlation function, which quantifys the temporal coordination of spikes across the two spike trains between two different neurons. In Chap. 3 and Chap. 4, we will see that it is informative and convenient to derive both the auto and cross- correlations between any pair of neurons in a unidectional network [ZP19] and in a chain of three couled neurons [ZPnu].

1.2 Classical (2D) Kuramoto model

The synchronization phenonenon [Pik+03] of coupled oscillators is of great importance in understanding systems such as populations of fireflies [BB68], circadian rhythms of animals [Yam+03], pulse-coupled neurons [Win67], Josephson junction circuits [SSW92], etc. In 1975, Kuramoto proposed a mathematically tractable model to describe the synchronization phenomenon of all-to-all pairwise coupled phase oscillators [Kur75], based on Winfree's analysis on synchronized community that can be considered as a threshold process [Win67]. The Kuramoto model is described by the following equation:

$$\begin{aligned}
\dot{\theta}_i &= \omega_i + \frac{K}{N} \sum_{j=1}^{N} \sin(\theta_j - \theta_i) \\
&= \omega_i + K\rho \sin(\Psi - \theta_i),
\end{aligned} \quad (1.22)$$

where θ_i is the phase of the i-th unit out of an ensemble with N coupled oscillators, ω_i is the corresponding natural frequency with distribution $g(\omega)$. By choosing a co-rotating reference frame, i.e., setting $\theta_i = \theta_i - \Omega t$, the distribution $g(\omega)$ with mean Ω can be investigated by $g(\omega)$ with zero mean. K is the coupling strength, which will facilitate synchronization of the oscillators when it's positive. ρ and Ψ are the

amplitude and phase of the order parameter, which is defined by

$$\rho e^{i\Psi} = \frac{1}{N} \sum_{j=1}^{N} e^{i\theta_j}. \tag{1.23}$$

In the thermodynamic limit $N \to \infty$, the continuity equation describing the evolution of the probability density $f(\theta, \omega, t)$ of the oscillators is straightforward. In this case, the discrete version of the definition of order parameter described by Eq. (1.23), is now replaced by a continuous one, i.e.,

$$\rho e^{i\Psi} = \int_{-\infty}^{\infty} \int_{0}^{2\pi} f(\theta, \omega, t) g(\omega) e^{i\theta} d\theta d\omega. \tag{1.24}$$

Using a self-consistent method [Kur84], Kuramoto obtained a closed integral form, from which, it suggested that there exist a critical coupling strength above which the synchronization was observed. The reason can be understood as the competition between the frequency of the oscillators, which desynchronize the population and the positive coupling strength, which facilitates the synchronization. Kuramoto model can also be used to describe the alignment of coupled agents [CGO19b], subject to a common field or force. In this sense, Eq. (1.22) can be reformulated as

$$\frac{d\hat{\boldsymbol{\sigma}}_i}{dt} = K(\boldsymbol{\rho} - (\boldsymbol{\rho} \cdot \hat{\boldsymbol{\sigma}}_i)\hat{\boldsymbol{\sigma}}_i) + \boldsymbol{\omega}_i \hat{\boldsymbol{\sigma}}_i, \tag{1.25}$$

where each unit vector $\hat{\boldsymbol{\sigma}}_i = (\cos\theta_i, \sin\theta_i)$ is subject to the mean field vector $\boldsymbol{\rho}$, i.e.,

$$\boldsymbol{\rho} = \frac{1}{N} \sum_{i=1}^{N} \boldsymbol{\sigma}_i, \tag{1.26}$$

$\boldsymbol{\omega}_i$ is an anti-symmetric matrix to describe the natural frequency of each unit. It is of the following form:

$$\boldsymbol{\omega} = \begin{pmatrix} 0 & \omega_i \\ -\omega_i & 0 \end{pmatrix}, \tag{1.27}$$

where the element ω_i is selected from a distribution $g(\omega)$.

After the Kuramoto model was proposed, many extensions have been done to investigate more complex phenomena. The noisy version of Kuramoto model was firstly investigated by Sakaguchi [Sak88]. The phase of each oscillator θ_i subject to random noise obeys the following Langevin equation:

$$\begin{aligned} \dot{\theta}_i &= \omega_i + \frac{K}{N} \sum_{j=1}^{N} \sin(\theta_j - \theta_i) + \xi_i(t) \\ &= \omega_i + K\rho \sin(\Psi - \theta_i) + \xi_i(t), \end{aligned} \tag{1.28}$$

Here $\xi(t)$ is the Guassian white noise with $< \xi_i(t) >= 0$ and $< \xi_i(t)\xi_j(t') = 2D\delta_{ij}\delta(t - t')$. The other parameters are defined the same way as in Eq. (1.22). Compared to the deterministic case ($D = 0$), the individual noise here prevents the oscillators from synchronization. Therefore, in terms of phase transition of the order parameter, the critical coupling K_c is expected to be larger than that in the deterministic case.
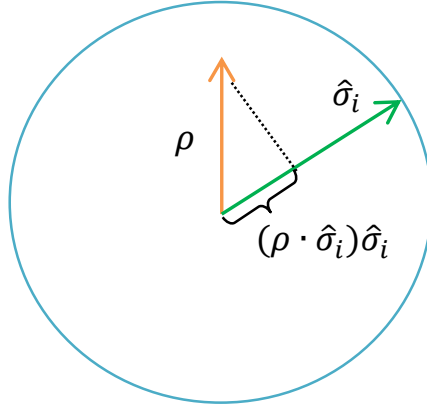
FIGURE 1.3: Schematic illustration of vector representation of two dimensional Kuramoto model.

1.2.1 Stationary solution by self-consistent method

In the case of thermodynamic limit, i.e., $N \to \infty$, the evolution of the probability density of the phase oscillators is described by the Fokker-Planck equation

$$\frac{\partial f(\theta, \omega, t)}{\partial t} = -\frac{\partial}{\partial \theta}(\omega - K\rho \sin(\Psi - \theta))f(\theta, \omega, t) + D\frac{\partial^2}{\partial \theta^2}f(\theta, \omega, t). \tag{1.29}$$

The stationary solution of Eq. (1.29) is subject to periodic boundary condition, i.e.,

$$f(\theta, \omega) = f(\theta + 2\pi, \omega). \tag{1.30}$$

It is first derived in Ref. [Sak88], and later in Ref. [BNS92] by an alternative form, which is

$$f(\theta, \omega) = \frac{1}{C(\omega)}e^{\frac{K\rho}{D}\cos(\Psi - \theta)}\int_0^{2\pi} d\theta_1 e^{-\frac{1}{D}[\omega\theta_1 + K\rho\cos(\Psi - \theta - \theta_1)]}. \tag{1.31}$$

Here $C(\omega)$ is the normalization constant with

$$C(\omega) = \int_0^{2\pi} d\theta e^{\frac{K\rho}{D}\cos(\Psi - \theta)}\int_0^{2\pi} d\theta_1 e^{-\frac{1}{D}[\omega\theta_1 + K\rho\cos(\Psi - \theta - \theta_1)]}. \tag{1.32}$$

Substituting Eq. (1.31) into Eq. (1.24), to the third order of ρ, we obtain

$$\rho = \frac{K\rho}{2}\left(\int_{-\infty}^{\infty} \frac{g(D\omega + \omega_0)}{\omega^2 + 1}g(D\omega + \omega_0) - \frac{K^2\rho^2}{2D^2}\int_{-\infty}^{\infty} g(D\omega + \omega_0)[\frac{1}{\omega^2 + 4} - \frac{\omega}{(\omega^2 + 1)^2}]\right), \tag{1.33}$$

which was first derived by Sakachuchi in Ref. Eq. (1.33) indicates the square root relationship in the vicinity of the critical point of the coupling strength K_c, which is given by

$$K_c = \frac{2D}{\int_{-\infty}^{\infty} g(\omega)/(1 + \omega^2/D^2)d\omega}. \tag{1.34}$$

Noteworthy, the above critical coupling is limited for the distribution of the frequency $g(\omega)$, which has to be an even function. Moreover, the result is obtained via the stationary solution of the corresponding Fokker-Planck equation (1.29) and hence the stability of the incoherent state is not yet revealed. It was firstly reported by

Strogatz and Mirollo in Ref. [SM91], where discrete and continuous spectrum are both considered, while the former one determines the instability of the incoherent state. The authors also proved that, for an even function $g(\omega)$ which is non-increasing on $[0, \infty)$, there is at most one solution for the eigenvalue λ, (we denote s in the following), which is necessarily real if the solution exists [MS90].

1.2.2 Linear stability of the incoherent state

The probability density of the incoherent state is

$$f_0(\theta, \omega, t) = \frac{1}{2\pi}, \tag{1.35}$$

which indicates that for any given ω, all the oscillators are uniformly distributed around the circle, i.e., there is no mean field to influence the oscillators. Assuming a small perturbation to the incoherent state, i.e.,

$$f(\theta, \omega, t) = f_0 + f_1(\theta, \omega)e^{st}, \tag{1.36}$$

substituting Eq. (1.36) into Eq. (1.29) and keeping only the linear part with respect to $f(\theta, \omega)_1$, we obtain the following equation:

$$sf(\theta, \omega) + \omega\frac{\partial f}{\partial \theta} - D\frac{\partial^2 f}{\partial \theta^2} = K f_0 \boldsymbol{\rho} \cdot \boldsymbol{\sigma}, \tag{1.37}$$

where $\boldsymbol{\rho} \cdot \boldsymbol{\sigma}$ in the r.h.s of the equation has the geometric meaning such that it represents the product of the first-order mean field and the unit vector, i.e.,

$$\boldsymbol{\rho} \cdot \boldsymbol{\sigma} = \begin{pmatrix} \rho_x \\ \rho_y \end{pmatrix} \cdot \begin{pmatrix} \cos\theta \\ \sin\theta \end{pmatrix} = \frac{1}{2}(\rho_x + i\rho_y)e^{-i\theta} + \frac{1}{2}(\rho_x - i\rho_y)e^{i\theta}. \tag{1.38}$$

By substituting the Fourier-series solution

$$f_1(\theta, \omega) = Ae^{i\theta} + A^*e^{-i\theta} \tag{1.39}$$

into Eq. (1.37), we obtain

$$f_1(\theta, \omega, t) = \frac{K(\rho_x + i\rho_y)}{s + D - i\omega}e^{-i\theta} + \frac{K(\rho_x - i\rho_y)}{s + D + i\omega}e^{i\theta}. \tag{1.40}$$

Since the mean field vector $\boldsymbol{\rho}$ is defined as

$$\begin{aligned} \boldsymbol{\rho} &= \int\int \boldsymbol{\sigma} f(\boldsymbol{\sigma}, \omega, t)g(\omega)d\boldsymbol{\sigma}d\omega \\ &= \int_{-\infty}^{\infty}\int_0^{2\pi} \begin{pmatrix} \frac{e^{i\theta}+e^{-i\theta}}{2} \\ \frac{e^{i\theta}-e^{-i\theta}}{2i} \end{pmatrix} f_1(\theta, \omega, t)g(\omega)d\theta d\omega \end{aligned} \tag{1.41}$$

substituting Eq. (1.40) into Eq. (1.41), we obtain a self-consistent equation about the order parameter:

$$\boldsymbol{\rho} = \frac{K}{2}\int_{-\infty}^{\infty} \begin{pmatrix} \frac{\rho_x(s+D)}{(s+D)^2+\omega^2} - \frac{\rho_y\omega}{(s+D)^2+\omega^2} \\ \frac{\rho_y(s+D)}{(s+D)^2+\omega^2} + \frac{\rho_x\omega}{(s+D)^2+\omega^2} \end{pmatrix} g(\omega)d\omega. \tag{1.42}$$

Since in 2D Kuramoto model a corotating frame can be found, the frequency distribution is usually chosen as an even function, leading to the vanishment of term

proportional to $\int \frac{\omega}{(s+D)^2 + \omega^2} g(\omega) d\omega$, i.e.,

$$\int_{-\infty}^{\infty} \frac{\omega}{(s+D)^2 + \omega^2} g(\omega) d\omega = 0. \tag{1.43}$$

Therefore, Eq. (1.42) can be further simplified as

$$1 = \frac{K}{2} \int_{-\infty}^{\infty} \frac{(s+D)}{(s+D)^2 + \omega^2} g(\omega) d\omega. \tag{1.44}$$

For an even and unimodal function $g(\omega)$, there is always a real eigenvalue s to determine the stability of the incoherent state [MS90; SM91]. Therefore, to obtain the critical coupling strength, it's straightforward to set $s = 0$. It's easy to check that K_c coincides with the result described by Eq. (1.34). For $g(\omega) = \delta(\omega)$, the eigenvalue in Eq. (1.44) is given by

$$s = \frac{K}{2} - D, \tag{1.45}$$

therefore the critical coupling strength is

$$K_c = 2D. \tag{1.46}$$

For a Cauchy distribution with zero mean, i.e., $g(\omega) = \frac{\gamma}{\pi(\omega^2 + \gamma^2)}$, it's also straightforward to obtain

$$s = \frac{K}{2} - D - \gamma, \tag{1.47}$$

so the critical coupling strength in this case is

$$K_c = 2(D + \gamma). \tag{1.48}$$

In conclusion, the individual noise always stabilizes the incoherent state and prevents the coupled oscillators from synchronization.

1.2.3 Recent development and state of the art

Kuramoto model has been a hot topic since its birth in 1975, with more and more phenomena observed in it and generalization beyond it. These developments include but are not limited to the low dimensional behavior of coupled oscillators [OA08; OA09] and macroscopic description of coupled neurons [MPR15], the chimera state [AS04; KB02; Ome18] and the application on complex networks [DB14; Rod+16] including adaptive networks [BSS20]. Moreover, the generalization of Kuramoto model on high dimensional space [OS06; Tan14; Loh09; CGO19b], where synchronization is more about the trajectory or velocity rather than phase locking in the classical case, has attracted a lot of attention. Interestingly, the even and odd dimensional cases are demonstrated to be different in terms of the transition from incoherent state to synchronization [CGO19b], but are subject to the same general low dimensional behavior macroscopically [CGO19a].

The dynamics concerning stability and bifurcation in Kuramoto model has been of great interest to physicists and mathematicians, with many related questions still open. In the book [Kur84], Kuramoto originally conjectured that as the coupling strength increases above the criticality, the incoherent state bifurcates supercritical to the partial synchronization state. The incoherent state should be stable below the criticality and unstable above it. These statements sounded reasonable physically but turned to be a difficult problem to prove mathematically. After the conjecture by

Kuramoto, the stability of the incoherent state was first investigated by Strogatz and Mirollo in [SM91; MS90], who later analyzed the stability for the partially locked state in [MS07].

Noteworthy, in [SM91] the incoherent state was claimed to be neutrally stable in the deterministic case while stable in the noisy case, due to the stabilizing effect of the noise on the incoherent state. It seems that the result is not quite in agreement with what Kuramoto conjectured originally. However, a recent paper by Chiba [CN11], where a center manifold reduction is used, demonstrated that Kuramoto's conjecture is actually right.

After the proposal of Ott-Antonsen (OA) ansatz [OA08], similar questions concerning the stability arise that, whether the OA manifold is attractive or not. The authors proved that the OA manifold is time-asymptotically attractive [OA09] when the frequency distribution has a nonzero width. It coincides with the intuition since that the relaxation to the OA manifold results from mixing phases of the oscillators with heterogeneous frequencies. However, in the case where the frequencies of all the oscillators are the same, i.e., the width of the frequency distribution is zero, the OA manifold is not attracting, in agreement with the results in [WS94; PR08; MMS09]. Additionally, the OA manifold is recently demonstrated to be not attracting in the finite N continuum case [EM20]. For the noisy version of Kuramoto model, the low dimensional behavior is different depending on whether the noise is common noise or individual noise. The common noise is a random force to which all the oscillators are subject and therefore it's within the framework of Watanabe-Strogatz theory and the Ott-Antonsen ansatz (to see [NK10; Pim+16; Gon+19]), while for the individual noise case, a circular cumulant expansion is believed to capture the low dimensional dynamics [Tyu+18].

Chapter 2

Delay-induced stochastic bursting in a single noisy excitable system

Time-delayed feedback and noise are factors that substantially contribute to the complexity of the dynamical behaviors. While noise generally destroys the coherence of oscillations, there are situations (e.g., stochastic and coherence resonances) where it plays a constructive role leading to a quite regular behavior [Abb+08; Nei07]. Also, delayed feedback can either increase or suppress coherence of oscillators [GRP03b; GRP03a; JBS04; BJS04]. The interplay of delay and noise is important for neural systems, where it has been studied both on the level of individual neurons [Pra+07; Sch+09; Li+10], of networks of coupled neurons [KMSG10; Hau+06], and of rate equations [GG15].

A significant progress in understanding the interplay of noise and delayed feedback has been achieved for bistable systems [TP01; Mas03]. Furthermore, variants of the bistable dynamics with highly asymmetric properties of the two states have been adopted to describe excitable systems under delay and noise [Pra+07; PJ08; KMSG10].

In this chapter, we develop another approach to the dynamics of excitable noisy systems with delayed feedback. We investigate a theta-neuron-like model [EK86], which is a paradigmatic example of an excitable system in mathematical and computational neuroscience. Under the action of small noise, this system demonstrates a random, Poisson sequence of spikes, as described in Sec. 1.1.1. We will show, that a small additional delayed feedback (large feedback can significantly modify the dynamics, see, e.g., [Kro+14]) leads to an interesting partially coherent spike pattern which we call *stochastic bursting*. Contrary to the bistable models, in our description we consider only the excitable state as a stochastic one, while the excitation itself is deterministic. The model is described by a scalar variable θ defined on a circle:

$$\dot{\theta} = a + \cos\theta + \epsilon(a + \cos\theta(t-\tau)) + \sqrt{D}\xi(t). \tag{2.1}$$

Here parameter a defines the excitability properties, parameter D describes the level of external noise (which we assume to be Gaussian white one, $\langle \xi(t) \rangle = 0$, $\langle \xi(t)\xi(t') \rangle = 2\delta(t-t')$), and ϵ is the amplitude of a delayed feedback. The feedback is chosen to vanish in the steady state of the system. Model (2.1), without delayed feedback, is very close to the theta-neuron model [EK86], extensively explored in different contexts in neuroscience (where inclusion of noise is very natural, while a delayed feedback is often attributed to the autapse effect, cf. [VDLG72; Li+10]), and to the active rotator model [PK96; Tes+07; Zak+03; Son+13]. In (2.1) we assume a simple additive action of the delayed feedback and of noise. For theta-neurons, one quite often explores multiplicative forcing, where the force terms are multiplied with factor $(1 - \cos\theta)$ (cf. [BK05], notice that our variable is shift by π to the variable used in [BK05]).

However, as will be clear from the analysis below, this brings only small quantitative corrections to the results, while the main qualitative conclusions remain valid – because the most sensitive to forcing region in the phase space is around $\theta \approx -\pi$, and in this domain the factor $(1 - \cos\theta)$ is nearly a constant.

For $|a| < 1$ the autonomous theta-neuron (without noise and feedback) is in an excitable regime: there are two nearby stationary states, one stable and one unstable. Both noise and the feedback can kick the system from the stable equilibrium so that it produces a "spike". Our goal in this paper is to describe the statistical properties of the appearing spike train. Before the full analysis, we briefly outline relatively simple cases of the purely deterministic dynamics (no noise) and the purely noisy dynamics (no delayed feedback).

2.1 Deterministic case

For an autonomous theta-neuron ($\epsilon = 0$, $D = 0$), one can represent the dynamics as an overdamped motion in an inclined periodic potential

$$\dot{\theta} = -\frac{dU}{d\theta}, \qquad U(\theta) = -a\theta - \sin\theta , \tag{2.2}$$

for which θ_s is a local minimum and θ_u is a local maximum, see Fig. 2.1 (a) and (b). As parameter a is close to the value of a SNIC bifurcation $a = 1$, the distance $\theta_u - \theta_s$ is small (correspondingly, the barier of the potential is small as well) and already a small external perturbation can produce a nearly 2π-rotation of θ. However, for large enough ϵ it can possess stable periodic oscillations. The form of the spike can be represented as a trajectory that starts at θ_u and ends at θ_s (marked red in Fig. 2.1 (a)):

$$\Theta_{sp}(t) = 2\arctan\left(\sqrt{\frac{1+a}{1-a}}\tanh\left(\frac{\sqrt{1-a^2}}{2}(t - t_0)\right)\right) . \tag{2.3}$$

Indeed, a perturbation of the equilibrium can result in a spike described by Eq. (2.3). After the delay time τ, a force

$$\epsilon H(t) = \epsilon(a + \cos\Theta_{sp}(t)) \tag{2.4}$$

will act on the theta-neuron. For a sufficiently large value of ϵ it will produce a new spike, which will also generate a new spike after time delay τ. The process will repeat until the peturbation is not large enough to induce a spike. In Fig. 2.2 we show critical values of ϵ in dependence on the delay time τ and on the excitability parameter a. Clearly, $\epsilon_c \to 0$ if the excitability parameter a approaches the bifurcation value $a_{SNIC} = 1$. Dependence on the delay time is also rather obvious: for large delays the critical value ϵ_c is delay-independent, while for delays comparable to the pulse duration (which is, according to (2.3), $\sim (1 - a^2)^{-1/2}$) there is a blocking effect which mimics a refractory period for a neuron after a spike.

2.2 Noisy case

For the purely noisy case without delay, we have described it in Sec. 1.1.1. Our main interest here is in the combined effects of time delay and noise with $D \neq 0, \epsilon \neq 0$. We simulate the Langevin dynamics described by Eq. (2.1) by the Euler-Maruyama method with discrete time interval $dt = 0.01$. Accordingly, we obtain the spike train in
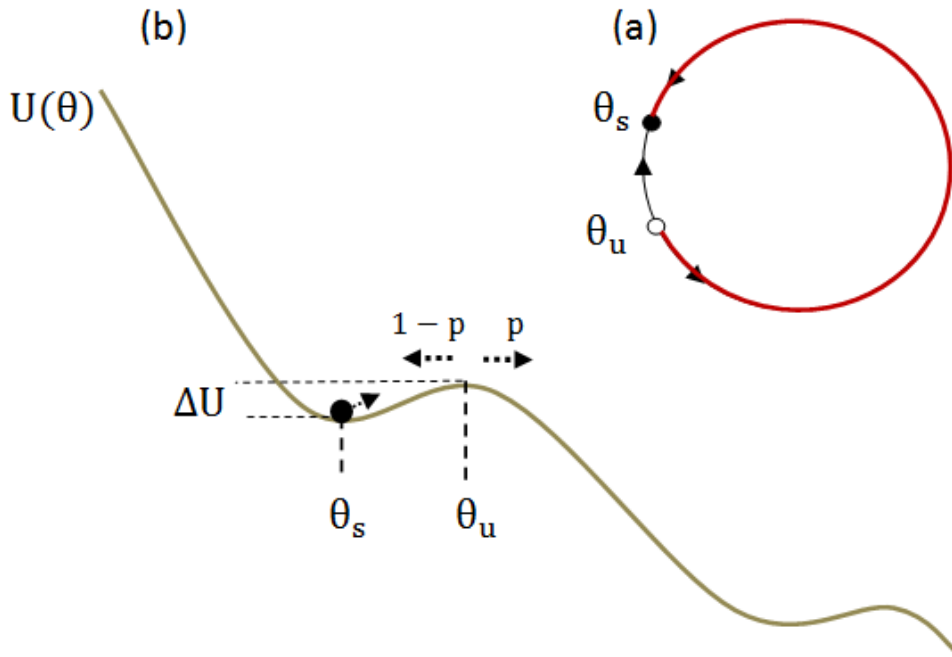
FIGURE 2.1: A sketch of the theta-neuron model Eq. (2.1). In (a), the red trajectory from θ_u to θ_s represents a spike, while the black curve shows relaxation without a spike. Panel (b) depicts how the 'phase particle' evolves in the effective potential $U(\theta)$, either overcoming the barrier (with probability p), or returning back to the equilibrium θ_s (with probability $1 - p$). Figure reprinted with permission from Ref. [ZP18].
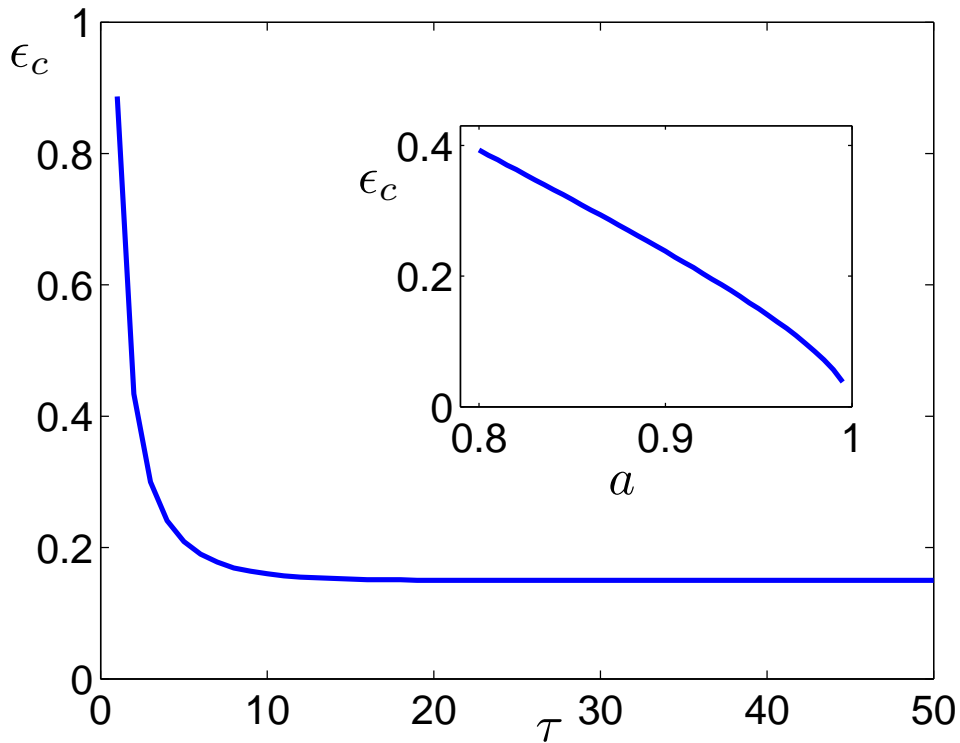
FIGURE 2.2: Critical value of ϵ in dependence on the delay time τ in the deterministic case with $a = 0.95$. The inset is the asymptotic value ϵ_c at large delay time for in dependence on excitability parameter a. Figure reprinted with permission from Ref. [ZP18].
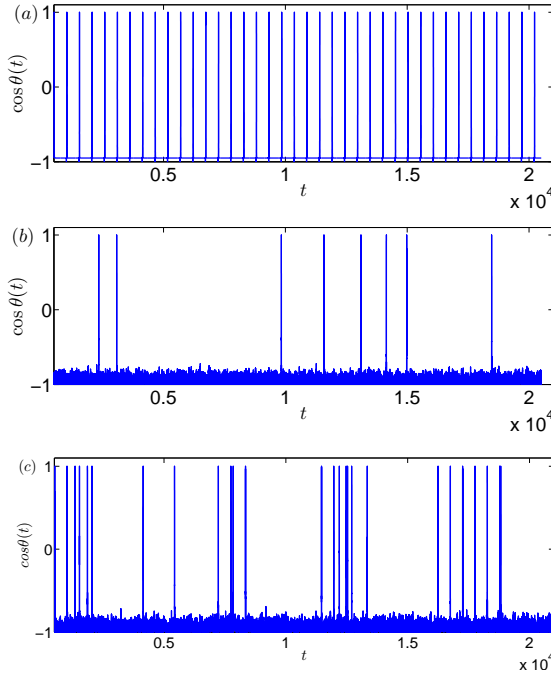
FIGURE 2.3: Panel (a) is the periodic solution in the deterministic case when $\epsilon > \epsilon_c$. Panel (b) shows the noisy case without delayed feedback, i.e $\epsilon = 0$, with the spike train obeying the Poisson statistics. Panel (c) is the case with both noise ($D = 0.005$) and delayed feedback ($\epsilon = 0.14$) , showing the *stochastic bursting* phenomenon. Many spikes with the interval close to τ are induced, depending on the delay force amplitude. The parameters are $a = 0.95, \tau = 500$. Figure reprinted with permission from Ref. [ZP18].

the case with both delay and noise ($D \neq 0, \epsilon \neq 0$) as shown in Fig. 2.3(c). Comparing with the purely periodic dynamics in the deterministic case (panel (a)) and with the Poisson sequence of spikes for delay-free case (panel (b)), in panel (c) we can see randomly appearing spikes, like in case (b), and "bursts" of several spikes separated by the delay time τ (like in case (a)). Qualitatively, this picture illustrates the two sources of spike formation: (i) due to a fluctuation of the noise driving, this source is delay-independent, and (ii) delay-induced spikes which appear due to a combined effect of delay forcing and noise. We call the former spikes spontaneous ones, or 'leaders', and the latter spikes as induced ones, or 'followers'.

An exact analytic approach to the noisy dynamics is hardly possible, because in presence of delay feedback and noise, the system is non-Markovian. Therefore we will next formulate an idealized point process model, which generalizes the Poisson point process in absence of the delayed feedback.

2.3   Point process model

Point processes are widely used to mathematically model physical processes that can be represented as a stochastic set of events in time or space, including spike trains. The spike train can be viewed as a sequence of pulses, fully determined via the spike appearance times t_j. In this case each spike is considered as a δ-pulse, we have $\sum_j \delta(t - t_j)$; more generally we can write $\sum_j H(t - t_j)$, where H is the waveform (2.4). In our model, we adopt the leader-follower relationship to describe the spiking pattern of type shown in Fig.2.3 (c). The spikes which appear when the delay feedback is weak, i.e. solely due to a large fluctuation of noise, we call "spontaneous" ones. As delay plays no
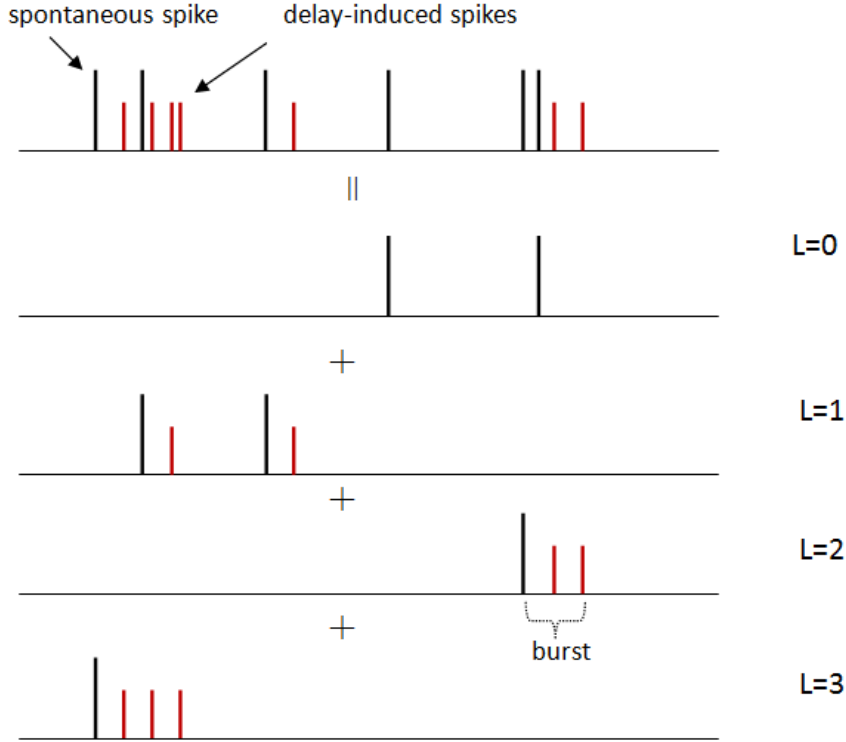
FIGURE 2.4: Schematic description of the point process. The black high pulses represent the spontaneous spikes (leaders) while the red low ones represent the delay-induced spikes (followers) (the difference in the height of spikes is just a schematic way to classify the events into leaders and followers, while they are of the same height in reality). A leader with a random number of its followers form a burst. The whole process can be viewed as a superposition of sub-processes with a fixed number of followers. Figure reprinted with permission from Ref. [ZP18].

role for these spikes, they form a Poisson process with a rate λ. Each spontaneous spike produces, after delay time τ, forcing (2.4). During this pulse forcing, the potential barrier decreases and there is an additional enlarged probability to overcome the barrier and to produce a "follower" spike. We denote the total probability to induce the follower spike as p (correspondingly, the probability to have no follower is $1 - p$). Of course, each induced spike can also produce a follower, with the same probability p. Thus, a leader spike induces a sequence of exactly L followers with probability $\varrho(L) = p^L(1 - p)$. The two parameters, λ and p, fully describe the point process, consisting of "bursts" as shown in Fig. 2.4. Each burst starts with a leader, which appears with a constant rate λ, these leaders form a Poisson process. The followers are separated by the time interval τ, their number in the burst is random according to the distribution $\varrho(L)$. Noteworthy, the bursts can overlap. Below we discuss the statistical properties of the point process following from the described model. It is rather simple to obtain the overall density of spikes. Indeed, the average number of followers of a leader is $\sum_{L=0}^{\infty} L\varrho(L) = \frac{p}{1-p}$, and hence the overall spike rate is

$$\mu = \lambda(1 + \frac{p}{1 - p}) = \frac{\lambda}{1 - p} . \tag{2.5}$$

Because the process is stationary, the probability to have a spike in a small time interval $(t, t + \Delta)$ does not depend on t and is equal to $\mu\Delta$. Correspondingly, the

probability that in a finite time interval T there is no one spike is $\exp[-\mu T]$.

2.4 Statistics of spike train

2.4.1 Interspike interval distribution

Now we derive the interspike interval (ISI) distribution, employing the renewal theory [Cox67; Ger+14]. Given a spike at time t and the next spike at time t', the probability to have no spike in the interval $[t, t']$ is called survivor or survival function. Let us separate the ISI, i.e $T = t' - t$, into three different cases, namely, $T > \tau, T = \tau$ and $T < \tau$. If $T < \tau$, the spikes at t and t' can be either spontaneous (leader) or delay-induced ones (followers of spikes preceding that at t), so the survival function is determined by the full rate μ: $S(T) = \exp(-\mu T)$. In contradistinction, for the case $T > \tau$, the next spike can be only a spontaneous one. The probability that there is no spike in $[t, t']$ is the product of three terms: the probability to have no spikes in the interval $[t, t + \tau)$ with survivor function

$$S_{\tau b} = \exp(-\mu \tau), \tag{2.6}$$

the probability $(1 - p)$ not to have a follower for the spike at t, and the probability to have no spike in the interval $[t + \tau, t']$, where only the spontaneous rate λ applies with the survivor function

$$S_{\tau a} = \exp(-\lambda(T - \tau)). \tag{2.7}$$

Thus, the survivor function for the case $T > \tau$ is

$$\begin{aligned} S(T) &= S_{\tau b}(1 - p) S_{\tau a} \\ &= (1 - p)e^{-\mu \tau - \lambda(T - \tau)}. \end{aligned} \tag{2.8}$$

Based on the above description and the relationship between the cumulative ISI distribution $Q(T)$ and the survivor function $Q(T) = 1 - S(T)$, the cumulative ISI distribution can be obtained as follows:

$$Q(T) = \begin{cases} 1 - e^{-\mu T}, & T < \tau, \\ 1 - (1 - p)e^{-\mu \tau - \lambda(T - \tau)}, & T \geq \tau. \end{cases} \tag{2.9}$$

According to the relationship between the cumulative ISI distribution and the ISI distribution density $P(T) = Q'(T)$, we can also obtain the ISI distribution density:

$$P(T) = \begin{cases} \mu e^{-\mu T}, & T < \tau, \\ p e^{-\mu \tau} \delta(T - \tau), & T = \tau, \\ \lambda(1 - p)e^{-\mu \tau - \lambda(T - \tau)}, & T > \tau. \end{cases} \tag{2.10}$$

We compare the obtained ISI distribution with the numerical result in Fig. 2.5.

2.4.2 Power spectral density

Next, we discuss the correlation properties of the point process. The spike train in our model can be represented as a superposition of sub-trains having a fixed number L of followers, see Fig. 2.4 for an illustration of this superposition. Let us denote $H(t)$ the shape of a spike (it is a delta-function for the point process model, but for a real process it is given by (2.3)). Then the time series can be written as sum of sub-series
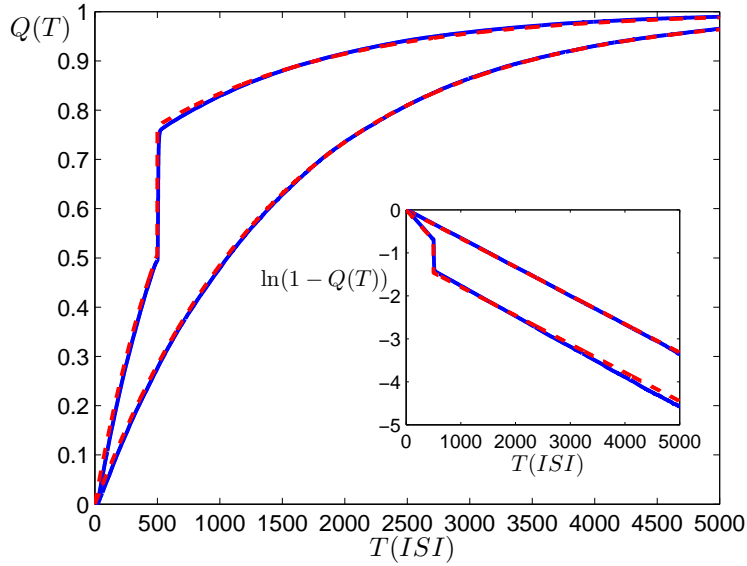
FIGURE 2.5: Cumulative ISI distribution $Q(T)$ vs $T(ISI)$. The blue curve corresponds to the simulation result, the dashed red curve corresponds to the point process with Eq. (2.9), where $\lambda = 6.64 \times 10^{-4}$ is calculated from Eq. (1.4) and $p = 0.53$ is calculated from Eq. (2.20). The upper two curves with a jump at $T = \tau$ correspond to the delay case with $\epsilon = 0.14$, while the lower two ones correspond to the case without delay, i.e $\epsilon = 0$. The inset in a logarithmic scale is to show the coincidence of the slopes, which validates the point process representation of the original model. Parameters are $a = 0.95, D = 0.005$ and $\tau = 500$. Figure reprinted with permission from Ref. [ZP18].

of bursts of size $L + 1$:

$$x(t) = \sum_{L=0}^{\infty} G_L(t) \otimes Y_L(t) \otimes H(t) \tag{2.11}$$

where terms G_L and Y_L describe the leaders and the followers for the bursts of size $L + 1$:

$$G_L(t) = \sum_i \delta(t - t_L^i); \quad Y_L(t) = \sum_{l=0}^{L} \delta(t - l\tau) . \tag{2.12}$$

The leaders of a sub-series of bursts of size $L+1$ form a Poisson process with the rate $\lambda \varrho(L)$, and the followers form a periodic set of spikes with separation τ. Here symbol $\otimes$ denotes a convolution.

According to the property of convolution and the independence of the sub-series for different L, the power spectral density is the sum of spectral densities of the series; inside each sub-series we have a product of spectral functions:

$$S_x(\omega) = \sum_{L=0}^{\infty} S_{G_L}(\omega) S_{Y_L}(\omega) S_H(\omega) . \tag{2.13}$$

Here $S_{G_L}(\omega)$ is the power spectral density of the spontaneous spikes, which have the Poisson statistics. The power spectral density of the Poisson process is a constant [Str67]:

$$S_{G_L}(\omega) = \lambda \varrho(L) = \lambda(1 - p)p^L . \tag{2.14}$$
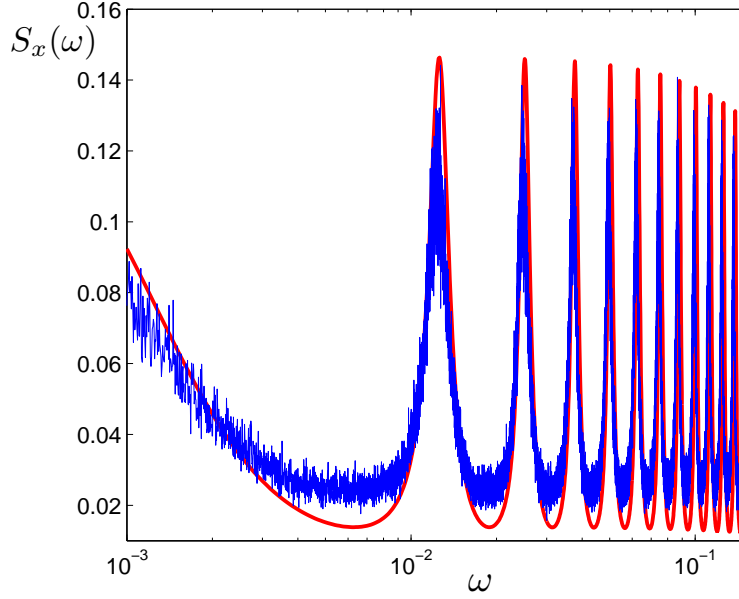
FIGURE 2.6: The power spectral density from the simulations (blue curve) and from the point process (red curve) described by Eq.(2.16), in which $\lambda = 6.64 \times 10^{-4}, p = 0.53$ are calculated from Eq.(1.4) and Eq.(2.20) respectively. The shape function is as Eq. (2.4) describes. Values of a, D and τ are the same as in Fig. (2.5), i.e $a = 0.95, D = 0.005$ and $\tau = 500$. Figure reprinted with permission from Ref. [ZP18].

The term $S_{Y_L}(\omega)$ is the power spectral density of the set of L points separated by time interval τ, i.e

$$S_{Y_L}(\omega) = \left| \int_0^\infty Y_L(t) e^{-i\omega t} dt \right|^2$$
$$= \frac{1 - \cos(L+1)\omega\tau}{1 - \cos\omega\tau}. \tag{2.15}$$

Finally, $S_H(\omega)$ is the power spectral density of the shape function

$$S_H(\omega) = \left| \int_{-\infty}^\infty H(t) e^{-i\omega t} dt \right|^2 .$$

Summarizing, we obtain the following expression for the power spectral density of the spike train

$$S_x(\omega) = \sum_{L=0}^\infty \frac{1 - \cos(L+1)\omega\tau}{1 - \cos\omega\tau} \lambda(1-p)p^L S_H(\omega)$$
$$= \frac{\lambda(1+p)}{1 + p^2 - 2p\cos\omega\tau} S_H(\omega). \tag{2.16}$$

The most important part of the spectrum is the first factor, thus we discuss the spectrum for the case of δ-pulses $S_H = 1$. For the limiting delay-free case, when $p = 0$, we have $S_x(\omega) = \lambda S_H(\omega)$, which corresponds to a purely Poisson process of spontaneous spikes. In another limiting case of extensive bursting $p \to 1$, the power spectral density becomes a periodic sequence of narrow Lorentzian-like peaks at frequencies $\omega = 0, \frac{2\pi}{\tau}, \frac{4\pi}{\tau}, \ldots$. The width of a peak is $\sim (1-p)$, while the amplitude scales $\sim (1-p)^{-2}$ (the total power of a peak diverges in this limit because the density of spike diverges). In Fig. 2.6 we compare the obtained expression for the spectral density with direct numerical modeling of Eq. (2.1).

2.5 Probability to induce a spike

As have been shown in the section 2.3 above, in our model, from the viewpoint of a point process, there are only two parameters: the spontaneous spiking rate λ (or J) and p, the probability to induce a spike by a delay force and noise. The expression for λ is given by formula (1.4). The main challenge that is discussed in this Section, is an analytical calculation of p.

From the simulations of Eq. (2.1), where the delay force can be switched off and on (corresponding to $\epsilon = 0$ and $\epsilon \neq 0$ respectively), the probability to induce a spike follows from the relation (2.5):

$$p = \frac{\langle n \rangle - \langle n_0 \rangle}{\langle n \rangle} \ . \tag{2.17}$$

Here $\langle n_0 \rangle$ is the average number of spikes within a large time interval without the time-delayed force, while $\langle n \rangle$ is the average number of spikes in presence of the delayed force within the same time interval.

2.5.1 Induced probability by the Fokker-Planck equation

Due to the nonlinear force and non-Markovian property of Eq. (2.1), it's hard to obtain the exact solution analytically, e.g., formulating it in terms of delay Fokker Planck equation [OY00; Fra05]. However, since a is close to 1 and the noise intensity is small, we can approximate the delay force with a deterministic time-dependent force based on the spike solution (2.3),(2.4). Thus, the problem reduces to consideration of a deterministically driven stochastic model

$$\dot{\theta} = a + \cos\theta + \epsilon H(t) + \sqrt{D}\xi(t). \tag{2.18}$$

where the force term is given by expression (2.4). The corresponding Fokker-Planck equation reads

$$\frac{\partial P(\theta, t)}{\partial t} = -\frac{\partial}{\partial \theta}\left[(a + \cos\theta + \epsilon H(t))P(\theta, t)\right] + D\frac{\partial^2 P(\theta, t)}{\partial \theta^2} \ . \tag{2.19}$$

In order to properly formulate the setup for this equation, we need to describe its dynamics qualitatively. As a starting state prior to incoming pulse $H(t)$, we can take a stationary distribution of the equation with $\epsilon = 0$, i.e. the stationary solution (1.3): $P(\theta, -T) = P_{st}(\theta)$, for $0 \leq \theta < 2\pi$. Here $-T$ is a starting point of pulse action. Under the action of the pulse, this state evolves, and $P(\theta, t)$ shifts in the positive direction of θ, and the flux of probability through the point $\theta = 0$ increases – this exactly describes increased local rates of a spike excitation during the action of the pulse. In order to control "multiple" pulse excitation (generation of two or more spikes during one acting pulse) it is convenient to choose the period of domain as 8π instead of 2π. Then, after the action of the pulse $H(t)$, a state $P(\theta, T)$ is reached. The net probability within the domain $[2\pi, 4\pi]$ can be interpreted as the probability to induce just one spike by the force $\epsilon H(t)$ as follows,

$$p = \int_{2\pi}^{4\pi} (P(\theta, T) - P_0(\theta, T))d\theta. \tag{2.20}$$

Here $P(\theta, T)$ is the solution of Eq. (2.19), while $P_0(\theta, T)$ is the corresponding solution of the unforced Fokker-Planck equation (i.e., of Eq. (2.19) with $\epsilon = 0$) – it describes
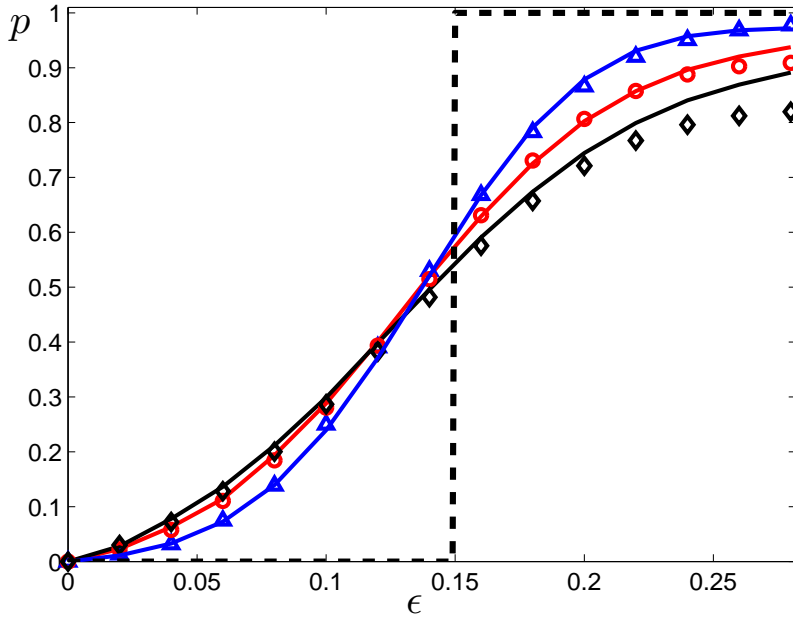
FIGURE 2.7: Probability to induce a spike by time delayed feedback for different delay force amplitudes. The blue triangles, red circles, and black diamonds represent the simuation results of Eq.(2.17) for $D = 0.005, 0.007, 0.009$ [we used the Euler-Maruyama method with time step $dt = 0.01$, integration interval was 5×10^5, and additionally averaging over 200 realizations was performed]. The solid lines with the same color is the corresponding numerical results of Eq.(2.20). The black dashed line is the deterministic solution with $\epsilon_c = 0.15$. Parameters are chosen as $a = 0.95, \tau = 500$. Figure reprinted with permission from Ref. [ZP18].

spontaneous spikes. The total probabilities in domains $[4\pi, 6\pi]$ and $[6\pi, 8\pi]$ (they correspond to the probabilities to induce 2 or 3 spikes) are actually very close to zero and therefore can be neglected.

Practically, we solve Eq. (2.19) with a spectral method. We represent the probability density as a (truncated) Fourier series as $P(\theta, t) = \sum_{m=-N}^{N} C_m(t) e^{i\frac{m}{4}\theta}$, and substitute it into the Fokker-Planck equation. In this way we obtain an large system of non-autonomous ODEs for the Fourier modes

$$\frac{dC_m}{dt} = \frac{m}{8i}C_{m-4} - (\frac{i}{4}ma + \frac{i}{4}m\epsilon H(t) + \frac{m^2}{16}D)C_m + \frac{m}{8i}C_{m+4}. \qquad (2.21)$$

We truncated this system at $N = 400$ and solved the above ODEs by the 4th order Runge-Kutta method with time step 0.001. As Fig. 2.7 depicts, the numerical method described fits well with the simulation results. We also investigated how the noise intensity influences the probability to induce a spike. To analyze the role of noise and delay, we compare the results in presence of noise with the deterministic case, where there is a critical value of ϵ to induce periodic spikes. Generally speaking, for $\epsilon < \epsilon_c$, noise enhances the spiking by cooperation with the delay feedback, while for $\epsilon > \epsilon_c$ noise can prevent spikes otherwise induced by the delay feedback.

2.5.2 Analytic approaches to calculate induced probability

As we have shown above, the problem reduces to the analysis of a pulse-driven Fokker-Planck equation. Such an analysis can be performed analytically in the limiting cases of an adiabatic (very long) pulse, and of a kicked (δ-function) driving. The adiabatic
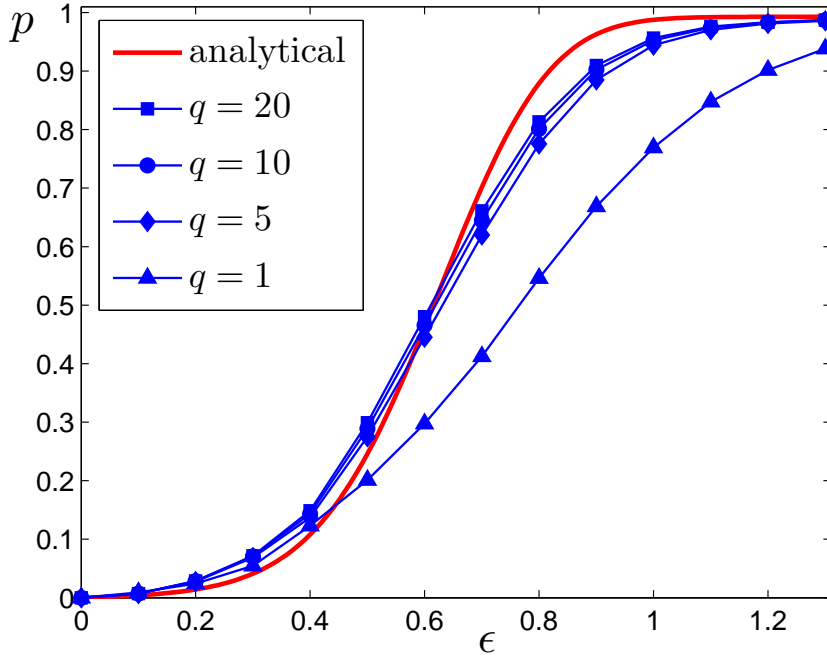
FIGURE 2.8: Probability to induce a spike by delayed pulses with different sharpness vs the amplitude of the delay force. The blue triangles, diamonds, circles and rectangles represent the simulation results of Eq. (2.22) with $q = 1$, 5, 10 and 20 respectively. The red curve is the analytical result from Eq. (2.25) for the δ-pulse. Parameters are chosen as $a = 0.995$, $D = 0.005$ and $\tau = 500$. Figure reprinted with permission from Ref. [ZP18].

approximation appears to be rather bad, while for a narrow pulse, as we show below, the approximation of a δ-kick appears to be satisfactory.

It is convenient to introduce a parameter to control the width of the forcing pulse. Therefore, Eq. (2.1) is modified into the following one:

$$\dot{\theta} = a + \cos\theta + \epsilon C_q(a + \cos\theta(t - \tau))^q + \sqrt{D}\xi(t) \ . \tag{2.22}$$

Here parameter q determines the effective width of the pulse, and C_q is the normalization coefficient defined as

$$C_q = \frac{1}{\int_{-\infty}^{\infty}(a + \cos\Theta_{sp}(t))^q dt},$$

being consistent with Eq. (2.1) when $q = 1$. For large values of q, the force in (2.22) is nearly a δ-pulse.

The analysis can be performed in terms of the so-called splitting probability. We start with an equilibrium solution of the autonomous Fokker-Planck equation 1.3, which for small noise is concentrated around the stable state (minimum of the potential). During the δ kick, the static potential and diffusion term don't play a role, and hence the effective evolution of the probability density from τ^- to τ^+ is just the shift

$$P(\theta, \tau^+) = e^{-\epsilon\frac{\partial}{\partial\theta}}P(\theta, \tau^-) = P_{st}(\theta - \epsilon). \tag{2.23}$$

Due to the noisy environment, the following evolution is a relaxation, described by the autonomous Fokker-Planck equation. During this evolution, a "particle" can overcome

the potential barrier, thus producing a spike, or return back to the stable state, this corresponds to not inducing a spike. The main contribution is from the points around $\theta_s + \epsilon$, for which we can approximate the potential by the inverted parabolic one. Evolution in such a potential is known as the splitting problem [Gar09]. If the 'phase particle' is initially at the position θ, the probability to eventually be right to the maximum θ_u is

$$\rho(\theta) = \frac{1}{2}\left(1 - \mathrm{erf}\left[(\theta_u - \theta)\sqrt{\frac{|U''(\theta_u)|}{D}}\right]\right). \tag{2.24}$$

Thus, the probability to induce a spike is

$$p(\epsilon) = \int_{\epsilon}^{2\pi+\epsilon} P_{st}(\theta - \epsilon)\rho(\theta)d\theta \ = \int_{0}^{2\pi} P_{st}(\theta)\rho(\theta + \epsilon)d\theta. \tag{2.25}$$

In Fig. 2.8 we compare the analytical expression for the delta-pulse with simulations for different values of parameter q. For $q = 1$ the analytic formula is not a good approximation, but for $q = 5$ and larger value, it fits numerics rather well.

2.6 Summary

We have demonstrated that the combined effect of time delay and noise can lead to interesting spike patterns in excitable neurons. We have shown that a weak positive (excitatory) time-delay feedback on the excitable neuron in a noisy environment leads to delay-induced stochastic bursting. As an ideal mathematical model to describe the spiking pattern we adopted a point process with the leader-follower relationship. The main restriction in the applicability of this model is a separation of time scales, which requires noise to be weak and the delay to be long. The model contains just two parameters, the rate λ of the appearance of spontaneous spikes, and the probability p to induce a follower spike. Roughly, the bursting pattern can be described as a sequence with randomly appearing bursts (with average inter-burst interval λ^{-1}), having random durations (as an average, each burst has $p(1-p)^{-1}$ spikes).

It is instructive to analyze the roles noise and time delay play in the model. When the amplitude of the delayed force is below the critical value of onset of delay-induced oscillations (i.e., $\epsilon < \epsilon_c$), noise and delay jointly induce spikes: delayed feedback reduces temporary the potential barrier to overcome due to noisy forcing. On the other hand, if the amplitude of the delayed force is above the threshold, i.e., $\epsilon > \epsilon_c$, and delay feedback is large enough to induce spikes in the deterministic case, the noise makes the probability to induce spikes to be less than one, so that the bursts remain finite. As a very rough estimation, one can say that exactly at $\epsilon = \epsilon_c$ the delayed force brings the system to the unstable state (maximum of the effective potential), from which noise can produce a spike with probability $1/2$. This estimate is confirmed by numerical results presented in Fig. 2.7, where the dashed line crosses the probability p curves at $p \approx 1/2$.

As we have shown in this chapter, two essential parameters determine the statistical properties of the stochastic bursting: the spontaneous excitation rate λ and the probability to induce a spike during the feedback p. While the former is the standard quantity, easily calculated from the stationary solution of the autonomous Fokker-Planck equation, the latter probability could be found only numerically (from the solution of forced Fokker-Planck equation) or with some additional approximations. We have found that the adiabatic approximation is not adequate for the theta-neuron considered here, while the approximation of a narrow, δ-function-like pulse gives a

qualitatively good result. A quantitative correspondence could be achieved, however, only when we modified the form of the delayed force making it narrower than in the original formulation.

Our basic system in this chapter was a one-dimensional equation similar to that of a theta-neuron. This significantly simplified the analysis based on the Fokker-Planck equation. However, we expect that the point process model of the dynamics will be valid in other, more realistic systems of Hodgkin-Huxley type, like the the noisy FitzHugh-Nagumo system with delayed feedback [Sch+09], provided the above-mentioned separation of the characteristic time scales is valid.

The approach based on the point process and multiscale approximation developed in this chapter is not limited to a single neuron case, while it can also be applied to networks of delay-coupled noisy theta-neurons. This will be described in Chap. 3 and Chap. 4.

Chapter 3

Stochastic bursting in unidirectionally delay-coupled systems

In Chap. 2 we observed the stochastic bursting in a single noisy system, under the influence of both time delay and noise. Since excitable systems such as neurons are usually coupled with each other in terms of complex networks, a natural question arises that whether or not the stochastic bursting also occurs in delay-coupled excitable systems.

In this chapter, we first extend the theory developed in Chap. 2 to the case of two mutually delay-coupled excitable units, and further to a simple but widely used network of unidirectional ring topology. After outlining the main features and approximations behind the theory of one unit, we describe *stochastic bursting* in two coupled units in detail. The generalization to a chain of neurons will be then straightforward. We consider in this chapter a network of unidirectionally coupled units, topology of which is illustrated in Fig. 3.1 (a). The units are generally different, and the propagation times for the interactions are also different. Each unit is described with a prototypic model for an excitable system, a noisy theta-neuron [EK86] (or, in other contexts, called active rotator [SK86]):

$$\dot{\theta}_i = a_i + \cos \theta_i + \epsilon_i(a_{i-1} + \cos \theta_{i-1}(t - \hat{\tau}_{i-1})) + \sqrt{D_i}\xi_i(t). \qquad (3.1)$$

Variable θ is defined on a circle $0 \leq \theta < 2\pi$. Here parameters a_i define the excitability property of the neurons. For $a_i < 1$, there is a stable and an unstable steady states for an isolated unforced unit, and these states collide in a SNIPER bifurcation at $a_i = 1$. Thus, close to this threshold, the unit is excitable: a small noise or a small force may induce a spike (nearly 2π-rotation of θ back to the stable state on the circle). Parameter D_i describes intensity of the Gaussian white noises $\xi_i(t)$, with $\langle \xi_i(t) \rangle = 0$, $\langle \xi_i(t)\xi_j(t') \rangle = 2\delta_{ij}\delta(t - t')$. Finally, parameters ϵ_i describe the strengths of delayed coupling. The coupling force, amplitude of which is ϵ_i, is chosen to vanish in the steady state of a driving unit. The forcing term on the r.h.s. of (3.1) produced by one spike can be represented as

$$H(t) = a + \cos \Theta_{sp}(t), \qquad (3.2)$$
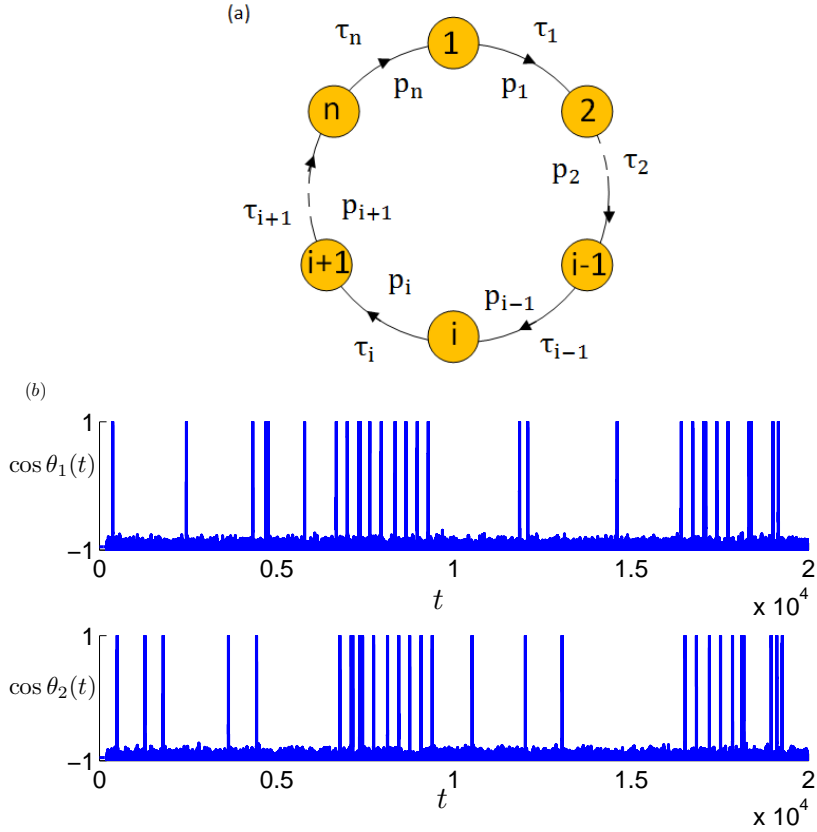
FIGURE 3.1: Panel (a): Schematic description of a ring of unidirectional delay-coupled noisy systems, where a spike in neuron i induces a spike to neuron $i + 1$ after delay time τ_i with probability p_i. Panel (b): The spike trains in a two-neuron network, obtained in direct simulations of Eq. (2.1). Values of parameters: $a = 0.95$, $D = 0.005$, $\hat{\tau}_1 = 100$, $\hat{\tau}_2 = 200$, and $\epsilon = 0.14$. Figure reprinted with permission from Ref. [ZP19].

with $\Theta_{sp}(t)$ being the deterministic trajectory connecting the unstable point (the threshold) with the stable one:

$$\Theta_{sp}(t) = 2 \arctan \left(\sqrt{\frac{1+a}{1-a}} \tanh \left(\frac{\sqrt{1-a^2}}{2}(t - t_0) \right) \right) . \tag{3.3}$$

3.1 Network dynamics and point process

To describe qualitatively the dynamics in the network, we start with a non-coupled unit. For a small noise, it produces independent spikes, constituting a Poisson process with the rate λ, which is described by Eq. (1.4) in Sec. 1.1.1.

With coupling, i.e. with $\epsilon \neq 0$, spikes of neuron $i - 1$ produce, with a delay, a kick to its next neighbor i. Such a kick facilitates excitation, so that it will cause a pulse in neuron i, as a combined effect of forcing and noise, with probability p_i. The timing of the induced spike is slightly shifted to the forcing, we will denote this shift $\bar{\tau}$ and define a new effective delay $\tau_i = \hat{\tau}_i + \bar{\tau}$ (we will mainly consider the shift $\bar{\tau}$ as a fixed one, but will briefly discuss the effect of fluctuations of this quantity in section 3.4.) Hence, to be more general, units are described by different quantities λ_i (rates with
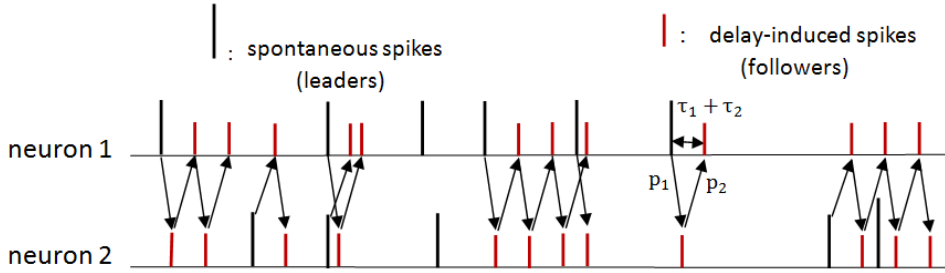
FIGURE 3.2: Schematic description of the point process with the leader-follower relationship for two neurons. A leader with a random number of its followers form a burst, and the followers could be in both neurons. The leaders appear in both neurons. Figure reprinted with permission from Ref. [ZP19].

which they "spontaneously" produce spikes due to noise), p_i (the probability with which a spike is induced by the incoming force), and τ_i (time delay in forcing).

    This allows us to describe the activity on the network as a point process, in which we neglect the duration of the spikes (approximate them as delta-functions), compared to the delay times τ and the inverse rate λ^{-1}. This is well justified for mammal brains, where the characteristic duration of a spike is $\sim 1ms$, while the delay time and the characteristic time interval between noise-induced spikes are of the order $\sim 100ms$ [SW12; Lon13]. The spike occurred at time t in neuron i, will produce a kick on neuron $i+1$ at time $t+\hat{\tau}_i$, and will generate a spike in neuron $i+1$ at time $t+\tau_i$ with probability p_i, as depicted schematically in Fig. 3.1 (a).

    Throughout the paper, in numerical illustrations we use parameters $a = 0.95$, $D = 0.005$. The small additional delay is $\bar{\tau} \approx 7$, it is much smaller than the characteristic delay times we use $\hat{\tau} \sim 100$ and the inverse of the spontaneous rate $\lambda^{-1} \approx 1506$. For these parameters of the neuron, we use the coupling strength $\epsilon = 0.14$, for which the probability to induce a spike by the forcing is $p = 0.53$ (for details of the calculation of this probability see Ref. [ZP18]). Empirically, this probability can be determined in simulations of one unit with a delayed self-feedback. One calculates the numbers of spikes, during a large time interval, in dependence on the coupling strength $N(\epsilon)$. Then,

$$p(\epsilon) = \frac{N(\epsilon) - N(0)}{N(\epsilon)} \ . \tag{3.4}$$

3.2   Two coupled units

3.2.1   Statistics of interspike intervals

It is instructive to start with the case where there are only two neurons in the ring, i.e. $n = 2$, and then to extend the theory to a more general case with arbitrary $n > 2$. When $n = 2$, the two delay-coupled neurons are denoted as i and j (i, j could be 1 or 2). We simulate Eq. (2.1) and obtain spike trains with bursts of each neuron as shown in Fig. 2.3(b). As outlined above, an idealized point process can be constructed to describe the bursting phenomenon, as illustrated in Fig. 3.2. Spontaneously generated spikes we denote as leaders. Each leader induces a finite set of followers (induced spikes), and together with them constitutes a coherent burst. In a burst, spikes in the two neurons appear alternatively with time intervals τ_1 and τ_2. The number of spikes in a burst is random. Noteworthy, similar to the case of one single neuron with delayed feedback (see Chap. 2) , the bursts can overlap; hence the analysis of the ISI

(inter-spike intervals) distribution of the spike train in each unit is nontrivial. Here the leaders in each neuron will have random followers in both the coupled neuron and the neuron itself, as explained schematically in Fig. 3.2.

First, we determine the overall rate of the spikes in each unit. The probability for a spike in unit i to induce a follower in the same unit is $p_i p_j$. Thus, the probability for a leader to have exactly m followers in the same unit is $(p_i p_j)^m (1 - p_i p_j)$. The average number of followers in the same unit is $\sum_m m(p_i p_j)^m (1 - p_i p_j) = (p_i p_j)(1 - p_i p_j)^{-1}$. The total average number of spikes in a burst is $1 + (p_i p_j)(1 - p_i p_j)^{-1} = (1 - p_i p_j)^{-1}$ Therefore, the total rate of spikes initiated in unit i is $\lambda_i (1 - p_i p_j)^{-1}$. For the spikes in unit i, initiated by a leader in unit j, we have first to find the rate of the first followers in unit i, which is $\lambda_j p_j$; the total rate of these spikes is thus $\lambda_j p_j (1 - p_i p_j)^{-1}$. Summing, we obtain the total rate of spikes μ_i as

$$\mu_i = \lim_{m \to \infty} (\lambda_i + \lambda_j p_j)[1 + p_i p_j + (p_i p_j)^2 + ... + (p_i p_j)^m] = \frac{\lambda_i + \lambda_j p_j}{1 - p_i p_j}. \tag{3.5}$$

To derive the statistics of the ISI, we assume that in one of the units there is a spike at time t, and the next spike at time $t' > t$, so that the inter-spike interval is $T = t' - t$. Three different cases should be distinguished, namely, $T > \tau_i + \tau_j, T = \tau_i + \tau_j$, and $T < \tau_i + \tau_j$. If $T < \tau_i + \tau_j$, the spikes at t and t' can be either spontaneous (leader) or delay-induced ones, but in the latter case they belong to different bursts, so they are independent. Therefore, the survival function, i.e., the probability that there is no spike in (t, t'), is determined by the full rate μ_i from (3.5): $S_i(T) = \exp(-\mu_i T)$.

In contradistinction, for the case $T > \tau_i + \tau_j$, the spike at time t' in neuron i can only be from a spontaneous one (leader) in neuron i itself, or the first induced spike (with probability p_j from neuron j). These events are independent on the occurrence of a spike at time t, and have the total rate $\lambda_i + \lambda_j p_j$. The probability that there is no any spike in (t, t') in neuron i is the product of three terms: the probability to have no spikes in the interval $(t, t + \tau_i + \tau_j]$ with the survival function $S_{\tau b} = \exp(-\mu_i(\tau_i + \tau_j))$, the probability $(1 - p_i p_j)$ not to have a follower for the spike at t, and the probability to have no spike in the interval $(t + \tau_i + \tau_j, t')$, where only the spontaneous total rate $\lambda_i + \lambda_j p_j$ applies with the survival function $S_{\tau a} = \exp(-(\lambda_i + \lambda_j p_j)(T - \tau_i - \tau_j))$. Thus, the survival function for the case $T > \tau_i + \tau_j$ is

$$S_i(T) = S_{\tau b}(1 - p_i p_j)S_{\tau a} = (1 - p_i p_j)e^{-\mu_i(\tau_i + \tau_j) - (\lambda_i + \lambda_j p_j)(T - \tau_i - \tau_j)}. \tag{3.6}$$

Based on the above description, and on the relationship between the cumulative ISI distribution $Q(T)$ and the survival function $S(T)$, which reads $Q(T) = 1 - S(T)$, the cumulative ISI distribution of neuron i can be obtained as follows:

$$Q_i(T) = \begin{cases} 1 - e^{-\mu_i T}, & T < \tilde{\tau}, \\ 1 - (1 - p_i p_j)e^{-\mu_i \tilde{\tau} - (\lambda_i + \lambda_j p_j)(T - \tilde{\tau})}, & T \geq \tilde{\tau}, \end{cases} \tag{3.7}$$

where $\tilde{\tau} = \tau_i + \tau_j$. We compare this expression with results of numerical simulations in Fig. 3.3. The point process described by Eq. (3.7) agrees well with direct simulations of Eq. (3.1), where we assumed the parameters of the two neurons to be the same, except for the time delays which are different.

3.2.2 Correlations and spectra

In the following, we derive the autocorrelation and the cross-correlation functions of the spike trains, and the corresponding power spectrum and the cross-spectrum. The
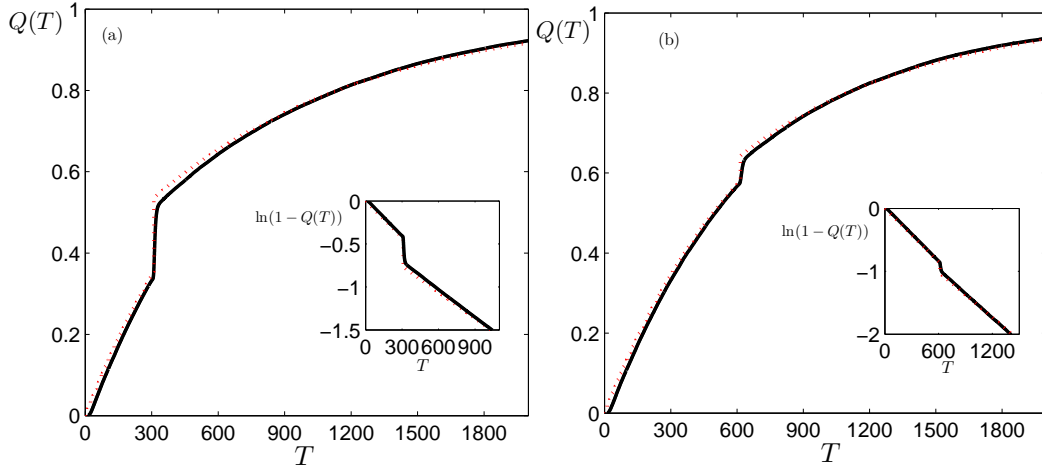
FIGURE 3.3: Cumulative ISI distribution $Q(T)$ vs T for $n = 2$ (panel (a)) and $n = 3$ (panel (b)) in a ring of unidirectional delay-coupled neurons. The black lines are direct numerical simulations of Eq. (2.1), where the values of parameters are chosen as: for $n = 2$, $\hat{\tau}_1 = 100$, $\hat{\tau}_2 = 200$ for $n = 3$, $\hat{\tau}_1 = 100$, $\hat{\tau}_2 = 200$, $\hat{\tau}_3 = 300$. Values of a, ϵ and D are chosen as $a = 0.95$, $\epsilon = 0.14$, $D = 0.005$ f or both cases. The red dotted lines correspond to the point process with Eq. (2.9) for cumulative ISI, where $\lambda = 6.64 \times 10^{-4}$, $p = 0.53$ are the same for both cases. The effective time delays are $\tau_1 = 107, \tau_2 = 207$ for $n = 2$ case. $\tau_1 = 107, \tau_2 = 207, \tau_3 = 307$ for $n = 3$ case. The inset is a logarithmic scale version to validate the piecewise-linear spiking rate. Figure reprinted with permission from Ref. [ZP19].

autocorrelation function is defined via a joint probability to have a spike in unit i within a small time interval $(t, t + \Delta t)$, and a spike in unit j within the time interval $(t + s, t + s + \Delta t)$, no matter whether or not there are any spikes between t and $t + s$. The joint probability of these events is defined as

$$P_{ij}(t, t + \Delta t; t + s, t + s + \Delta t) = \begin{cases} W_i(t, t + \Delta t)P_{ij}(t + s|t, \Delta t), & s \geq 0, \\ W_j(t, t + \Delta t)P_{ji}(t|t + s, \Delta t), & s < 0. \end{cases} \quad (3.8)$$

Here $W_i(t, t + \Delta t) = \mu_i \Delta t$ is the probability to observe a spike in neuron i within the time interval $[t, t + \Delta t]$. The quantity $P_{ij}(t + s|t, \Delta t)$ is the probability to induce a spike in neuron j at time $t + s$, given a spike in neuron i at time t.

Correlations and spectra within one unit

We first calculate the conditional probability (3.8) for the same unit. The conditional probability to have one induced spike with time shift $\tilde{\tau}$ is $p_i p_j$, while it is $(p_i p_j)^k$ for the k-th induced spike with delay $k\tilde{\tau}$. Therefore,

$$P_{ii}(t + s|t, \Delta t) = \delta(s)\Delta t + p_i p_j \delta(s - \tilde{\tau})\Delta t + \cdots + (p_i p_j)^k \delta(s - k\tilde{\tau})\Delta t + \cdots$$

$$= \sum_{k=0}^{\infty} (p_i p_j)^k \delta(s - k\tilde{\tau})\Delta t, \quad s \geq 0; \quad (3.9)$$

$$P_{ii}(t|t + s, \Delta t) = P_{ii}(t - s|t, \Delta t), s < 0,$$

where $\delta(\cdot)$ is the Dirac delta function. Since the correlation function can be seen as the mean rate of the joint event, after substituting Eq. (3.8) and (3.9), the auto-correlation

function is

$$
\begin{aligned}
C_{ii}(s) &= \langle (x_i(t) - \langle x_i \rangle)(x_i(t+s) - \langle x_i \rangle) \rangle \\
&= \frac{1}{T} \int_0^T dt \lim_{\Delta t \to 0} \frac{P_{ii}(t, t+\Delta t; t+s, t+s+\Delta t)}{\Delta t^2} = \mu_i \sum_{n=-\infty}^{\infty} (p_i p_j)^{|n|} \delta(s - n\tilde{\tau}),
\end{aligned}
$$

(3.10)

where we use the fact that P_{ii} is t-independent, and have taken into account that $\langle x_i \rangle = \mu_i$.

Taking the Fourier transform of the correlation function, we obtain the power spectral density

$$
S_{ii}(\omega) = \int_{-\infty}^{\infty} C_{ii}(s) e^{-i\omega s} ds = \frac{(\lambda_i + \lambda_j p_j)(1 + p_i p_j)}{1 + (p_i p_j)^2 - 2 p_i p_j \cos \omega(\tau_i + \tau_j)}.
$$

(3.11)

The derivations above are based on the time series $x_i(t)$ represented as a sum of delta-peaks, i.e., $x_i(t) = \sum_{i=1}^{N} \delta(t - t_i)$. For a train of realistic spikes, the shape function can be straightforwardly taken into account as done in Ref. [ZP18], namely the spectrum (3.11) should be just multiplied by the squared amplitude of the Fourier transform of the pulse shape. For example, if observable (2.4) is used, the spike train x_i will be convoluted with the shape function $H(t)$. Hence, the power spectral density and the cross-spectral density in the following illustrations will be multiplied by the spectral density of $H(t)$, which we denote as $S_H(\omega)$. For simplicity, in the formulas below we still use the delta-peak representation of x_t, while we multiply by $S_H(\omega)$ to compare with numerical correlations and spectra obtained by simulations of Eq. (2.1). This comparison is shown in Fig. 3.4(a), the theoretical predictions based on the point process analysis agree well with the results of direct simulation of Eq. (2.1).

Cross-correlations and cross-spectra for two units

The conditional probability of the joint event between the two neurons can be expressed similarly to formula (3.9) above:

$$
\begin{aligned}
P_{ij}(t+s|t, \Delta t) &= p_i \delta(s - \tau_i)\Delta t + \cdots + p_i(p_i p_j)^k \delta(s - k\tilde{\tau} - \tau_i)\Delta t + \cdots \\
&= \sum_{k=0}^{\infty} p_i(p_i p_j)^k \delta(s - k\tilde{\tau} - \tau_i)\Delta t, \quad s \geq 0; \\
P_{ji}(t|t+s, \Delta t) &= p_j \delta(s + \tau_j)\Delta t + \cdots + p_j(p_i p_j)^k \delta(s + k\tilde{\tau} + \tau_j)\Delta t + \cdots \\
&= \sum_{k=0}^{\infty} p_j(p_i p_j)^k \delta(s + k\tilde{\tau} + \tau_j)\Delta t, \quad s < 0.
\end{aligned}
$$

(3.12)

This allows us to obtain the cross-correlation function of the two neurons, by substituting Eq. (3.12) into Eq. (3.8), leading to the Eq. (3.13):

$$
\begin{aligned}
C_{ij}(s) &= \lim_{\Delta t \to 0} \frac{P_{ij}(t, t+\Delta t; t+s, t+s+\Delta t)}{\Delta t^2} \\
&= \mu_i \sum_{n=0}^{\infty} p_i(p_i p_j)^n \delta(s - n\tilde{\tau} - \tau_i) + \mu_j \sum_{n=0}^{\infty} p_j(p_i p_j)^n \delta(s + n\tilde{\tau} + \tau_j).
\end{aligned}
$$

(3.13)
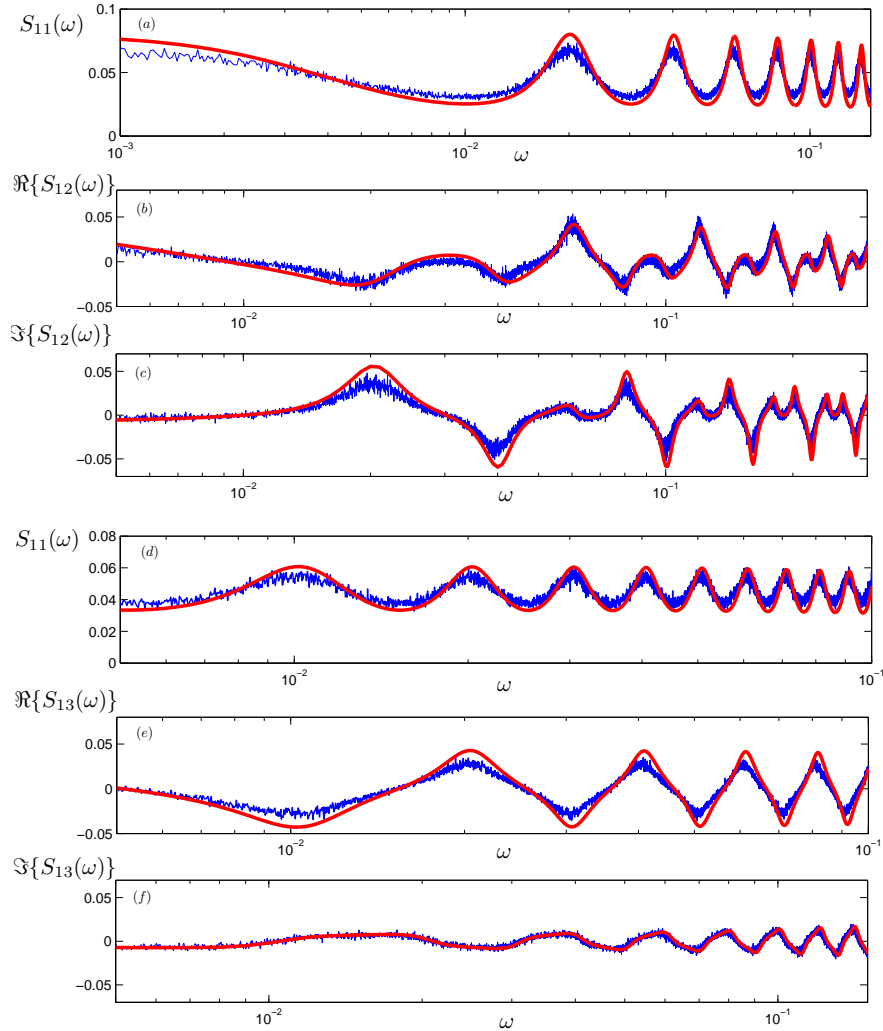
FIGURE 3.4: Panels (a)-(c) show the power spectral density of neuron 1, and the real part and the imaginary part of the cross-spectral density S_{12}, respectively, for two delay-coupled neurons. The blue lines are from direct simulation of Eq. (2.1) and the red lines are the analytical results from Eq. (3.11), Eq. (3.15) and Eq. (3.16) for (a)-(c), respectively. Panels (d)-(f) show the power spectral density, the real part and the imaginary part of the cross-spectral density S_{13}, respectively, for the ring of $n = 3$ neurons. The blue lines show numerical simulations of Eq. (2.1) with $n = 3$. The red lines are the analytical results from Eq. (3.24), Eq. (3.26) and Eq. (3.27) for (d)-(f), respectively. The parameter values in the simulation and the analytical expressions are chosen the same as in Fig. 3.3. Noteworthy, all the power and corss-spectral density are multiplied by the power spectral density of the shape function S_H, similar to Ref. [ZP18]. Figure reprinted with permission from Ref. [ZP19].

The cross-spectral density is the Fourier transform of the cross-correlation function:

$$S_{ij}(\omega) = \int_{-\infty}^{\infty} C_{ij}(s)e^{-i\omega s}ds = \mu_i p_i \frac{e^{-i\omega \tau_i}}{1 - p_i p_j e^{-i\omega \tilde{\tau}}} + \mu_j p_j \frac{e^{i\omega \tau_j}}{1 - p_i p_j e^{i\omega \tilde{\tau}}}. \tag{3.14}$$

It is instructive to present explicitly the real part

$$\mathrm{Re}\,[S_{ij}] = \frac{p_i(\mu_i - \mu_j p_i p_j)\cos\omega\tau_i + p_j(\mu_j - \mu_i p_i p_j)\cos\omega\tau_j}{1 + (p_i p_j)^2 - 2p_i p_j \cos\omega\tilde{\tau}}, \tag{3.15}$$

and the imaginary part

$$\mathrm{Im}\,[S_{ij}] = \frac{p_i(\mu_i - \mu_j p_i p_j)\sin\omega\tau_i - p_j(\mu_j - \mu_i p_i p_j)\sin\omega\tau_j}{1 + (p_i p_j)^2 - 2p_i p_j \cos\omega\tilde{\tau}}. \tag{3.16}$$

of the cross-spectrum.

Unlike the power spectral density described by a real-valued function (3.11), the cross-spectral density is generally a complex-valued function. It is real-valued only when the two neurons are totally identical, i.e., $\lambda_i = \lambda_j = \lambda$, $p_i = p_j = p$, and $\tau_1 = \tau_2 = \tau$, resulting in a simple expression

$$S_{ij}(\omega) = \frac{2\lambda p(1 + p)\cos\omega\tau}{1 + p^4 - 2p^2 \cos 2\omega\tau}, \tag{3.17}$$

which is very similar to the power spectral density of a single unit (3.11). We compare the theoretical cross-spectra with simulations in Figs. 3.4b,c.

Correlation and spectra of the total output from the network

If we consider correlations and spectra from the viewpoint of the total network output, the cross-correlations between all the pulses should be calculated. A joint probability could be defined as having a spike in any unit within a small time interval $(t, t + \Delta t)$, and a spike in any unit within the time interval $(t + s, t + s + \Delta t)$, no matter whether or not there are any spikes between t and $t+s$. The joint probability $\hat{P}$ of these events is the sum of all contributions:

$$\hat{P}(t, t + \Delta t; t + s, t + s + \Delta t) = \sum_{i=1}^{2}\sum_{j=1}^{2} P_{ij}, \tag{3.18}$$

where P_{ij} is described by Eq. (3.8). Thus the correlation function is

$$\hat{C}(s) = \frac{1}{T}\int_{0}^{T} dt \lim_{\Delta t \to 0} \frac{\hat{P}(t, t + \Delta t; t + s, t + s + \Delta t)}{\Delta t^2} = \sum_{i=1}^{2}\sum_{j=1}^{2} C_{ij} \tag{3.19}$$

where C_{ij} is described by Eq. (3.10) when $i = j$ and by Eq. (3.13) when $i \neq j$. The spectral density of the total output , i.e. of the observable $X(t) = x_1(t) + x_2(t)$, is obtained as a Fourier transform of $\hat{C}(s)$, leading to

$$S_X(\omega) = \sum_{i=1}^{2} \mu_i \frac{1 - (p_i p_j)^2 + 2p_i(\cos\omega\tau_i - p_i p_j \cos\omega\tau_j)}{1 + (p_i p_j)^2 - 2p_i p_j \cos\omega\tilde{\tau}}. \tag{3.20}$$
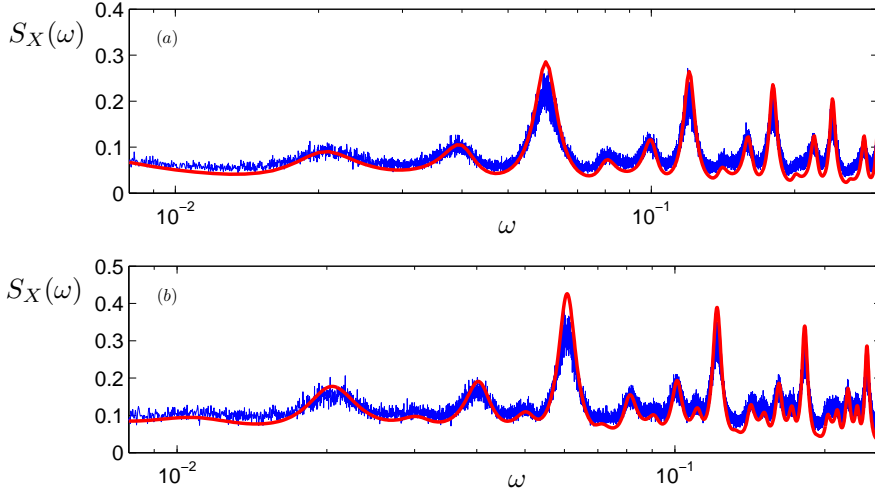
FIGURE 3.5: Power spectral density of the total output from the networks with $n = 2$ (panel (a)) and $n = 3$ (panel (b)). The blue curves correspond to the simulation results and the red lines are the theoretical expressions Eq. (3.20) for $n = 2$ and Eq. (3.28) for $n = 3$. Values of parameters are chosen the same as in Fig. 2.5 and Fig. 3.4. Figure reprinted with permission from Ref. [ZP19].

As is shown in Fig. 3.5 (a), the theoretical spectra of the total output agrees well with simulation results.

3.3 General network

The case of many neurons with $n > 2$ in the ring topology is a direct extension of the $n = 2$ case as described above; thus the analysis follows the same steps, only the expressions are more involved. First, we extend the cumulative ISI distribution for neuron i in the ring as follows,

$$Q_i(T) = \begin{cases} 1 - e^{-\mu_i T}, & T < \tilde{T}, \\ 1 - (1 - \tilde{P})e^{-\mu_i \tilde{T} - \tilde{\mu}_i (T - \tilde{T})}, & T \geq \tilde{T}. \end{cases} \tag{3.21}$$

Here $\tilde{T} = \sum_{i=1}^{n} \tau_i$ is the total round-trip delay time acround the ring, $\tilde{P} = \prod_{j=1}^{n} p_j$ is the probability to have a completed round trip around the ring, and $\tilde{\mu}_i$ is the spiking rate of all first spikes in bursts that include neuron i:

$$\begin{aligned} \tilde{\mu}_i &= \lambda_i + \lambda_{i-1} p_{i-1} + \lambda_{i-2} p_{i-2} p_{i-1} + \cdots + \lambda_{i-n+1} p_{i-1} \cdots p_{i-n+1} \\ &= \lambda_i + \sum_{l=1}^{n-1} \lambda_{i-l} \prod_{j=1}^{l} p_{i-j}. \end{aligned} \tag{3.22}$$

Here λ_i is the rate of spontaneous spikes in neuron i itself, $\lambda_{i-1} p_{i-1}$ is the rate of spontaneous spikes in neuron $i - 1$ that induce also a spike in neuron i, and so on. Noteworthy, due to the ring structure of the coupling, λ_i is a periodic function, i.e., $\lambda_i = \lambda_{i+n} = \lambda_{i-n}$. The total activity in the network is characterized by the rate μ_i, to which the rates from all spikes (both leaders and followers) contribute. Thus,

similarly to Eq. (3.5), we get

$$\mu_i = \lim_{m \to \infty} \tilde{\mu}_i (1 + \tilde{P} + \tilde{P}^2 + \cdots + \tilde{P}^m) = \frac{\tilde{\mu}_i}{1 - \tilde{P}}. \qquad (3.23)$$

Differently formulated, the expression above follows from the fact that a spike can have m followers (in the same unit) with probability $\tilde{P}^m(1 - \tilde{P})$. Using the same method as in the $n = 2$ case described above, we obtain the power spectral density of neuron i in the ring by Fourier transform of the correlation function (not presented):

$$S_{ii}(\omega) = \frac{\tilde{\mu}_i(1 + \tilde{P})}{1 + \tilde{P}^2 - 2\tilde{P}\cos\omega\tilde{T}}. \qquad (3.24)$$

The cross-spectral density of spike trains in neuron i and neuron j is:

$$S_{ij}(\omega) = \mu_i \bar{P}_{ij} \frac{e^{-i\omega T_{ij}}}{1 - \tilde{P}e^{-i\omega\tilde{T}}} + \mu_j \bar{P}_{ji} \frac{e^{i\omega T_{ji}}}{1 - \tilde{P}e^{i\omega\tilde{T}}}, \qquad (3.25)$$

The real part of which is:

$$\text{Re}\,[S_{ij}] = \frac{\bar{P}_{ij}(\mu_i - \mu_j\tilde{P})\cos\omega T_{ij} + \bar{P}_{ji}(\mu_j - \mu_i\tilde{P})\cos\omega T_{ji}}{1 + \tilde{P}^2 - 2\tilde{P}\cos\omega\tilde{T}}, \qquad (3.26)$$

and the imaginary part of which is

$$\text{Im}\,[S_{ij}] = \frac{\bar{P}_{ij}(\mu_i - \mu_j\tilde{P})\sin\omega T_{ij} - \bar{P}_{ji}(\mu_j - \mu_i\tilde{P})\sin\omega T_{ji}}{1 + \tilde{P}^2 - 2\tilde{P}\cos\omega\tilde{T}}. \qquad (3.27)$$

Here $T_{ij} = \tau_i + \cdots + \tau_{j-1}$ is the delay time from neuron i to neuron j along the direction of the ring , i.e. clockwise as depicted in Fig. 2.3, with probability $\bar{P}_{ij} = \prod_{l=i}^{j-1} p_l$. Correspondingly, $T_{ji} = \tilde{T} - T_{ij}$ is the delay time from neuron j to come to neuron i with probability $\bar{P}_{ji}$ and $\bar{P}_{ij}\bar{P}_{ji} = \tilde{P}$. The spectral density of total output, i.e. $X = \sum_{i=1}^{n} x_i(t)$, from the network is

$$S_X(\omega) = \sum_{i=1}^{n} \sum_{j=i+1}^{i+n-1} \mu_i \frac{1 - \tilde{P}^2 + 2\bar{P}_{ij}(\cos\omega T_{ij} - \tilde{P}\cos\omega T_{ji})}{1 + \tilde{P}^2 - 2\tilde{P}\cos\omega\tilde{T}}. \qquad (3.28)$$

In the case that all the units are totally identical, i.e. $\lambda_i = \lambda$, $p_i = p$ and $\tau_i = \tau(i = 1, \cdots, n)$, $S_X(\omega)$ reduces to $S_X(\omega) = \frac{n\lambda(1+p)}{1+p^2-2\cos\omega\tau}$.

Generally, the model works for any network size n, but for simplicity we choose $n = 3$ for comparison with numerics. The cumulative ISI described by Eq. (3.21), spectra described by Eqs. (3.24), (3.26), (3.27) and (3.28) agree well with direct simulation of Eq. (2.1), as shown in Fig. 2.5(b), Fig. 3.4(d)-(f) and Fig. 3.5(b), respectively. Noteworthy, similar to the case $n = 2$, the cross-spectrum S_{ij} is generally a real-valued function only if n is an even number and neurons i and j are symmetric, i.e., $|i - j| = n/2$.

To further demonstrate that our theory works for a larger network, we choose $n = 10$ and calculate the cross-spectra between neurons at different distances, e.g. between neurons 1 and 3, and between neuron 1 and 4. As shown in Fig. 3.6, the analytical results agree well with the simulations. Noteworthy, as ϵ goes larger, the duration of the delay-induced pulse becomes shorter, leading to a smaller empirical
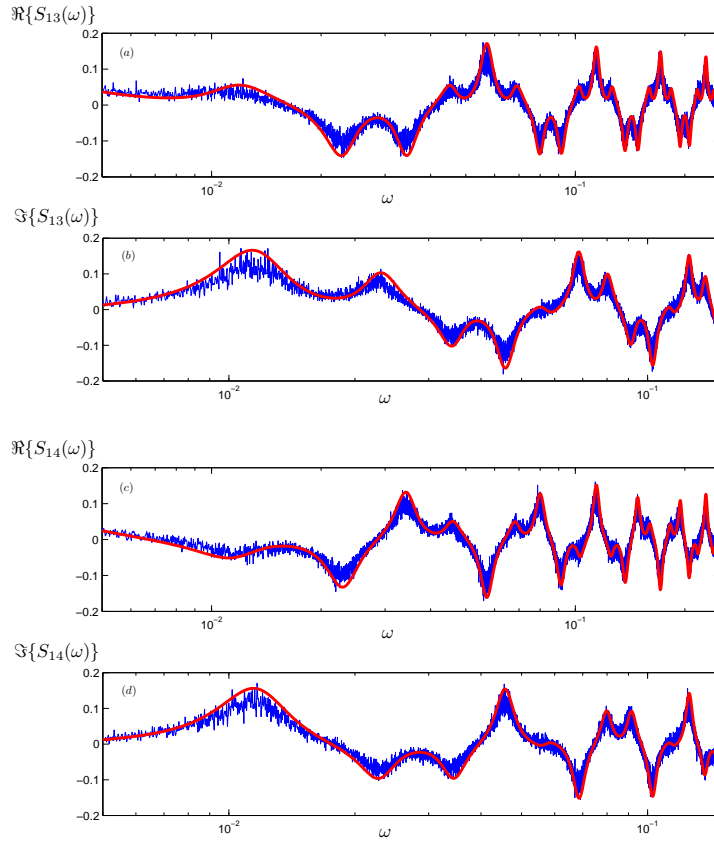
FIGURE 3.6: Cross-spectra between 1 and neuron 3 (panel (a) and panel (b) for real and imaginary part respectively, and between neuron 1 and neuron 4 (panel (c) and (d) for real and imaginary part respectively). The blue lines show numerical simulations of Eq. (2.1) where values of parameters are $a = 0.95, D = 0.005, \epsilon = 0.2, \tau_i = 50(i = 1, \cdots, 10)$. The red lines are the analytical results from Eq. (3.26) and Eq. (3.27), where $\lambda_i = 6.64 \times 10^{-4}$ is the same as described in the $n = 2$ and $n = 3$ cases and $p_i = 0.85(i = 1, \cdots, 10)$ is calculated from Eq. (2.17). Figure reprinted with permission from Ref. [ZP19].

time shift $\bar{\tau}$. In the case depicted in Fig. 3.6, $\bar{\tau} \approx 5$ for $\epsilon = 0.2$.

3.4 Summary

In conclusion, we investigated the stochastic bursting phenomenon in the unidirectionally delay-coupled noisy excitable systems. Under the condition of time-scale separation, an idealized version of coupled point processes with a leader-follower relationship was formulated. Roughly speaking, occurrence of stochastic bursting is based on three ingredients: excitability of the system, excitatory coupling with a fixed time delay, and noise. Excitability combined with noise results in the spontaneous spikes with a constant spiking rate, which are leaders of the bursts. A relatively weak coupling is not strong enough to induce a follower deterministically, but it leads to an increased probability to have a follower, characterized by the crucial parameter p. The leader with the followers form a burst, which is rather coherent (because of the fixed time interval between the followers, nearly equal to the delay time), but has a random number of spikes in it.

To characterize the stochastic bursting, the cumulative ISI distribution was derived; simulations demonstrated a good agreement with the theoretical prediction.

Furthermore, via the calculation of the joint probability of the spikes, the autocorrelation function of a single neuron spike train, the cross-correlation function of any pair of neurons in the unidirectional ring, and the autocorrelation function of the total output from the network are derived analytically. Calculation of the spectra and of the cross-spectra is then straightforward. Noteworthy, the model in the present paper not only shows an interesting coherent spiking pattern but also provides an alternative way to investigate the cross-spectrum of different neurons beyond the linear response theory (see, e.g., Refs. [LDL05; OBH09; Tro+12; VSL14], to name a few), which is widely used in the analysis of correlated neuronal networks.

Above we assumed, based on the time scale separation, that the delay times are constants. A generalization to the case of random delay times is also possible and will be presented in details elsewhere; here we discuss a simple version of this analysis. The essential point where the fixed delays appear, is the representation of the correlation function (3.10) as a sum of delta-peaks at times $n\tilde{\tau}$. If we assume the delay times to be independent Gaussian variables with mean value $\tilde{\tau}$ and standard deviation κ, then one has to replace in (3.10) delta-functions by Gaussian peaks $\delta(t - n\tilde{\tau}) \rightarrow (2n\pi\kappa^2)^{-1/2} \exp[-(t - n\tilde{\tau})^2/(2n\kappa^2)]$. In the spectrum (3.11), this correction corresponds to the replacement $p_i p_j \rightarrow p_i p_j \exp[-n\omega^2\kappa^2/2]$. Around the main frequency peaks (i.e. with small values of n), the effect of this correction is, as expected, small, due to the time scale separation $\kappa \ll \tilde{\tau}$.

In this chapter, we restricted our discussion to a unidirectional coupling in a ring topology, because here overlapping of incoming spikes is not possible under the condition of the time-scale separation. Such an overlap happens, e.g., in a network of delay-coupling neurons demonstrating polychronization [Izh06]; study of stochastic bursting in such a setup will be discussed in Chap. 4.

Chapter 4

Stochastic bursting in a chain of excitable units with delayed coupling

In our previous chapters, we have demonstrated that a coherent spike pattern which we call *stochastic bursting* can appear in simple excitable units due to the combined effect of time-delayed feedback and noise. Noise plays a two-fold role in the stochastic bursting. On one hand, it leads to spontaneous, quite rare statistically independent spikes. On the other hand, when a delayed feedback pulse enters like an excitatory under-threshold kick, noise results in an increased probability to create a new, induced spike. Thus, a spontaneous spike (the leader) can be followed by a sequence of induced spikes (the followers) separated approximately by the delay time interval. Because the creation of a follower is a random event, the overall burst has a random number of spikes. We describe stochastic bursting statistically in the case of a single excitable unit in Chap. 2, and for networks of unidirectionally delay-coupled units in Chap. 3. What these two cases have in common is that any two delay-induced kicks do not overlap. This allowed a full statistical description of the bursting as a point process, where the only parameters are the spontaneous rate of excitation, and the probability to excite a follower.

The point process model is an idealization based on the time scale separation: it is assumed that the characteristic duration of a spike is much less than other characteristic times in the system, the delay time and the characteristic time interval between the pulses (which depends on the spontaneous rate and the probability of induced spikes). However, it's not the case when neurons have multiple feedback or more complex coupling topology, where two or more delay-induced spikes could overlap with some probability. From the viewpoint of Fokker-Planck formalism, the non-markovian nature of the Langevin equation in our model prevents us from obtaining an analytic formula to describe how the phase density evolves, as many cases related to both noise and delay. Thus, in this case, the point-process representation is still a good option to describe the statistics of spike train in each neuron and between different neurons, if an appropriate approximation is adopted.

In the present chapter, we extend the theory of stochastic bursting on the case where incoming delayed pulses can overlap. Here, generally, one needs to define the probability to induce a spike by two incoming pulses. We restrict our attention below to the case of weak coupling, where this probability can be represented through one-pulse probabilities. This allows for an analytical treatment that results in explicit expressions for the power spectrum of the spike trains. First, in Section 4.1, we investigate the stochastic bursting phenomenon in a noisy excitable unit with multiple delay feedbacks. Then, in Section 4.2, we extend the theory to a network of three delay-coupled units, with a star-type coupling.
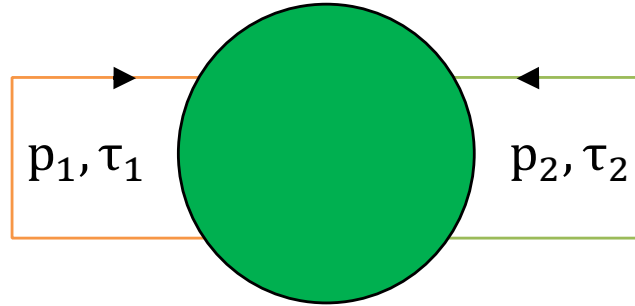
FIGURE 4.1: Schematic description of a noisy excitable unit with two feedback loops.

4.1 One excitable unit with multiple delayed feedbacks

The main goal of this chapter is to extend the theory of stochastic bursting to the situations where an overlap of delayed feedback pulses is possible. The simplest case is one unit with two delayed feedbacks, Fig. 4.1. As a model we consider a scalar equation on a circle $0 \leq \theta < 2\pi$, which is a prototypical example of excitability:

$$\dot{\theta} = a + \cos\theta + \epsilon_1(a + \cos\theta(t - \hat{\tau}_1)) + \epsilon_2(a + \cos\theta(t - \hat{\tau}_2)) + \xi(t), \qquad (4.1)$$

Here parameter $a < 1$ defines the excitability level, parameters ϵ_1, ϵ_2 are coupling strength for the two delayed feedbacks with delay times $\hat{\tau}_1$ and $\hat{\tau}_2$, respectively. The system is driven by a Gaussian white noise $\xi(t)$ with intensity D, i.e. $\langle \xi(t) \rangle = 0$, $\langle \xi(t)\xi(t') \rangle = 2D\delta(t - t')$. Without feedback (i.e. $\epsilon_1 = \epsilon_2 = 0$), the spiking rate is described by Eq. (1.4) in Sec. 1.1.1. Below we will assume this rate to be small, i.e. the characteristic time interval between the noise-excited spikes is much larger than the duration of the spikes. Below we will also assume, that this separation of times is valid for characteristic times of the delayed feedback: the delay times $\hat{\tau}_1$, $\hat{\tau}_2$ and their difference $|\hat{\tau}_1 - \hat{\tau}_1|$ are much larger than the duration of a pulse. If just one delay feedback term is present, the bursting appears as described in Chap. 2.

We now qualitatively describe the phenomenon of stochastic bursting, illustrated in Fig. 4.2. Because a feedback force acts as a kick on the unit after delay time $\hat{\tau}$, there is an increased probability p for a next pulse to be induced. Thus, each spontaneously excited pulse can have a random number of "followers" separated by a time interval $\tau = \hat{\tau} + \tau_r$, together they constitute a regular burst. Here we take into account, that the delay-induced effect is not instant, but rather it takes some relatively small response time τ_r for the unit to generate a spike after receiving a delayed kick, as described in Chap. 3. Generally speaking, the delay-induced spike occurs with some deviation around the effective time delay, i.e., not exactly at $t + \hat{\tau} + \tau_r$, but for simplicity, we assume the deviation can be ignored. The essential parameter of the stochastic bursting is the probability p to induce a follower, we discussed in Chap. 2 the ways to calculate it.

In the case of two delayed feedback, after a spontaneous pulse at time t, there are two times $t + \tau_1$ and $t + \tau_2$ at which the followers can appear, with probabilities p_1 and p_2, these probabilities are the same as for single time-delay feedbacks, as shown schematically in Fig. 4.2 (b). However, at the next level, there is an interaction of delayed kicks, which makes the problem essentially more difficult than that of one delayed feedback. Indeed, if both followers at times $t + \tau_1$ and $t + \tau_2$ are present, at time $t + \tau_1 + \tau_2$ there will be an overlap of two incoming feedback kicks. Generally, there are many such overlaps possible, at times $t + k\tau_1 + l\tau_2$ with k and l being both positive integers. Thus, another probability $p^{(2)}$ to induce a spike mediated by
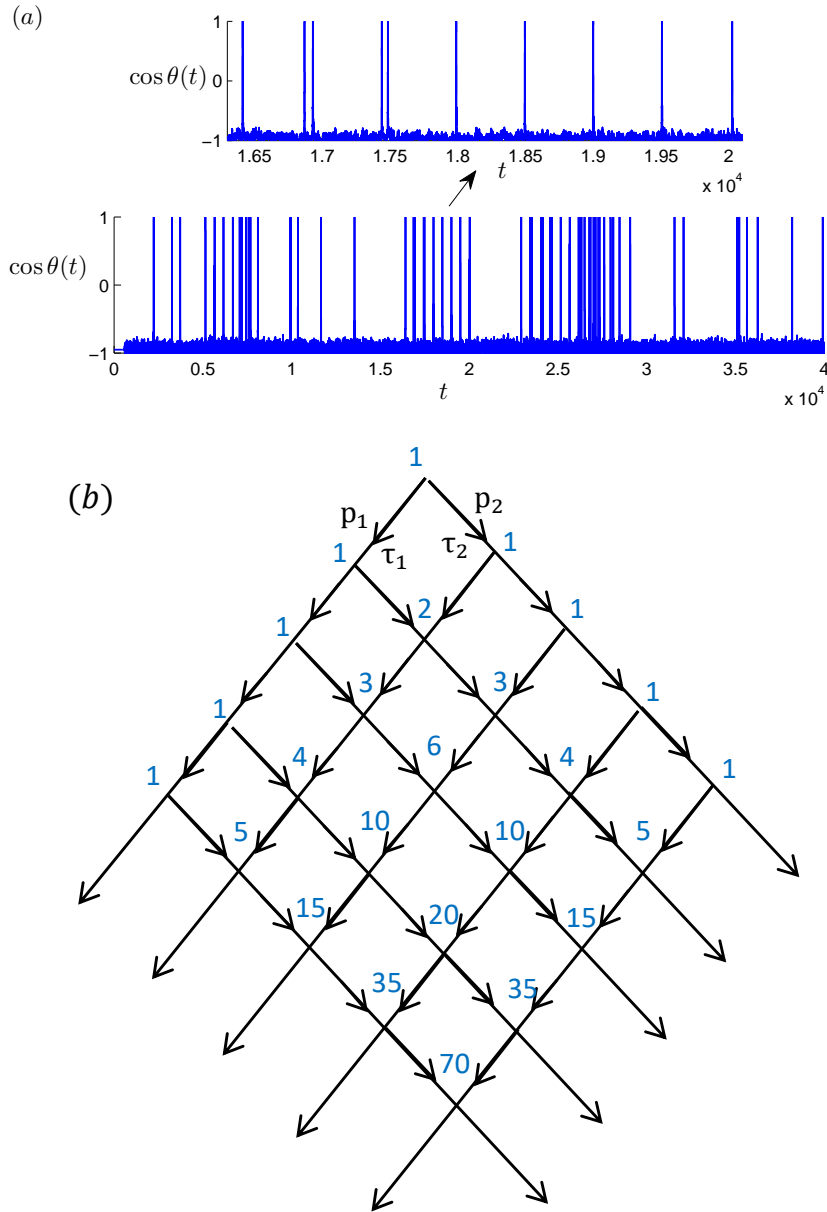
FIGURE 4.2: (a) Spike train of a neuron with two feedback, with values of parameters chosen as $a = 0.95, D = 0.005, \epsilon_1 = 0.12, \hat{\tau}_1 = 500, \epsilon_2 = 0.1$, and $\hat{\tau}_2 = 600$. Zooming in a burst shows many spikes with interval of around 500 and 600. (b): Representation in directed tree lattice, where the cross position of the lattice, i.e. $k\tau_1 + l\tau_2$ with k, l being non-negative integers, represents where there is potentially a delay-induced spike with probability $P(k\tau_1 + l\tau_2)$. The blue numbers near the intersection $k\tau_1 + l\tau_2$ is the number of paths to go to that point, i.e., $\binom{k+l}{k}$ in Eq. (4.4).
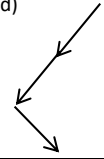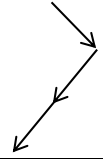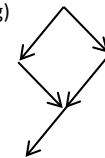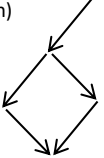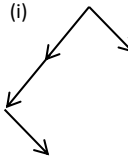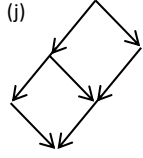
	(a)	(b)	(c)	(d)	(e)
configuration					
probability	$(1-p_2)p_1p_2$	$(1-p_1)p_1p_2$	$p_1p_2p^{(2)}$	$(1-p_2)^2p_1^2p_2$	$(1-p_1)p_1^2p_2$
	(f)	(g)	(h)	(i)	(j)
configuration					
probability	$(1-p_2) \times (1-p_1)p_1^2p_2$	$p_1^2p_2p^{(2)}(1-p_1)$	$(1-p_2)p_1^2p_2p^{(2)}$	$p_1^2p_2^2(1-p^{(2)})$	$p_1^2p_2p^{(2)}p^{(2)}$

FIGURE 4.3: Configurations and the corresponding probability to induce a spike at the cross section $\tau_1 + \tau_2$ (a)-(c) and $2\tau_1 + \tau_2$ (d)-(j) of the lattice shown in Fig. 4.2 (b).

the overlap of two incoming kicks is needed. Generally, this probability should be calculated extra with the same methods as p_1, p_2 are determined. However, when two feedbacks are both weak, we can assume a linear dependence of the probability to induce a follower on the incoming pulse amplitude, which makes an approximation $p^{(2)} \approx p_1 + p_2$ reasonable. It's easy to see that potential followers of a spontaneous spike form a tree as illustrated in Fig. 4.2 (b). If we compare the leader to the parent and compare the followers to the offsprings, the stochastic process here is very similar to the reproduction and extinction problem in theoretical ecology. Both of them can be described by the branching process [Ath06] in probability theory.

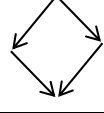On this tree there can be non-branching paths, which correspond just to sequences of followers separated by time intervals $\tau_{1,2}$, which appear with probabilities $p_{1,2}$. However, any branching leads to an overlap, so we have to use $p^{(2)}$ to calculate the probability to observe the corresponding induced spike.

It is instructive to start with the simplest overlap at time $\tau_1 + \tau_2$. The probability to induce a spike at this time can be calculated as

$$
\begin{aligned}
\tilde{P}(\tau_1 + \tau_2) &= (1-p_2)p_1p_2 + (1-p_1)p_1p_2 + p_1p_2p^{(2)} \\
&\approx 2p_1p_2,
\end{aligned}
\tag{4.2}
$$

where the first line in Eq. (4.2) describes contributions of different configuration with corresponding probabilities, as shown in Fig. 4.3 (a)-(c).

Similarly, we can calculate the probability to induce a spike at the cross section $2\tau_1 + \tau_2$ as

$$
\begin{aligned}
\tilde{P}(2\tau_1 + \tau_2) &= (1-p_1)p_1^2p_2 + (1-p_1)(1-p_2)p_1^2p_2 \\
&\quad + (1-p_2)(1-p_2)p_1^2p_2 + p_1^2p_2p^{(2)}p^{(2)} \\
&\quad + (1-p_2)p_1^2p_2p^{(2)} + p_1p_2(1-p^{(2)})p_1p_2 \\
&\quad + p_1p_2p^{(2)}(1-p_1)p_1 \\
&\approx 3p_1^2p_2.
\end{aligned}
\tag{4.3}
$$

The corresponding configurations and their probabilities are shown in Fig. 4.3 (d)-(j).

Now, by induction, it is easy to extend to the general case. One can easily check that the general expression

$$\tilde{P}(k\tau_1 + l\tau_2) = \binom{k+l}{k} p_1^k p_2^l \qquad (4.4)$$

is consistent with calculation of the induced probability $\tilde{P}(k\tau_1 + l\tau_2)$ on the base of the "parent" probabilities $\tilde{P}((k-1)\tau_1 + l\tau_2)$ and $\tilde{P}(k\tau_1 + (l-1)\tau_2)$. By iteration of the relationship

$$\tilde{P}(k\tau_1 + l\tau_2) = \tilde{P}((k-1)\tau_1 + l\tau_2)p_1 + \tilde{P}(k\tau_1 + (l-1)\tau_2)p_2 \qquad (4.5)$$

on the directed tree lattice, it's easy to obtain Eq. (4.4). We stress that expression (4.4) is valid only under assumption $p^{(2)} \approx p_1 + p_2$, in a general case $p^{(2)} \neq p_1 + p_2$ we could not derive a simple expression for these probabilities.

Having determined the probabilities of the followers, we now derive statistical properties of the bursts. To calculate the total firing rate μ, we have to determine the average number of spikes in a burst. The probability to have k spikes with τ_1 separation and l spikes with τ_2 separation in the burst, is the product of $\tilde{P}(k\tau_1 + l\tau_2)$ and probability $1 - p_1 - p_2$, which is the probability to generate no spikes further. Thus, the total fitring rate is

$$\mu = \lambda(1 - p_1 - p_2) \sum_{k,l} \tilde{P}(k\tau_1 + l\tau_2)(k+l)$$

$$= \frac{\lambda}{1 - p_1 - p_2} \ . \qquad (4.6)$$

We check this relation numerically in Fig. 4.4. Throughout the paper, the values of parameters for a and D are fixed as $a = 0.95$, $D = 0.005$. This yields the spontaneous spike rate $\lambda = 6.64 \times 10^{-4}$, as calculated from Eq. (1.4). The probabilities to induce a spike can be calculated by virtue of solving a forced Fokker-Planck equation numerically like described in Chap. 2. For the delay coupling amplitudes $\epsilon = 0.1$ and $\epsilon = 0.12$, this gives values $p = 0.25$ and $p = 0.39$, respectively. Furthermore, in this case, the empirical value of the response time τ_r is approximately $\tau_r \approx 7$. In Fig. 4.4, we set the value of ϵ_1 fixed, i.e., $\epsilon_1 = 0.12$ and thus $p_1 = 0.39$, and vary the strength of the second feedback ϵ_2. As shown if Fig. 4.4, the analytic result described by Eq. (4.6) predicts well the spike rate when ϵ_2 is small and moderate; deviations appear for large values of ϵ_2.

Our next goal is to calculate correlations and spectra of stochastic bursting in this system. The autocorrelation function $C(s)$ can be represented in terms of the joint probability to have a spike in the time interval $(t, t + \Delta t)$ and a spike in the time interval $(t + s, t + s + \Delta t)$:

$$C(s) = \frac{1}{T} \int_0^T dt \lim_{\Delta t \to 0} \frac{P(t, t + \Delta t; t + s, t + s + \Delta t)}{\Delta t^2} \qquad (4.7)$$
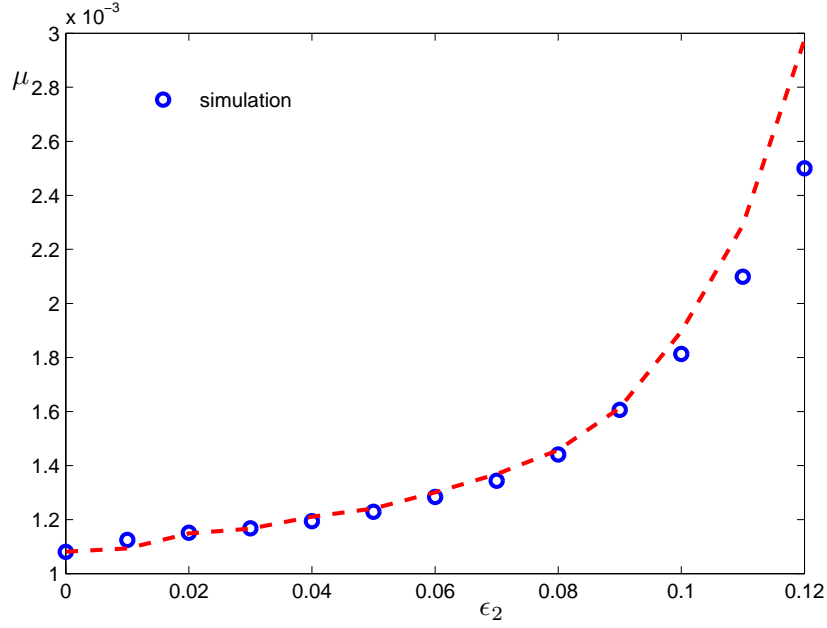
FIGURE 4.4: Spike rate of the single excitable unit with two delayed feedback, where ϵ_1 is set to be 0.12 and ϵ_2 is varied. The blue circles represent the result by direct simulation of Eq. (4.1) and the red dashed line represents the analytical result described by Eq. (4.6). Here τ_1 and τ_2 are chosen as 500 and 600 respectively.

Due to our representation of the burst as a point process,

$$C(s) = \mu \sum_{k,l} \tilde{P}(k\tau_1 + l\tau_2)\delta(s \pm (k\tau_1 + l\tau_2)) =$$

$$\mu \sum_{k,l} \binom{k+l}{k} p_1^k p_2^l \delta(s \pm (k\tau_1 + l\tau_2))$$

The Fourier transform of the correlation function gives the power spectrum:

$$
\begin{aligned}
S(\omega) &= \int_{-\infty}^{\infty} ds\, C(s) e^{-i\omega s} = \\
&= \mu \sum_{k,l; k+l>0} \binom{k+l}{k} p_1^k p_2^l e^{ik\omega\tau_1 + il\omega\tau_2} + \text{c.s.} + \mu \\
&= \mu \sum_{m=0}^{\infty} (p_1 e^{i\omega\tau_1} + p_2 e^{i\omega\tau_2})^m + \text{c.s.} - \mu = \\
&= 2\text{Re}\left(\frac{\mu}{1 - p_1 e^{i\omega\tau_1} - p_2 e^{i\omega\tau_2}}\right) - \mu
\end{aligned}
$$

(4.8)

We compare this theoretical prediction with the results of numerical simulation in Fig. 4.5(a).

Using the same method, a noisy excitable unit with m delays described by the following Langevin equation

$$
\begin{aligned}
\dot{\theta} = a + \cos\theta + \epsilon_1(a + \cos\theta(t - \hat{\tau}_1)) + \cdots \\
+ \epsilon_m(a + \cos\theta(t - \hat{\tau}_m)) + \xi(t),
\end{aligned}
$$

(4.9)
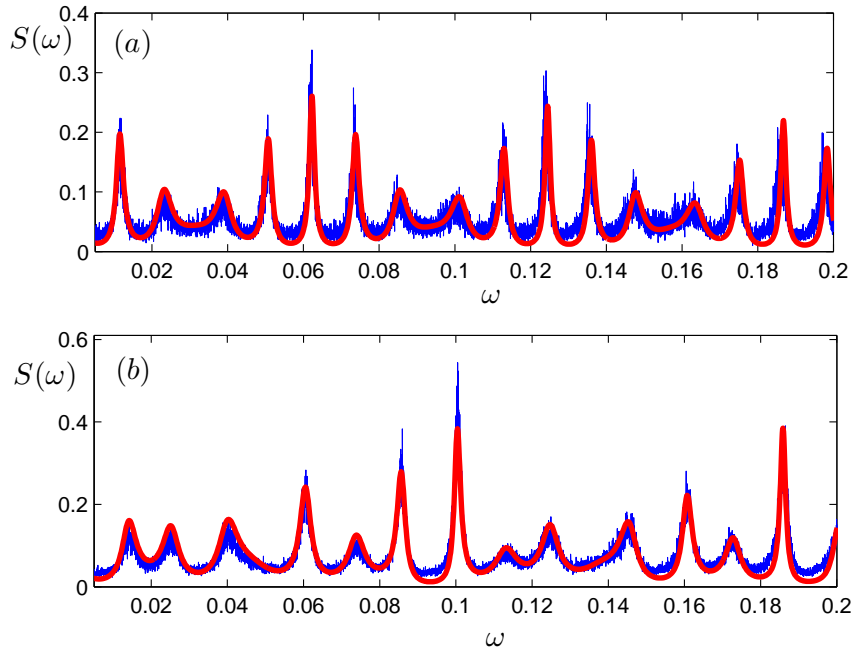
FIGURE 4.5: Power spectral density of a noisy excitable unit with two delay feedback (a) and three delay feedback. For the direct simulation of Eq. (4.1), with the results shown in blue lines, parameters are chosen as $\epsilon_1 = 0.12, \hat{\tau}_1 = 500, \epsilon_2 = 0.1, \hat{\tau}_2 = 600$ in two-delay case and $\epsilon_1 = \epsilon_2 = \epsilon_3 = 0.1, \hat{\tau}_1 = 300, \hat{\tau}_2 = 430, \hat{\tau}_3 = 500$. for Eq. (4.9) in three-delay case. The red lines are the analytic results described by Eq. (4.8) for two-delay case and Eq. (4.9) for three-delay case.

can be studied. Here, the total spike rate can be expressed as $\mu = \lambda/(1 - \sum_{l=1}^{m} p_l)$, where p_l is the probability to induce a spike by the delay feedback with strength ϵ_l and time delay $\hat{\tau}_l$. The power spectral density of the corresponding spike train is described by the following formula:

$$S^{(m)}(\omega) = 2\mathrm{Re}\left(\frac{\mu}{1 - \sum_{l=1}^{m} p_l e^{i\omega\tau_l}}\right) - \mu, \tag{4.10}$$

where $\tau_l = \hat{\tau}_l + \tau_r$. Since the condition of time- scale separation becomes harder to fulfill for large m (one needs the time intervals between pulses to be large), practically only the case $m = 3$ is tested in Fig. 4.5(b).

As shown in Fig. 4.5 (a) and (b), the analytic results described by Eq. (4.8) for two delayed feedback and Eq. (4.10) for three delayed feedback agree well with the direct simulation of the Langevin Eq. (4.1) and (4.9) respectively.

4.2   Delay-coupling in a chain of three units

Here we use the approach above to study a network of three delay-coupled noisy excitable units. The scheme of coupling is presented in Fig. 4.6, i.e., it is a star-type network with a central unit 2 (a hub) coupled to peripheral units 1,3. The Langevin
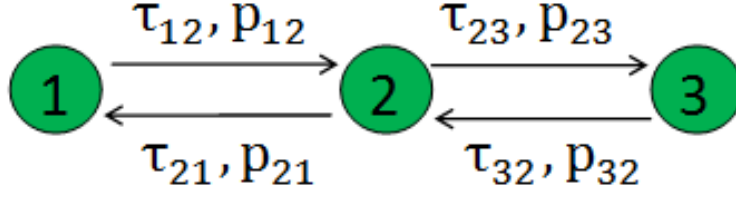
FIGURE 4.6: schematic description of three delay-coupled noisy excitable units in a chain, where p_{ij} is the probability to induce a spike due to delay feedback with strength ϵ_{ij} and time delay τ_{ij}.

equations, describing this network, read

$$
\begin{aligned}
\dot{\theta}_1 &= a + \cos\theta_1 + \epsilon_{21}(a + \cos\theta_2(t - \hat{\tau}_{21})) + \xi_1(t), \\
\dot{\theta}_2 &= a + \cos\theta_2 + \epsilon_{12}(a + \cos\theta_1(t - \hat{\tau}_{12})) \\
&\quad + \epsilon_{32}(a + \cos\theta_3(t - \hat{\tau}_{32})) + \xi_2(t), \\
\dot{\theta}_3 &= a + \cos\theta_3 + \epsilon_{23}(a + \cos\theta_2(t - \hat{\tau}_{23})) + \xi_3(t).
\end{aligned}
\tag{4.11}
$$

Here $\epsilon_{ij}(i, j = 1, 2, 3)$ is the delay feedback strength from unit i to unit j with delay time $\hat{\tau}_{ij}$, and $\xi_i(t)(i = 1, 2, 3)$ is the Gaussian white noise in unit i with $\langle\xi_i(t)\rangle = 0$, $\langle\xi_i(t)\xi_j(t')\rangle = 2D\delta_{ij}\delta(t - t')$. In the absence of delay feedback, i.e., $\epsilon_{ij} = 0$, the three units fire spontaneously with constant rates $\lambda_i(i = 1, 2, 3)$, described by Eq. (1.4). For simplicity, the noise intensities here in the three units are chosen to be the same. When the delayed feedback is included, i.e., $\epsilon_{ij} \neq 0$, each spontaneous spike in unit 1 will induce another spike in unit 2 with probability p_{12} after time delay τ_{12}, and the induced spike in unit 2 will generate spikes in unit 1 with probability p_{21} after time delay τ_{21}, and in unit 3 with probability p_{23} after time delay τ_{23}. Here τ_{ij} includes the response time, i.e., $\tau_{ij} = \hat{\tau}_{ij} + \tau_r$.

Thus, each spontaneous spike, which plays the role of leader, is followed by random number of induced spikes (followers) across the network. Noteworthy, the above description is based on time-scale separation as described in Sec. 4.1. The relation to the model of one excitable unit with two feedbacks described in Section 4.1 above is evident when one considers effective feedbacks from unit 2 to itself: there are two effective delay feedback channels, one with the probability $p_{21}p_{12}$ and time delay $\tau_{21} + \tau_{12}$ to induce a spike back into unit 2 itself through unit 1, and the other one through unit 3 with probability $p_{23}p_{32}$ and time delay $\tau_{23} + \tau_{32}$. Therefore, the total spike rate of unit 2 can be represented as

$$
\mu_2 = \frac{\lambda_2 + p_{12}\lambda_1 + p_{32}\lambda_3}{1 - (p_{21}p_{12} + p_{23}p_{32})},
\tag{4.12}
$$

Here the numerator $\lambda_2 + p_{12}\lambda_1 + p_{32}\lambda_3$ represents the total rate of first spikes in a burst in unit 2. These are spikes initiated spontaneously in unit 2 (rate λ_2), and the first followers in unit 2 of spikes spontaneously created in units 1 and 3 (rates $p_{12}\lambda_1$ and $p_{32}\lambda_3$, respectively). The denominator in (4.12) comes from the same summation as in Eq. (4.6).

Similarly, we can express the total spike rate of neuron 1 μ_1 as

$$
\begin{aligned}
\mu_1 &= \lambda_1 + \mu_2 p_{21} \\
&= \lambda_1 + \frac{\lambda_2 + p_{12}\lambda_1 + p_{32}\lambda_3}{1 - (p_{21}p_{12} + p_{23}p_{32})}p_{21},
\end{aligned}
\tag{4.13}
$$
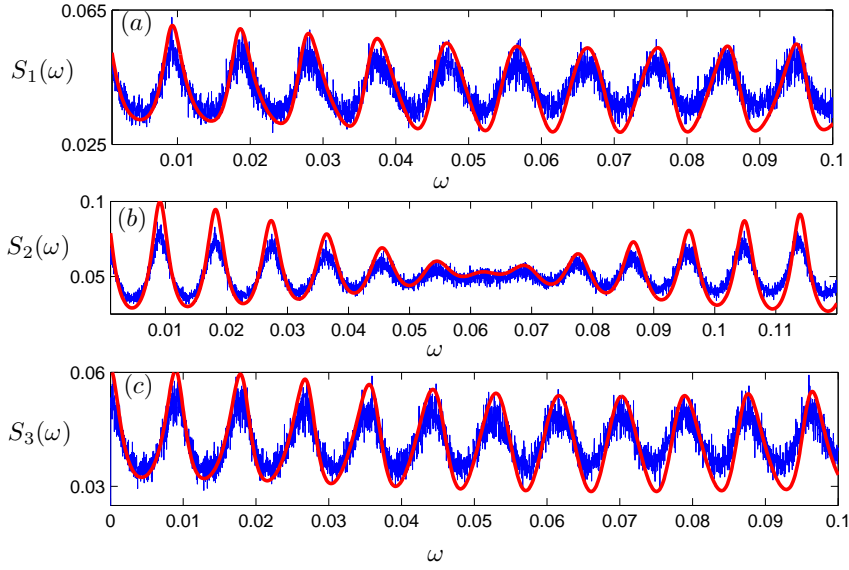
FIGURE 4.7: Power spectral density of neuron 1 (a), 2 (b) and 3 (c) in a chain of three delay-coupled noisy excitable neurons. Values of parameters are $\epsilon_1 = \epsilon_2 = \epsilon_3 = 0.12$, $\tau_{12} = 350, \tau_{21} = 300, \tau_{23} = 300, \tau_{32} = 400, a = 0.95$ and $D = 0.005$. Noteworthy, all the power density are multiplied by the power spectral density of the shape function S_H, similar to Ref. [ZP18; ZP19].

since the leading spikes in unit 1 is either from the spontaneous ones created in unit 1, or induced from spontaneous spikes of unit 2. For the unit 3, the total rate is

$$
\begin{aligned}
\mu_3 &= \lambda_3 + \mu_2 p_{23} \\
&= \lambda_3 + \frac{\lambda_2 + p_{12}\lambda_1 + p_{32}\lambda_3}{1 - (p_{21}p_{12} + p_{23}p_{32})} p_{23}.
\end{aligned}
\tag{4.14}
$$

Using the same method as described in Sec. 4.1, we can write the power spectral density of a spike train in unit 2 as

$$
S_2(\omega) = 2\text{Re}\left(\frac{\mu_2}{1 - \bar{p}_1 e^{i\omega\bar{\tau}_1} - \bar{p}_2 e^{i\omega\bar{\tau}_2}}\right) - \mu_2,
\tag{4.15}
$$

where $\bar{p}_1 = p_{21}p_{12}$, $\bar{\tau}_1 = \tau_{21} + \tau_{12}$, $\bar{p}_2 = p_{23}p_{32}$ and $\bar{\tau}_2 = \tau_{23} + \tau_{32}$. Similarly, taking into account all the delayed feedback loops connecting neuron 1, we obtain the power spectral density of neuron 1 as follows,

$$
\begin{aligned}
S_1(\omega) &= 2\text{Re}\left(\frac{\mu_1}{1 - (\bar{p}_1 e^{i\omega\bar{\tau}_1} + \bar{p}_1\bar{p}_2 e^{i\omega T}\sum_{n>0}(\bar{p}_2 e^{i\omega\bar{\tau}_2})^n)}\right) - \mu_1 \\
&= 2\mu_1\text{Re}\left(\frac{1 - \bar{p}_2 e^{i\omega\bar{\tau}_2}}{1 - \bar{p}_1 e^{i\omega\bar{\tau}_1} - \bar{p}_2 e^{i\omega\bar{\tau}_2}}\right) - \mu_1.
\end{aligned}
\tag{4.16}
$$

Here $T = \bar{\tau}_1 + \bar{\tau}_2$ in the first equality and $\bar{p}_1\bar{p}_2 e^{i\omega T}\sum_{n>0}(\bar{p}_2 e^{i\omega\bar{\tau}_2})^n)$ is due to the summation of all the feedback loops starting from neuron 1, connecting neuron 2 and 3 and then going back to neuron 1. By the same method, the power spectral density of

neuron 3 is

$$S_3(\omega) = 2\mu_3 \mathrm{Re}\left(\frac{1 - \bar{p}_1 e^{i\omega\bar{\tau}_1}}{1 - \bar{p}_1 e^{i\omega\bar{\tau}_1} - \bar{p}_2 e^{i\omega\bar{\tau}_2}}\right) - \mu_3. \tag{4.17}$$

We compare these expressions with the results of direct numerical simulations of model (4.11) in Fig. 4.7 (a)-(c).

For networks of coupled units, it is instructive to calculate cross-correlations and cross-spectra. The cross-correlation between neuron 1 and 2 can be described in terms of the joint probability $P_{12}(t, t + \Delta t; t + s, t + s + \Delta t)$ that there is a spike in the time interval $(t + \Delta t)$ in neuron 1 and a spike in the time interval $(t + s, t + s + \Delta t)$ in neuron 2, i.e.,

$$
\begin{aligned}
C_{12}(s) &= \lim_{\Delta t \to 0} \frac{P_{12}(t, t + \Delta t; t + s, t + s + \Delta t)}{\Delta t^2} \\
&= \mu_1 p_{12} \sum_{k,l} \tilde{P}(k\bar{\tau}_1 + l\bar{\tau}_2)\delta(s - (k\bar{\tau}_1 + l\bar{\tau}_2 + \tau_{12})) \\
&\quad + \mu_2 p_{21} \sum_{k,l} \tilde{P}(k\bar{\tau}_1 + l\bar{\tau}_2)\delta(s + (k\bar{\tau}_1 + l\bar{\tau}_2 + \tau_{21})).
\end{aligned}
\tag{4.18}
$$

Here $\tilde{P}(k\bar{\tau}_1 + l\bar{\tau}_2)$ is the probability to induce a spike at time $k\bar{\tau}_1 + l\bar{\tau}_2$ after a spike and according to Eq. (4.4) it is

$$\tilde{P}(k\bar{\tau}_1 + l\bar{\tau}_2) = \binom{k + l}{k}\bar{p}_1^k\bar{p}_2^l. \tag{4.19}$$

Substituting Eq. (4.19) into Eq. (4.18) we obtain the cross-correlation function

$$
\begin{aligned}
C_{12}(s) &= \mu_1 p_{12} \sum_{k,l} \binom{k + l}{k}\bar{p}_1^k\bar{p}_2^l\delta(s - (k\bar{\tau}_1 + l\bar{\tau}_2 + \tau_{12})) \\
&\quad + \mu_2 p_{21} \sum_{k,l} \binom{k + l}{k}\bar{p}_1^k\bar{p}_2^l\delta(s + (k\bar{\tau}_1 + l\bar{\tau}_2 + \tau_{21})).
\end{aligned}
\tag{4.20}
$$

So the cross-spectral density between neuron 1 and 2 is just Fourier-transfrom the cross-correlation function, i.e.,

$$
\begin{aligned}
S_{12}(\omega) &= \int_{-\infty}^{\infty} C_{ij}(s)e^{-i\omega s}ds \\
&= \frac{\mu_1 p_{12} e^{-i\omega\tau_{12}}}{1 - \bar{p}_1 e^{-i\omega\bar{\tau}_1} - \bar{p}_2 e^{-i\omega\bar{\tau}_2}} + \frac{\mu_2 p_{21} e^{i\omega\tau_{21}}}{1 - \bar{p}_1 e^{i\omega\bar{\tau}_1} - \bar{p}_2 e^{i\omega\bar{\tau}_2}}.
\end{aligned}
\tag{4.21}
$$

As shown in Fig. 4.8 (a) and (b) for the real and imaginary parts of the cross-spectral density, the analytic results agree well with direct simulation of Eq. (4.10).
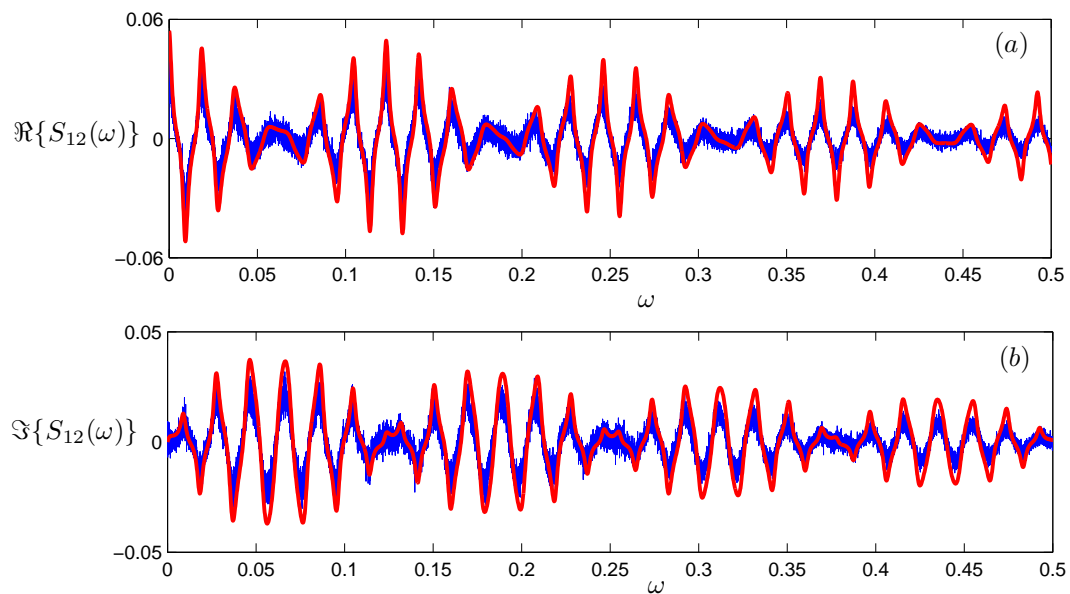
FIGURE 4.8: Real part (a) and imaginary part (b) of the cross-spectral density between neuron 1 and 2 in a chain of three delay-coupled noisy excitable neurons. Values of parameters are chosen the same as in Fig. 4.7. Noteworthy, the cross-spectral density are also multiplied by the power spectral density of the shape function S_H as in Fig. 4.7.

4.3   Summary

In summary, we investigated stochastic bursting in a single noisy excitable unit with multiple feedback and a star-type network of three delay-coupled units. Our analysis is based on two approximations. One is that of time-scale separation, valid for weak noise and large delay times. It allows us to model the process as a point one, so that only time instants of spikes are relevant for correlations and spectra. Another approximation is based on the assumption that the induced probabilities are small, and the probability for two overlapping inputs to induce a spike can be represented as a sum of the corresponding one-input probabilities. This latter assumption appeared to be extremely helpful, as it allowed us to express the probabilities of induced spikes in a simple closed form. As a result, also the spectra of the point stochastic bursting process have been analytically represented in a closed form. These power spectral and cross-spectral densities agree well with direct simulation of the original Langevin equation (4.8), (4.9) and (4.11). Our approach works well for a small number of interacting units and a small number of feedback loops, because here the time-scale separation is well justified. In a network with a large number of units and many connections, the spikes become denser, and the point process approximation may be violated. Similarly, for strong feedbacks, the probability to induce a spike by overlapping inputs will be violated as well. From the viewpoint of applications, we would like to mention that correlation functions of the spike trains is an important indicator in computational neuroscience [DLR+07; Doi+16; JR16; LCL05; NL03; Per+11]. Our analytic results could be potentially compared with observed correlations and spectra, shedding light on the origin of observed correlations.

Chapter 5

Three-dimensional Kuramoto Model

In Chap. 1.2, we introduce the basic property of the classical Kuramoto model, where the evolution of phase is in one-dimensional space, or alternatively, the dynamics of coupled unit vectors evolve in two-dimensional space as described by Eq. (1.25). However, in many real physical systems in nature, collective motions occur in three dimensions, e.g., fish schools [Par+80], flocks of birds [MD78] and bacterial colonies [War+19]. It's of great importance and interest to see how Kuramoto model can describe these complex collective motion in three-dimensional space. Recently, several versions of the high-dimensional Kuramoto model have been proposed, i.e., a swarm model to describe the synchronous behavior on a sphere [OS06; Tan14], non-Abelian Kuramoto model [Loh09], and generalized D-dimensional Kuramoto model [CGO19a; CGO19b]. Tanaka extends the Watanabe–Strogatz theory [WS94] to the high-dimensional case by the projection transformation (the Möbius transformation) and also extends the Ott–Antonsen theory [OA08] to capture the low-dimensional behavior in the continuum limit system. Lohe describes non-Abelian generalizations of the Kuramoto model in terms of a chirally covariant model [Loh09], for any classical compact Lie group. Lohe also generalizes the Watanabe–Strogatz theory to a higher-dimensional vector transform which deals with vector oscillator models of synchronization [Loh18]. The relationship between these three versions of the high-dimensional Kuramoto model is discussed in Ref. [LMS19], where the natural hyperbolic geometry on a unit ball in the high-dimensional space is explained as the reason of the three intimately related generalizations.

Similar to the vector form of the two-dimensional Kuramoto model described by
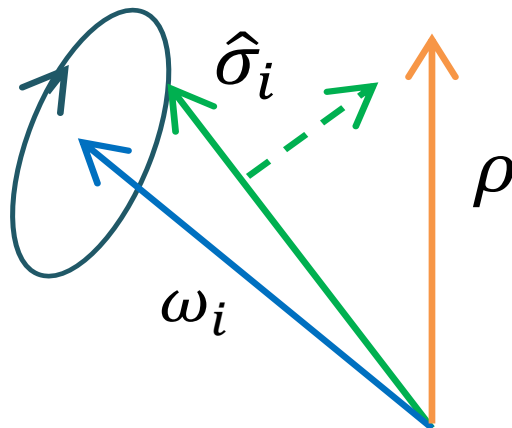

FIGURE 5.1: Schematic description of 3 dimensional Kuramoto model.

Eq. (1.25), the three-dimensional version as reported in Ref. [CGO19b] is described by the following equation:

$$\frac{d\hat{\boldsymbol{\sigma}}_i}{dt} = \frac{K}{N}\sum_{j}^{N}[\hat{\boldsymbol{\sigma}}_j - (\hat{\boldsymbol{\sigma}}_j \cdot \hat{\boldsymbol{\sigma}}_i)\hat{\boldsymbol{\sigma}}_i] + \boldsymbol{\omega}_i \times \hat{\boldsymbol{\sigma}}_i, \tag{5.1}$$

where $\hat{\boldsymbol{\sigma}}_i$ is the unit vector of agent i in an ensemble of size N, K is the coupling strength between every two agents. $\boldsymbol{\omega}_i = \omega_i \hat{\boldsymbol{\omega}}_i$ is the natural frequency vector of agent i and is chosen from a distribution $g_d(\hat{\boldsymbol{\omega}})$ for the direction vector $\hat{\boldsymbol{\omega}}$ and another distribution $g(\omega)$ for the amplitude ω. Defining the order parameter as

$$\boldsymbol{\rho} = \frac{1}{N}\sum_{j}^{N}\hat{\boldsymbol{\sigma}}_j, \tag{5.2}$$

we can rewrite Eq. (5.1) in terms of each agent coupled to the mean field:

$$\frac{d\hat{\boldsymbol{\sigma}_i}}{dt} = K(\boldsymbol{\rho} - (\boldsymbol{\rho} \cdot \hat{\boldsymbol{\sigma}}_i)\hat{\boldsymbol{\sigma}}_i) + \boldsymbol{\omega}_i \times \hat{\boldsymbol{\sigma}}_i. \tag{5.3}$$

Here $\boldsymbol{\rho}$ can either be a mean field or an external force in general, as schematically illustrated in Fig. 5.1.

As reported in Ref. [CGO19b], the cross product term $\boldsymbol{\omega}_i \times \hat{\boldsymbol{\sigma}}_i$ is represented alternatively by the matrix multiplication of an antisymmetric matrix W_i and the unit vector $\hat{\boldsymbol{\sigma}}_i$, in order to generalize to any dimension. In the odd-dimensional Kuramoto model, the transition to synchrony always occurs at the coupling strength $K \to 0^+$, e.g., a very small coupling strength will lead to synchrony with the order parameter $\rho \geq 0.5$ in three dimensions, while the even-dimensional version displays the second-order phase transition (continuous). In this thesis, we focus on the three-dimensional case that has real physical meaning in nature, as we will show below. Strikingly and in stark contrast to the classical (2d) Kuramoto model, despite heterogeneous frequency amplitudes and directions, the global coupling leads to a finite translational collective motion for arbitrary small coupling strength $K \to 0^+$, when $\hat{\boldsymbol{\sigma}}_i \cdot \hat{\boldsymbol{\omega}}_i = \pm 1$ in the direction of the mean field ($\hat{\boldsymbol{\sigma}}_i \cdot \boldsymbol{\rho} > 0$). Here, frequency heterogeneity is not sufficient to prevent alignment. Below we will firstly introduce the fixed points in the three-dimensional Kuramoto model and the self-consistent description of the mean field and explore the stochastic dynamics with noise.

5.1   Self-consistent solution in the deterministic case

First, we study the fixed points of the unit vector, which obeys the following equation:

$$K[\boldsymbol{\rho} - (\boldsymbol{\rho} \cdot \hat{\boldsymbol{\sigma}}_i)\hat{\boldsymbol{\sigma}}_i] + \boldsymbol{\omega} \times \hat{\boldsymbol{\sigma}}_i = 0. \tag{5.4}$$

Defining $\beta = \frac{\omega_i}{K\rho}$ with ρ being the amplitude of the order parameter, after some calculations (see Appendix A) we obtain the fixed points:

$$\hat{\boldsymbol{\sigma}}_i^f = \frac{1}{\beta^2 + b^2}(\beta\hat{\boldsymbol{\omega}}_i \times \hat{\boldsymbol{\rho}} + b\hat{\boldsymbol{\rho}} + a\beta^2\hat{\boldsymbol{\omega}}_i). \tag{5.5}$$

Here $b = \hat{\boldsymbol{\rho}} \cdot \hat{\boldsymbol{\sigma}}_i^f$ and $a = \hat{\boldsymbol{\omega}}_i \cdot \hat{\boldsymbol{\sigma}}_i^f$. We see that the r.h.s of Eq. (5.5) contains the fixed point self-consistently. By multiplying the both sides of Eq. (5.5), we obtain the fixed point solution with respect to the mean field $\boldsymbol{\rho}$, the frequency unit vector $\hat{\boldsymbol{\omega}}$ and β in
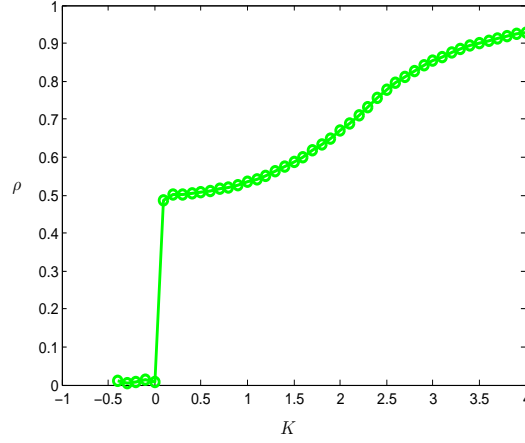
FIGURE 5.2: The amplitude of order parameter vs the coupling strength. The transition to synchrony occurs when the coupling strength $K \to 0^+$ and the corresponding order parameter is always 0.5 regardless of the frequency distribution.

terms of a scalar equation:

$$b = \hat{\boldsymbol{\rho}} \cdot \hat{\boldsymbol{\sigma}}_i^f = \pm \sqrt{\frac{1 - \beta^2 + \sqrt{(1-\beta^2)^2 + 4\beta^2 (\hat{\boldsymbol{\rho}} \cdot \hat{\boldsymbol{\omega}}_i)^2}}{2}}. \tag{5.6}$$

Here the plus and minus signs correspond to the stable and unstable fixed points respectively. Therefore, the amplitude of the order parameter having integrals with respect to both the direction $\hat{\boldsymbol{\omega}}$ and the amplitude ω of the frequency vector $\boldsymbol{\omega}$ is

$$
\begin{aligned}
\rho &= \int \int \hat{\boldsymbol{\rho}} \cdot \hat{\boldsymbol{\sigma}}^f g_d(\hat{\boldsymbol{\omega}}) g(\omega) d\hat{\boldsymbol{\omega}} d\omega \\
&= \int \int \cos \Theta(\beta, \hat{\boldsymbol{\omega}}) g_d(\hat{\boldsymbol{\omega}}) g(\omega) d\hat{\boldsymbol{\omega}} d\omega \\
&= \int \int \cos \Theta(\beta, \hat{\boldsymbol{\omega}}) g_d(\hat{\boldsymbol{\omega}}) g(K\beta\rho) K\rho d\hat{\boldsymbol{\omega}} d\beta.
\end{aligned}
\tag{5.7}
$$

Here Θ is the angle between the stable fixed points $\hat{\boldsymbol{\sigma}}^f$ and the direction of the order parameter (mean field) $\boldsymbol{\rho}$. Divided by ρ for both sides, an integral equation for general frequency distribution can be obtained as follows [CGO19b]:

$$1 = \int \int \cos \Theta(\beta, \hat{\boldsymbol{\omega}}) g_d(\hat{\boldsymbol{\omega}}) g(K\beta\rho) K d\hat{\boldsymbol{\omega}} d\beta. \tag{5.8}$$

We consider an isotropic distribution for the frequency direction ($g_d(\hat{\boldsymbol{\omega}}) = \frac{1}{4\pi}$) and a Maxwell-Boltzmann distribution for the amplitude, i.e., $g(\omega) = 4\pi (\frac{1}{2\pi\delta})^{3/2} \omega^2 e^{-\frac{\omega^2}{2\delta}}$, as in [CGO19b]. Therefore the integral equation (5.8) becomes

$$1 = \frac{K^3 \rho^2}{2\sqrt{2\pi}\delta^3} \int_{-1}^{1} d\nu \int_{-\infty}^{\infty} d\beta \sqrt{\frac{1 - \beta^2 + \sqrt{(1-\beta^2)^2 + 4\beta^2(\nu)^2}}{2}} \beta^2 e^{-(K\beta\rho)^2/(2\delta^2)} \tag{5.9}$$

where $\nu = \hat{\boldsymbol{\rho}} \cdot \hat{\boldsymbol{\omega}}$. Noteworthy, since the distribution of the frequency unit vector $\hat{\boldsymbol{\omega}}$ is isotropic here, the location of the stable fixed points σ_i is of rotational symmetry about the mean field $\boldsymbol{\rho}$. Substituting $K \to 0^+$, it's not difficult to prove that $\rho = 0.5$ regardless of the frequency distribution $g(\omega)$, as shown in Fig. 5.2. This is because

the fixed points of the agents $\boldsymbol{\sigma}$ are uniformly distributed on the upper hemisphere with $\boldsymbol{\rho} \cdot \hat{\boldsymbol{\sigma}} > 0$.

In general, the mean field $\boldsymbol{\rho}$ can appear in terms of various kinds of forms, depending on the parameter regime and bifurcation. For instance, $\boldsymbol{\rho}$ can be a constant vector with both amplitude and direction fixed, or either of them fixed, i.e., an oscillatory mean field with the amplitude varying periodically but the direction fixed, or with the amplitude fixed but direction rotating periodically. The latter case corresponds to the so-called *collective oscillation*, which is widely studied both in nonlinear dynamics and in experimental biophysics. We refer the readers to a recent work about the collective oscillation in an *E. Coli* colony [Che+17], where the local coupling between the cells makes the system self-organized into the weak synchronization state. For the three-dimensional Kuramoto model, we will also discuss the collective oscillation in Sec. 5.2.2 and Sec. 5.3.2.

5.2 Three-dimensional Kuramoto model with noise

As a ubiquitous influence in nature, noise plays an important role in the collective dynamics of the chemical, physical and biological systems, reminiscent of another prominent model to describe collective motion, i.e., the Vicsek model [Vic+95]. Therefore, understanding the three-dimensional Kuramoto model with noise is of considerable interest.

The three-dimensional noisy Kuramoto model obeys the following equation:

$$\frac{d\hat{\boldsymbol{\sigma}}_i}{dt} = \frac{K}{N} \sum_j^N [\hat{\boldsymbol{\sigma}}_j - (\hat{\boldsymbol{\sigma}}_j \cdot \hat{\boldsymbol{\sigma}}_i)\hat{\boldsymbol{\sigma}}_i] + (\boldsymbol{\omega}_i + \boldsymbol{\xi}_i(t)) \times \hat{\boldsymbol{\sigma}}_i, \tag{5.10}$$

Here $\boldsymbol{\xi_i}(t)$ is the Gaussian white noise individually for agent i, with the components in $\boldsymbol{x}, \boldsymbol{y}, \boldsymbol{z}$ directions being independent, i.e.,

$$
\begin{aligned}
\langle \xi_i^k \rangle &= 0 \quad (k = x, y, z), \\
\langle \xi_i^k(t)\xi_i^l(t') \rangle &= 2D\delta_{kl}\delta(t - t') \quad (k, l = x, y, z),
\end{aligned}
\tag{5.11}
$$

with D being the noise intensity. The other variables are the same as in the deterministic model (5.1). Also, defining the order parameter as

$$\boldsymbol{\rho} = \frac{1}{N} \sum_j^N \hat{\boldsymbol{\sigma}}_j, \tag{5.12}$$

we can rewrite Eq. (5.10) as

$$\frac{d\hat{\boldsymbol{\sigma}}_i}{dt} = K(\boldsymbol{\rho} - (\boldsymbol{\rho} \cdot \hat{\boldsymbol{\sigma}}_i)\hat{\boldsymbol{\sigma}}_i) + (\boldsymbol{\omega}_i + \boldsymbol{\xi}_i(t)) \times \hat{\boldsymbol{\sigma}}_i, \tag{5.13}$$

Positive coupling strength K always promotes the alignment of each agent $\hat{\boldsymbol{\sigma}}_i$, while individual noise is believed to prevent the agents from alignment (synchronization), as described in the two-dimensional noisy Kuramoto model [Sak88; SM91]. Therefore, it is expected that there exists a critical coupling strength K_c, above which the incoherent state ($\rho = 0$) will lose stability and hence the system will enter into the partial synchronization state.
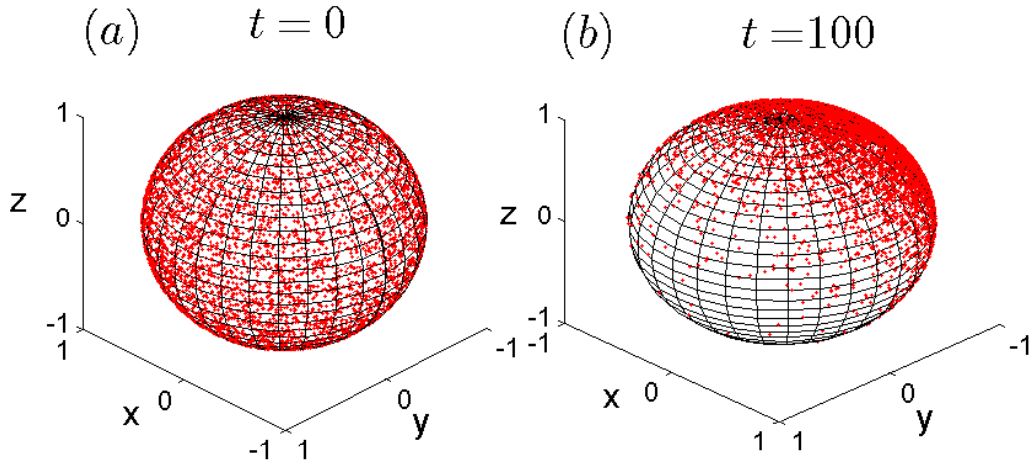
FIGURE 5.3: Visualization of 10000 coupled agents (red dots) in a noisy environment, as described by Eq. (5.10). Each agent has no natural frequency, the noise intensity is $D = 0.5$ and the coupling strength is $K = 2.5$. (a) is the initial state with agents distributed isotropically on the sphere, and (b) is when the observation time is $t = 100$, displaying alignment or synchronization.

The Fokker-Planck equation to describe the probability density $f(\boldsymbol{\sigma}, \boldsymbol{\omega}, t)$ of the agents is

$$\frac{\partial f}{\partial t} + \boldsymbol{\nabla}_s \cdot (f(\boldsymbol{\sigma}, \boldsymbol{\omega}, t)\boldsymbol{V}) = D\boldsymbol{\nabla}_s^2 f(\boldsymbol{\sigma}, \boldsymbol{\omega}, t), \tag{5.14}$$

where velocity $\boldsymbol{V}$ is given by

$$\boldsymbol{V} = K(\boldsymbol{\rho} - (\boldsymbol{\rho} \cdot \hat{\boldsymbol{\sigma}})\hat{\boldsymbol{\sigma}}) + \boldsymbol{\omega} \times \hat{\boldsymbol{\sigma}}. \tag{5.15}$$

Here $\boldsymbol{\nabla}_s$ is the nabla operator along the surface of the three-dimensional unit sphere.

Below we will discuss two different situations, i.e., the case without natural frequency and the case with a general frequency distribution. In the former case, we will derive the exact analytical solution to the corresponding Fokker-Planck equation, while in the latter case we will analyze the linear stability of the incoherent state ($\rho = 0$). By a general frequency distribution, we mean there is a distribution $g_d(\hat{\boldsymbol{\omega}})$ for the direction and the other distribution $g(\omega)$ for the amplitude.

5.2.1 Noisy Kuramoto Model without Natural Frequency

Firstly we consider the case where there is no natural frequency, i.e., $g(\boldsymbol{\omega}) = \delta(\boldsymbol{\omega})$. By direct simulation of the Langevin Eq. (5.10), we observe that a positive coupling strength above some critical value, will lead to the agents' alignment (synchronization), as shown in Fig. 5.3. Due to that there is no probability current in this case, the stationary solution obeys the following equation:

$$fK(\boldsymbol{\rho} - (\boldsymbol{\rho} \cdot \hat{\boldsymbol{\sigma}})\hat{\boldsymbol{\sigma}}) = D\boldsymbol{\nabla}_s f. \tag{5.16}$$

Without loss of generality, we set $\boldsymbol{\rho} = \rho\hat{\boldsymbol{z}}$ and multiply both sides of Eq. (5.16) by $\hat{\boldsymbol{z}}$. The resulting one-dimensional differential equation for the rotational symmetric

density has the Boltzmann-type solution

$$f(\theta, \phi) = f(\theta) = \frac{K\rho}{4\pi D \sinh\left(\frac{K\rho}{D}\right)} \exp\left(\frac{K\rho}{D}\cos\theta\right). \tag{5.17}$$

The amplitude of the order parameter is

$$
\begin{aligned}
\rho &= \int_0^{2\pi}\int_0^\pi \boldsymbol{\rho}\cdot\hat{\boldsymbol{\sigma}} f(\theta,\phi)\sin\theta d\theta d\phi \\
&= \coth\left(\frac{K\rho}{D}\right) - \frac{D}{K\rho}.
\end{aligned}
\tag{5.18}
$$

Denoting $\epsilon = \frac{K\rho}{D}$ the system state has the parametric form

$$
\begin{aligned}
\rho &= \coth\epsilon - 1/\epsilon, \\
K/D &= \epsilon^2/(\epsilon\coth\epsilon - 1),
\end{aligned}
\tag{5.19}
$$

with $0 < \epsilon < \infty$ between the transition point at $\epsilon \to 0$, where $\rho \to 0$ and the noise free limit $\epsilon \to \infty$, where $\rho \to 1$.

These analytical results show good agreement with direct simulation of Eq. (5.10), as depicted in Fig. 5.5 (a). Expanding Eq. (5.18) to the third order of ρ we obtain

$$\rho \approx \frac{K\rho}{3D} - \frac{K^3\rho^3}{45D^3}, \tag{5.20}$$

leading to the criticality with square-root relationship:

$$\rho \approx \sqrt{\frac{15D^2(K-3D)}{K^3}}. \tag{5.21}$$

We recall that similar criticality of square-root relationship also holds true in the classical (2D) Kuramoto model. A natural question arises that whether there is a general formula about it. Below we will generalize it to the case in any q ($q \geq 2$) dimension.

Generalization to q-dimensional case

Similar to the three-dimensional noisy Kuramoto model without natural frequency discussed above, it's straightforward to extend to the q-dimensional ($q \geq 2$) case, where $\hat{\boldsymbol{\sigma}}$ is a q-dimensional unit vector coupled to the mean field $\boldsymbol{\rho}$. Since the cross product is not well defined in high-dimensional space, we replace the cross product of the noise and the unit vector, i.e., $\boldsymbol{\xi}_i(t) \times \hat{\boldsymbol{\sigma}}_i$, by $A_i\hat{\boldsymbol{\sigma}}_i$ with A_i being an $q \times q$ antisymmetric matrix with noise entries. For instance, the antisymmetric matrix A_i in 3 dimensions ($q = 3$) is

$$A_i = \begin{pmatrix} 0 & -\xi_i^z(t) & \xi_i^y(t) \\ \xi_i^z(t) & 0 & -\xi_i^x(t) \\ -\xi_i^y(t) & \xi_i^x(t) & 0 \end{pmatrix}. \tag{5.22}$$

The noise entries are Gaussian white and independent for each agent, as defined in Eq. (5.11). It's easy to check that $\boldsymbol{\xi}_i(t) \times \hat{\boldsymbol{\sigma}}_i = A_i\hat{\boldsymbol{\sigma}}_i$. The antisymmetric matrix of independent noise entries ensures that the agents diffuse along the surface of the unit

ball B^q in $\mathbb{R}^q$. Therefore, the high-dimensional generalization of the noisy Kuramoto model without natural frequency is described by the following equation:

$$\frac{d\hat{\boldsymbol{\sigma}}_i}{dt} = K(\boldsymbol{\rho} - (\boldsymbol{\rho} \cdot \hat{\boldsymbol{\sigma}}_i)\hat{\boldsymbol{\sigma}}_i) + A_i\hat{\boldsymbol{\sigma}}_i, \tag{5.23}$$

The stationary solution obeys the same equation as Eq. (5.16) but in any q ($q \geq 2$) dimensions. The stationary distribution of the agents is

$$f(\boldsymbol{\rho}, \hat{\boldsymbol{\sigma}}) = C_q(\epsilon)e^{\epsilon\hat{\boldsymbol{\rho}}\cdot\hat{\boldsymbol{\sigma}}}, \tag{5.24}$$

where $\hat{\boldsymbol{\rho}}$ is the unit vector in the direction of the mean field $\boldsymbol{\rho}$, i.e., $\boldsymbol{\rho} = \rho\hat{\boldsymbol{\rho}}$. The ϵ is defined as $\epsilon = \frac{K\rho}{D}$ with D being the noise intensity. The normalization condition $\int f(\boldsymbol{\rho}, \hat{\boldsymbol{\sigma}})d\hat{\boldsymbol{\sigma}} = 1$ leads to the dimension-dependent normalization constant

$$C_q(\epsilon) = \frac{\epsilon^{q/2-1}}{(2\pi)^{q/2}I_{q/2-1}(\epsilon)}. \tag{5.25}$$

Here $I_s(\cdot)$ denotes the modified Bessel function of the first kind and order s, which satisfies

$$I_s(\epsilon) = \frac{(\epsilon/2)^s}{\Gamma(s+\frac{1}{2})\Gamma(\frac{1}{2})} \int_{-1}^{1} e^{\epsilon t}(1-t^2)^{s-\frac{1}{2}}dt, \tag{5.26}$$

with Γ being the Gamma function. Therefore, it follows that

$$\begin{aligned}
\int_S e^{\epsilon\hat{\boldsymbol{\rho}}\cdot\hat{\boldsymbol{\sigma}}}d\hat{\boldsymbol{\sigma}} &= B(\frac{q-1}{2}, \frac{1}{2})^{-1} \int_{-1}^{1} e^{\epsilon t}(1-t^2)^{(q-3)/2}dt \\
&= \frac{(2\pi)^{q/2}}{\epsilon^{q/2-1}}I_{q/2-1}(\epsilon),
\end{aligned} \tag{5.27}$$

corresponding to the inverse of the normalization constant in Eq. (5.25). The same result for the Vicsek model is reported by Degond and collaborators in Ref. [DDM14]. In directional statistics, the distribution described by Eq. (5.24) on the $(q-1)$-sphere $\mathbb{R}^q$ is called von Mises–Fisher distribution, which was first used to describe the interaction of electric dipoles in an electric field [MJ99]. In the case $\epsilon \to 0$, $f(\boldsymbol{\rho}, \hat{\boldsymbol{\sigma}}) \to \frac{\Gamma(q/2)}{2\pi^{q/2}}$ and $f(\boldsymbol{\rho}, \hat{\boldsymbol{\sigma}}) \to \delta(\hat{\boldsymbol{\sigma}} - \hat{\boldsymbol{\rho}})$ when $\epsilon \to \infty$. Defining the order parameter

$$\boldsymbol{\rho} = \int \hat{\boldsymbol{\sigma}}f(\boldsymbol{\rho}, \hat{\boldsymbol{\sigma}})d\hat{\boldsymbol{\sigma}}, \tag{5.28}$$

then the amplitude of the order parameter is

$$\begin{aligned}
\rho &= \int \hat{\boldsymbol{\rho}} \cdot \hat{\boldsymbol{\sigma}}f(\boldsymbol{\rho}, \hat{\boldsymbol{\sigma}})d\hat{\boldsymbol{\sigma}} \\
&= \frac{I_{q/2}(\epsilon)}{I_{q/2-1}(\epsilon)},
\end{aligned} \tag{5.29}$$

The second line of Eq. (5.29) is done by substituting Eq. (5.24) and Eq. (5.25) into the first line of Eq. (5.29).

We recall that in the classical Kuramoto model with $q = 2$, the order parameter is given by

$$\rho = \frac{I_1(\epsilon)}{I_0(\epsilon)}, \tag{5.30}$$

corresponding to our result described by Eq. (5.29) with $q = 2$. Also, in the three-
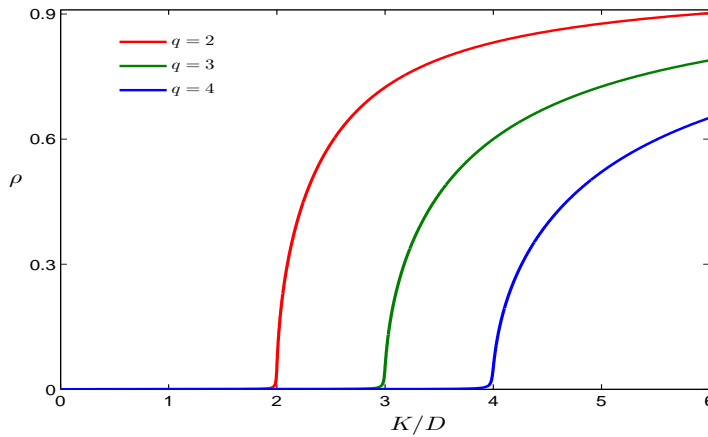
FIGURE 5.4: Self-consistent solution of q-dimensional noisy Kuramoto model without natural frequency, as described by Eq. (5.29).

dimensional case, the result coincides with Eq. (5.18) and Eq. (5.19), i.e.,

$$\frac{I_{3/2}(\epsilon)}{I_{3/2-1}(\epsilon)} = \coth{(\epsilon)} - \frac{1}{\epsilon}. \tag{5.31}$$

Expanding Eq. (5.29) to the third order of ϵ, we obtain (see Appendix B)

$$\rho \approx \frac{K\rho}{qD} - \frac{K^3\rho^3}{2D^3}\left(\frac{1}{q^2} - \frac{1}{q(q+2)}\right), \tag{5.32}$$

which indicates the square-root relationship of the criticality in general q dimension, i.e.,

$$\rho \approx \sqrt{\frac{q(q+2)(K - qD)D^2}{K^3}} \tag{5.33}$$

The critical coupling strength for the incoherent state ($\rho = 0$) to lose stability is qD with D here being the noise intensity in q-dimensional noisy Kuramoto model, as shown in Fig. 5.4.

Above, we derive the analytical solution of the probability density of the agents and hence obtain the self-consistent solution of the order parameter, in the case without natural frequency. However, for a general distribution both in direction and amplitude of the frequency in three dimensions, it's difficult to obtain the exact analytical solution of the corresponding Fokker-Planck equation. This is due to the fact that the probability current in three dimensions is dependent on both the azimuthal angle ϕ and the polar angle θ of the agent $\hat{\boldsymbol{\sigma}}$. Therefore, in the following section, we will investigate the linear stability of the incoherent state ($\rho = 0$) and we will restrict our discussion to the three-dimensional case ($q = 3$) because of its real physical meaning in nature. Various types of the distribution of the direction of the natural frequency will be considered, and the critical coupling strength K_c for the incoherent state to lose stability will be calculated in each case.

5.2.2 Linear Stability of the Incoherent State

Here we consider the linear stability of the incoherent state in the three-dimensional Kuramoto model with general frequency distribution. We rewrite the Fokker-Planck

equation (5.14) (see Appendix C) as

$$
\begin{aligned}
&\frac{\partial f}{\partial t} + K(\boldsymbol{\nabla}_s f(\hat{\boldsymbol{\sigma}}, \boldsymbol{\omega}, t) - 2f(\hat{\boldsymbol{\sigma}}, \boldsymbol{\omega}, t)\hat{\boldsymbol{\sigma}}) \cdot \boldsymbol{\rho} \\
&+ (\boldsymbol{\omega} \times \hat{\boldsymbol{\sigma}}) \cdot \boldsymbol{\nabla}_s f(\hat{\boldsymbol{\sigma}}, \boldsymbol{\omega}, t) = D\boldsymbol{\nabla}_s^2 f(\hat{\boldsymbol{\sigma}}, \boldsymbol{\omega}, t)
\end{aligned}
\tag{5.34}
$$

Considering a small perturbation to the distribution $f(\hat{\boldsymbol{\sigma}}, \boldsymbol{\omega}, t)$, i.e.,

$$
f(\hat{\boldsymbol{\sigma}}, \boldsymbol{\omega}, t) = f_0(\hat{\boldsymbol{\sigma}}, \boldsymbol{\omega}) + \eta(\hat{\boldsymbol{\sigma}}, \boldsymbol{\omega})e^{st}.
\tag{5.35}
$$

and then substituting Eq. (5.35) into Eq. (5.34), we obtain to the linear order in ρ and η the equation

$$
s\eta(\hat{\boldsymbol{\sigma}}, \boldsymbol{\omega}) + (\boldsymbol{\omega} \times \boldsymbol{\sigma}) \cdot \boldsymbol{\nabla}_s \eta(\hat{\boldsymbol{\sigma}}, \boldsymbol{\omega}) - D\boldsymbol{\nabla}_s^2 \eta(\hat{\boldsymbol{\sigma}}, \boldsymbol{\omega}) = 2K(\boldsymbol{\rho} \cdot \boldsymbol{\sigma})f_0(\hat{\boldsymbol{\sigma}}, \boldsymbol{\omega}).
\tag{5.36}
$$

Assuming without loss of generality $\boldsymbol{\omega} = \omega\hat{\boldsymbol{\omega}} = \omega\hat{\boldsymbol{z}}$, we obtain a simplified equation

$$
s\eta(\theta, \phi, \omega) + \omega\frac{\partial}{\partial\phi}\eta(\theta, \phi, \omega) - D\boldsymbol{\nabla}_s^2 \eta(\theta, \phi, \omega) = 2K(\boldsymbol{\rho} \cdot \hat{\boldsymbol{\sigma}})f_0(\theta, \phi, \omega),
\tag{5.37}
$$

where the uniform incoherent distribution $f_0 = \frac{1}{4\pi}$ and $\boldsymbol{\rho} \cdot \hat{\boldsymbol{\sigma}}$ in the r.h.s of Eq. (5.37) is only related to the first spherical harmonics, i.e.,

$$
\begin{aligned}
\boldsymbol{\rho} \cdot \hat{\boldsymbol{\sigma}} &= \rho_z\cos\theta + \rho_x\sin\theta\cos\phi + \rho_y\sin\theta\sin\phi \\
&= \sqrt{\frac{4\pi}{3}}\rho_z Y_1^0 + \sqrt{\frac{2\pi}{3}}(\rho_x + i\rho_y)Y_1^{-1} - \sqrt{\frac{2\pi}{3}}(\rho_x - i\rho_y)Y_1^1.
\end{aligned}
\tag{5.38}
$$

Here Y_1^0, Y_1^1 and Y_1^{-1} are the first spherical harmonics with the expressions

$$
\begin{aligned}
Y_1^0(\theta, \phi) &= \sqrt{\frac{3}{4\pi}}\cos\theta, \\
Y_1^{-1}(\theta, \phi) &= \sqrt{\frac{3}{8\pi}}\sin\theta e^{-i\phi}, \\
Y_1^1(\theta, \phi) &= -\sqrt{\frac{3}{8\pi}}\sin\theta e^{i\phi}.
\end{aligned}
\tag{5.39}
$$

In order to solve Eq. (5.37), we express $\eta(\theta, \phi, \omega)$ in terms of the linear combination of the spherical harmonics

$$
\eta(\theta, \phi, \omega) = \sum_{l=0}^{\infty}\sum_{m=-l}^{l} b_l^m Y_l^m(\theta, \phi),
\tag{5.40}
$$

where $Y_l^m(\theta, \phi)$ is the spherical harmonics defined as

$$
Y_l^m(\theta, \phi) = \sqrt{\frac{(2l+1)}{4\pi}\frac{(l-m)!}{(l+m)!}}P_l^m(\cos\theta)e^{im\phi}.
\tag{5.41}
$$

Here $P_l^m(\cos\theta)$ is the associated Legendre polynomial. On the surface of the sphere the action of the diffusion term reduces to

$$
\boldsymbol{\nabla}_s^2 Y_l^m(\theta, \phi) = -l(l+1)Y_l^m(\theta, \phi).
\tag{5.42}
$$

Substituting Eq. (5.40), (5.41), (5.42) into Eq. (5.37), we obtain a linear system of equations for the coefficients b_l^m

$$
\sum_{l=0}^{\infty} \sum_{m=-l}^{l} b_l^m [s + im\omega + Dl(l+1)] Y_l^m(\theta, \phi)
$$
$$
= \sqrt{\frac{1}{3\pi}} K\rho_z Y_1^0 + \sqrt{\frac{1}{6\pi}} K(\rho_x + i\rho_y) Y_1^{-1} - \sqrt{\frac{1}{6\pi}} K(\rho_x - i\rho_y) Y_1^1. \tag{5.43}
$$

Eq. (5.43) can be solved due to the orthonormality of the spherical harmonics, i.e.,

$$
\int_{\theta=0}^{\pi} \int_{\phi=0}^{2\pi} Y_l^m Y_{l'}^{m'*} \sin\theta d\theta d\phi = \delta_{mm'}\delta_{ll'},
$$

where δ_{ij} is the Kronecker delta and the complex conjugation of Y_l^m is defined as

$$
Y_l^{m*}(\theta, \phi) = (-1)^m Y_l^{-m}(\theta, \phi).
$$

Since the l.h.s. of Eq. (5.43) only depends on Y_l^m with $l = 1$ the components b_l^m with $l > 1$ decay exponentially at rates $Dl(l+1)$. For $l = 1$ the coefficients b_1^0, b_1^{-1} and b_1^1 are calculated as follows,

$$
b_1^0 = \sqrt{\frac{1}{3\pi}} \frac{K\rho_z}{s + 2D}; \quad b_1^{-1} = \sqrt{\frac{1}{6\pi}} \frac{K(\rho_x + i\rho_y)}{s + 2D - i\omega};
$$
$$
b_1^1 = -\sqrt{\frac{1}{6\pi}} \frac{K(\rho_x - i\rho_y)}{s + 2D + i\omega}; \quad b_l^m = 0(l > 1). \tag{5.44}
$$

Accordingly, the perturbation to the distribution, i.e., the solution of Eq. (5.37), is only related to the first harmonics, i.e.,

$$
\eta(\theta, \phi, \omega, t) = \sqrt{\frac{1}{3\pi}} \frac{K\rho_z}{s + 2D} Y_1^0 + \sqrt{\frac{1}{6\pi}} \frac{K(\rho_x + i\rho_y)}{s + 2D - i\omega} Y_1^{-1} - \sqrt{\frac{1}{6\pi}} \frac{K(\rho_x - i\rho_y)}{s + 2D + i\omega} Y_1^1. \tag{5.45}
$$

By integrating with respect to the unit vector $\hat{\boldsymbol{\sigma}}$ and the frequency vector $\omega\hat{\boldsymbol{\omega}}$, we obtain the perturbation to the order parameter

$$
\boldsymbol{\rho}(t) = \int \int \int_s \hat{\boldsymbol{\sigma}} \eta(\hat{\boldsymbol{\sigma}}, \boldsymbol{\omega}, t) g_d(\hat{\boldsymbol{\omega}}) g(\omega) d\hat{\boldsymbol{\sigma}} d\hat{\boldsymbol{\omega}} d\omega, \tag{5.46}
$$

where $g_d(\hat{\boldsymbol{\omega}})$ is the distribution of direction of the frequency, e.g., $1/(4\pi)$ for the isotropic case, and $g(\omega)$ is the distribution of amplitude of the frequency.

First let's calculate the integral with respect to $\hat{\boldsymbol{\sigma}}$, i.e., the frequency-dependent mean field

$$
\boldsymbol{R} = \int_s \hat{\boldsymbol{\sigma}} \eta(\hat{\boldsymbol{\sigma}}, \boldsymbol{\omega}, t) d\hat{\boldsymbol{\sigma}}
$$
$$
= \frac{2K}{3} \begin{pmatrix} \frac{\rho_x\lambda - \rho_y\omega}{\lambda^2 + \omega^2} \\ \frac{\rho_y\lambda + \rho_x\omega}{\lambda^2 + \omega^2} \\ \frac{\rho_z}{\lambda} \end{pmatrix}. \tag{5.47}
$$

where $\lambda = s + 2D$. According to the convention above, $\hat{\boldsymbol{\omega}}$ is directed along $\hat{\boldsymbol{z}}$ while the direction of $\boldsymbol{\rho}$ is arbitrary. However, expression (5.47) can be rewritten in a covariant

form, allowing for arbitrary directions of $\boldsymbol{\rho}$ and $\hat{\boldsymbol{\omega}}$

$$\boldsymbol{R} = \frac{2K}{3} \left[\frac{\lambda\boldsymbol{\rho}}{\lambda^2 + \omega^2} + \frac{\omega\hat{\boldsymbol{\omega}} \times \boldsymbol{\rho}}{\lambda^2 + \omega^2} + \left(\frac{1}{\lambda} - \frac{\lambda}{\lambda^2 + \omega^2} \right) \hat{\boldsymbol{\omega}} \left(\hat{\boldsymbol{\omega}} \cdot \boldsymbol{\rho} \right) \right]. \tag{5.48}$$

Finally defining the averages

$$h_1 = \int\limits_{-\infty}^{\infty} \frac{\lambda}{\lambda^2 + \omega^2} g(\omega) d\omega, \quad h_2 = \int\limits_{-\infty}^{\infty} \frac{\omega}{\lambda^2 + \omega^2} g(\omega) d\omega, \tag{5.49}$$

and $h_3 = \frac{1}{\lambda} - h_1$, the antisymmetric matrix Ξ with

$$\Xi = \int_{S^1} \begin{pmatrix} 0 & -\hat{\omega}_z & \hat{\omega}_y \\ \hat{\omega}_z & 0 & -\hat{\omega}_x \\ -\hat{\omega}_y & \hat{\omega}_x & 0 \end{pmatrix} G(\hat{\boldsymbol{\omega}}) |d\hat{\boldsymbol{\omega}}| \tag{5.50}$$

and the frequency direction covariance matrix W with

$$W = \int_{S^1} \begin{pmatrix} \hat{\omega}_x^2 & \hat{\omega}_x\hat{\omega}_y & \hat{\omega}_x\hat{\omega}_z \\ \hat{\omega}_x\hat{\omega}_y & \hat{\omega}_y^2 & \hat{\omega}_y\hat{\omega}_z \\ \hat{\omega}_x\hat{\omega}_z & \hat{\omega}_y\hat{\omega}_z & \hat{\omega}_z^2 \end{pmatrix} G(\hat{\boldsymbol{\omega}}) |d\hat{\boldsymbol{\omega}}|, \tag{5.51}$$

we can express $\boldsymbol{\rho}$ self-consistently as

$$\boldsymbol{\rho} = \frac{2K}{3} \left[h_1 \mathbb{1} + h_2 \Xi + h_3 W \right] \boldsymbol{\rho}. \tag{5.52}$$

The eigenvalue problem (5.52) has a solution if the dispersion relation

$$\det \left[\frac{2K}{3} \left(h_1 \mathbb{1} + h_2 \Xi + h_3 W \right) - \mathbb{1} \right] = 0 \tag{5.53}$$

holds. Both, the real and the imaginary part of the determinant on the l.h.s. must be zero which at criticality where $s = i\Omega$ and other system parameters fixed, occurs for a discrete set of points (K_l, Ω_l). At the smallest coupling strength $K_c = \min_l K_l$ the incoherent state loses stability and a nonzero mean field with frequency Ω_c emerges. For any critical mode with (K_l, Ω_l) the mode with $(K_l, -\Omega_l)$ is also critical. Moreover, there is always at least one solution $(K_l, \Omega_l = 0)$ since the determinant is a cubic polynomial in K with real coefficients when $\Omega = 0$. For an isotropic or axial symmetric distribution $G(\hat{\boldsymbol{\omega}})$ the matrix can become reducible and the determinant a product of linear or quadratic functions in K. With $\hat{\boldsymbol{z}}$-axial symmetry of frequency directions the matrix W is diagonal with $\langle \hat{\omega}_z^2 \rangle_G = \Lambda_z^2$, $\langle \hat{\omega}_x^2 \rangle_G = \langle \omega_y^2 \rangle_G = \Lambda_{xy}^2$ and Matrix Ξ has only $\pm\mu_z = \pm \langle \hat{\omega}_z \rangle_G$ as nonzero entries, i.e., Eq. (5.53) becomes

$$\begin{vmatrix} \frac{2K}{3}(h_1 + \Lambda_{xy}^2 h_3) - 1 & -\frac{2K}{3}\mu_z h_2 & 0 \\ \frac{2K}{3}\mu_z h_2 & \frac{2K}{3}(h_1 + \Lambda_{xy}^2 h_3) - 1 & 0 \\ 0 & 0 & \frac{2K}{3}(h_1 + h_3\Lambda_z^2) - 1 \end{vmatrix} = 0. \tag{5.54}$$

Then the matrix determinant is a product of two factors so that one of the two equations

$$0 = h_1 + \Lambda_z^2 h_3 - \frac{3}{2K} \tag{5.55}$$

$$0 = \left(h_1 + \Lambda_{xy}^2 h_3 - \frac{3}{2K}\right)^2 + \mu_z^2 h_2^2 \tag{5.56}$$

must hold. If $h_2 \mu_z$ is zero, the numbers of left and right rotating oscillators around each rotation axis are equal and we can immediately find the solutions with $\Omega = 0$ as

$$
\begin{aligned}
K_1 &= \frac{3}{2} \frac{1}{\Lambda_z^2 h_3 + h_1}\bigg|_{\lambda=2D}, \\
K_2 &= \frac{3}{2} \frac{1}{\Lambda_{xy}^2 h_3 + h_1}\bigg|_{\lambda=2D},
\end{aligned} \tag{5.57}
$$

The smaller one of K_1 and K_2 determines the critical coupling strength, i.e.,

$$K_c = \min(K_1, K_2). \tag{5.58}$$

With Lorentzian frequency distribution $g(\omega) = \frac{1}{\pi} \frac{\gamma}{(\omega-\omega_0)^2+\gamma^2}$ the integrals (5.49) can directly be evaluated (see Appendix D) as

$$h_1 = \frac{\lambda + \gamma}{(\lambda + \gamma)^2 + \omega_0^2}, \quad h_2 = \frac{\omega_0}{(\lambda + \gamma)^2 + \omega_0^2}, \quad h_3 = \frac{1}{\lambda} - h_1. \tag{5.59}$$

In this case and when $h_2\mu_z = 0$ one can show, by inspecting the imaginary part of the r.h.s. in Eq. (5.58) with $\lambda = 2D + i\Omega$, that no oscillatory instabilities with $\Omega \neq 0$ exist. Here we consider four cases:

- Case (i), the direction of the frequency vector is a constant unit vector $\hat{\boldsymbol{\omega}}_1$, i.e., $g_d(\hat{\boldsymbol{\omega}}) = \delta(\hat{\boldsymbol{\omega}} - \hat{\boldsymbol{\omega}}_1)$. In this case, $\Lambda_{xy}^2 = 0, \Lambda_z^2 = 1$ and therefore the coupling strength determined by (5.57) are

$$
\begin{aligned}
K_1 &= \frac{3}{2(h_3 + h_1)} = 3D, \\
K_2 &= \frac{3}{2h_1} = \frac{3}{2} \frac{(2D + \gamma)^2 + \omega_0^2}{2D + \gamma}.
\end{aligned} \tag{5.60}
$$

It's easy to prove that $K_1 < K_2$, since h_3 is always larger than zero regardless of the width γ of the frequency distribution, i.e.,

$$h_3 = \frac{\gamma^2 + \omega_0^2 + \lambda\gamma}{\lambda\left((\lambda + \gamma)^2 + \omega_0^2\right)} > 0. \tag{5.61}$$

Therefore, the critical coupling strength for the incoherent state to lose stability in this case is

$$K_c = K_1 = 3D. \tag{5.62}$$

As shown in Fig. 5.5(b), for $D = 0.5$, the critical coupling strength is always 1.5, regardless of the width γ and mean ω_0 of the amplitude distribution for the frequency.
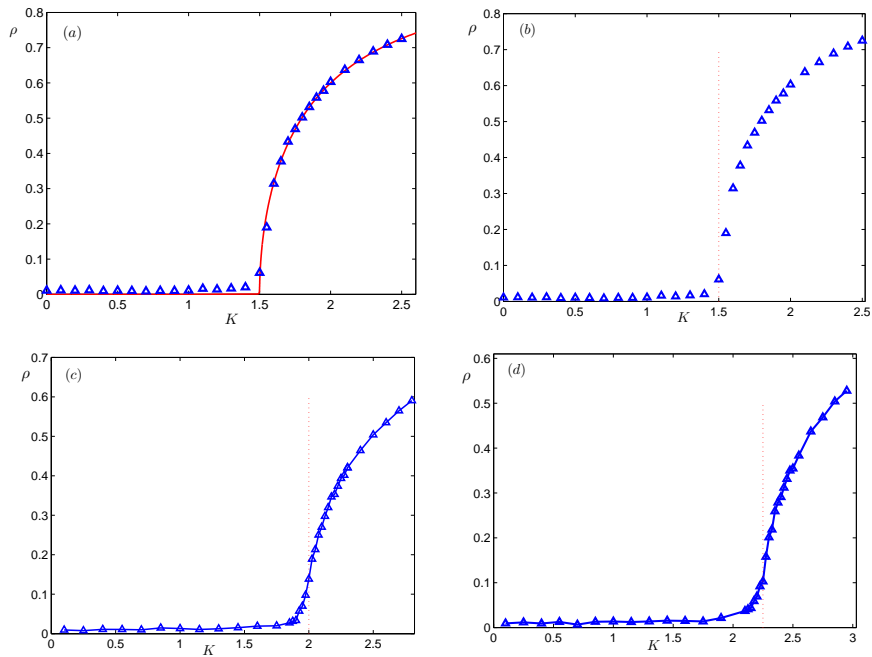
FIGURE 5.5: Transition to synchrony in the three-dimensional noisy Kuramoto model described by Eq. (5.10), where the number of coupled agents is $N = 1 \times 10^4$ and the noise intensity is $D = 0.5$. (a) is for the case where there is no natural frequency and the red curve is the analytic self-consistent solution described by Eq. (5.18). (b) is for Case (i), where the frequency direction is a constant vector, i.e., here we choose $\hat{\boldsymbol{\omega}}_1 = \hat{\boldsymbol{z}}$. (c) is for Case (ii), where the frequency vectors are located uniformly in the $x - y$ plane. (d) is for Case (iii), where the distribution of the frequency direction is isotropic. The amplitudes of frequency in (b), (c) and (d) are all chosen from the same Cauchy distribution $g(\omega) = \frac{\gamma}{\pi(\omega^2 + \gamma^2)}$ with width $\gamma = 1$. The blue triangles in (a)-(d) represent the direct simulations of Eq. (5.10) and all the red dotted lines in (b)-(d) indicate the analytical critical value K_c above which the incoherent state loses stability, i.e., Eq. (5.62) for Case (i), Eq. (5.64) for Case (ii) and Eq. (5.65) for Case (iii).

FIGURE 5.6: Two dimensional visualization of 20000 coupled agents (red dots) for $K = 1.8$ in Case (i) (left) and $K = 2.3$ in Case (ii) (right). The noise intensity in both cases is $D = 0.5$ and the observatio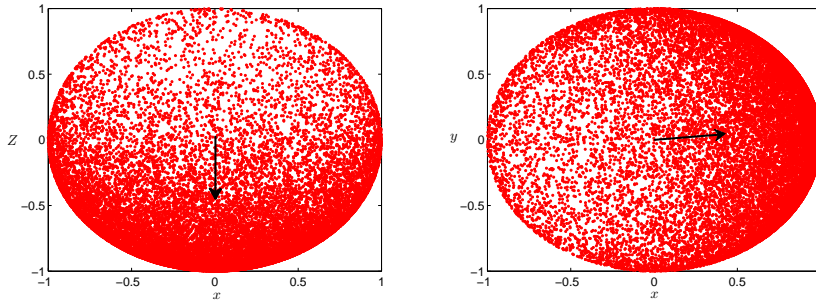n time is $t = 200$. The black arrows represent the mean field $\boldsymbol{\rho}$, which is close to the $\boldsymbol{z}$ direction for Case (i) and is in the x-y plane for Case (ii).

- Case (ii), all the frequency vectors are located uniformly on a plane. Without loss of generality, here we choose the $x - y$ plane. The direction distribution of the frequency is $g_d(\hat{\boldsymbol{\omega}}) = g_d(\vartheta, \psi) = \frac{\delta(\vartheta - \pi/2)}{2\pi}$, with ϑ and ψ being the polar angle and azimuthal angle of the unit vector $\hat{\boldsymbol{\omega}}$ respectively. In this case, $\Lambda^2_{xy} = 1/2$, $\Lambda^2_z = 0$ and k_1 and k_2 determined by Eq. (5.57) are

$$K_1 = \frac{3}{h_3 + 2h_1} = \frac{6D(\gamma + 2D)}{\gamma + 4D},$$
$$K_2 = \frac{3}{2h_1} = \frac{3}{2}\frac{(2D + \gamma)^2 + \omega_0^2}{2D + \gamma}. \tag{5.63}$$

Due to the inequality in (5.61), one can also easily prove that $K_1 < K_2$ always holds regardless of the width γ and mean ω_0 for the Lorentzian frequency distribution. Accordingly, the smaller one of the coupling strengths $\min(K_1, K_2) = K_1$ determines the critical coupling strength K_c for the incoherent state to lose stability in this case, i.e.,

$$K_c = K_1 = \frac{6D(\gamma + 2D)}{\gamma + 4D}. \tag{5.64}$$

As shown in Fig. 5.5 (c), the analytical result predicted by Eq. (5.64) coincides well with direct simulation of the Langevin equation (5.10).

Close to the criticality, the mean field vector is in the direction of $\hat{\boldsymbol{z}}$ for Case (i) and in the $x - y$ plane in Case (ii), as shown in Fig. 5.6. This can be checked easily by the linear mean-field equation (5.52)

- Case (iii), the frequency vector is isotropic, i.e., $g_d(\vartheta, \psi) = \frac{1}{4\pi}$. In doing the simulation, we choose a vector $\boldsymbol{\omega_g}$, of which each element is selected from Gaussian distribution to make it isotropic, and then normalize it to obtain an isotropic unit vector, i.e., $\hat{\boldsymbol{\omega}} = \boldsymbol{\omega_g}/|\boldsymbol{\omega_g}|$. In this case, $\Lambda^2_{xy} = \Lambda^2_z = 1/3$ determines the critical coupling strength and thus Eq. (5.58) is reduced to:

$$K_c = \frac{9}{2(3h_1 + h_3)} = \frac{9D(\gamma + 2D)}{(\gamma + 6D)}. \tag{5.65}$$

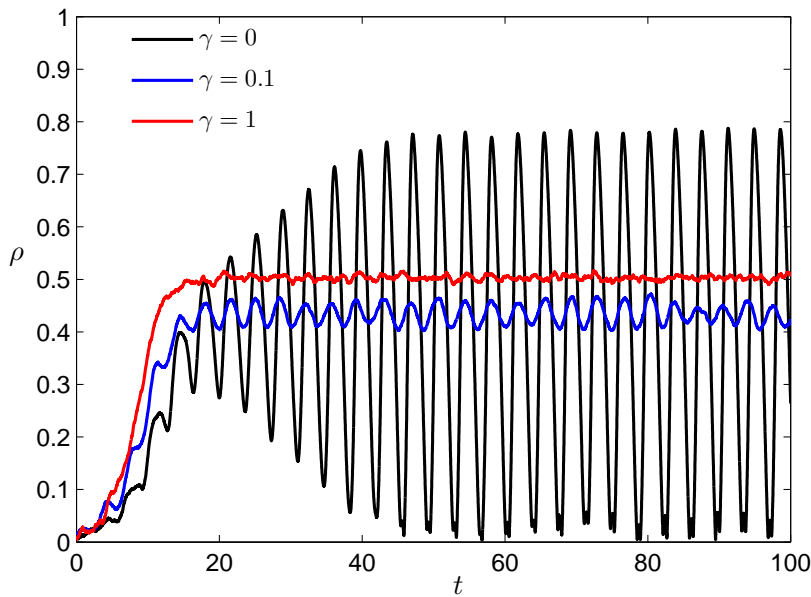As shown in Fig. 5.5(d), the theoretical prediction described by Eq. (5.65)

FIGURE 5.7: The order parameter evolves as a function of time, from the simulation of
Eq. (5.10). Here the noise intensity is $D = 0.1$, the frequency vectors are isotropic with the
amplitude a Cauchy distribution $g(\omega) = \frac{\gamma}{\pi((\omega-\omega_0)^2+\gamma^2)}$. Here the coupling strength is $K = 2$,
the mean value of frequency amplitude ω_0 is 2 and γ is chosen as 0(black), 0.1(blue) and
1(red) respectively.

matches well with the direct simulation of the Langevin Eq. (5.10), where the
small mismatch is expected due to the finite-size effect.

The individual noise always stabilizes the incoherent state, as in the classical
Kuramoto model [SM91], and a transition to collective motion occurs at finite
coupling strength.

- Case (iv), asymmetric amplitude distribution for the frequency. Interestingly,
  when $g(\omega)$ is symmetric but with a non-zero mean value, there will be more
  rich dynamics displaying. Suppose the amplitude distribution of the frequency
  $g(\omega)$ is the Cauchy distribution with the form $g(\omega) = \frac{\gamma}{\pi((\omega-\omega_0)^2+\gamma^2)}$ while the
  direction distribution of the frequency is still isotropic as in Case (iii). With
  the same procedure as in Case (iii), one can easily obtain the critical coupling
  strength for the incoherent state to lose stability

$$K_c = \frac{9\lambda[(\lambda+\gamma)^2 + \omega_0^2]}{2[(\lambda+\gamma)(3\lambda+\gamma) + \omega_0^2]}\bigg|_{\lambda=2D}. \tag{5.66}$$

The richer dynamics in this case lies in, in the regime where the incoherent
state is unstable, that the amplitude of the order parameter can be oscillatory,
as demonstrated in Ref. [Rit98] for $\gamma = 0$. Here we show this phenomenon
for different width γ in Fig. 5.7. This is induced by the symmetry-breaking
of the amplitude distribution of the frequency $g(\omega)$. However, more detailed
descriptions such as the phase diagram are needed, based on the nonlinear mean-
field equation. This is beyond the linear stability analysis we studied in this
chapter and we leave it to future work.
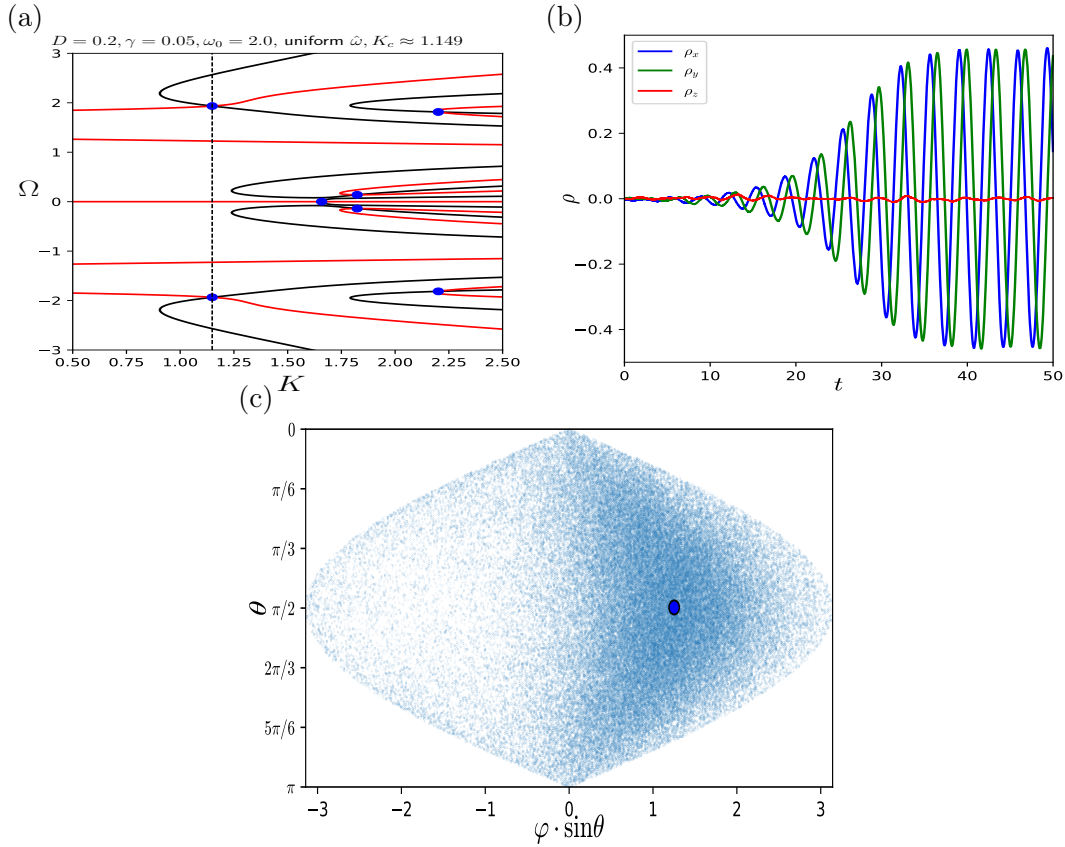
(a)

(b)

(c)

FIGURE 5.8: (a) Lines of zero real part (bold) and zero imaginary part (light) of the determinant (5.53) as function of coupling strength K and mode frequency Ω. The nonzero frequency $\Omega_c \approx 1.95$ of the unstable mode with the smallest coupling strength $K_c \approx 1.149$ signifies a Hopf bifurcation from the incoherent state. (b) Time series of the x, y and z component from $N = 4 \times 10^4$ uniformly distributed initial agents at $K = 1.6$ demonstrating a uniformly rotating mean field in the xy-plane. (e) Snapshot of the agents (small dots) and the mean field (black circle) in a Mercator equal-area projection of the unit sphere. Figure reprinted with permission from Ref. [ZTP20].

Compared with an equivalent model called random top model [Rit98], in which the analysis is hard to follow and is limited to the special case with $\gamma = 0$, the three-dimensional noisy Kuramoto model we proposed here and the linear stability analysis we did as above have more general solutions, e.g., for the critical coupling strength K_c in Case (i)-(iv).

One common feature in Case (i)-(iv) is that when taking the limit $D \to 0$, the critical coupling strengths derived in all cases approach zero, coinciding with the deterministic case where the transition occurs infinitely close to zero, i.e., $K_c \to 0^+$ (see Sec. 5.1).

Symmetry-breaking induced Hopf bifurcation

All the cases (i)-(iv) discussed above have a fixed direction of the mean field $\hat{\boldsymbol{\rho}}$, with the collective frequency $\Omega_c = 0$ in the vicinity of criticality $K \to K_c$. This is due to the high symmetry of both the direction and the amplitude distribution for the frequency, i.e., $g_d(\hat{\boldsymbol{\omega}})$ and $g(\omega)$ respectively. As long as this kind of symmetry is broken to some degree, the mean field can be rotating, leading to collective oscillation. Here we show a non-trivial example where the incoherent state becomes unstable undergoing

a Hopf bifurcation, which appears in terms of a non-zero collective frequency Ω in the dispersion relation (5.53).

We consider the axial symmetric example of a uniform distribution $G(\hat{\boldsymbol{\omega}})$ on the upper half sphere with $\Lambda_{xy}^2 = \Lambda_z^2 = 1/3$ and $\mu_z = 1/2$, a narrow Lorentzian frequency amplitude distribution $g(\omega)$ with mean value $\omega_0 = 2.0$ and scale factor $\gamma = 0.05$, and noise strength $D = 0.2$. The zeros of dispersion relation (5.53) are shown in Fig. 5.8(a), where two solutions of (5.56) have the smallest coupling strength $K_c \approx 1.149$ at a frequency $\Omega_c \approx \pm 1.95$. Due to the fact that $\mu_z h_2$ is non-zero in this case, the numbers of left and right rotating oscillators around each rotation axis are not equal, and hence the collective frequency Ω of the mean field can also be non-zero, i.e., the mean field $\boldsymbol{\rho}$ can be rotating instead of being static in the stationary state. In direct simulations, we find that the mean field is rotating in the xy-plane, as shown in Fig. 5.8(b). Moreover, we plot the snapshot of the agents $\hat{\boldsymbol{\sigma}} = (\sin\theta\cos\phi, \sin\theta\sin\phi, \cos\theta)$ on the three-dimensional sphere, as shown in Fig. 5.8(c). It demonstrates further that the mean field in this case is located in the $x - y$ plane. In Sec. 5.3.2 we will see that, by interpreting $\hat{\boldsymbol{\sigma}}$ as the velocity vector of a microswimmer, the Hopf bifurcation will lead to the collective oscillation of the particles where the center of mass of them is rotating while the individual particles are diffusing outwards.

5.3 Three-dimensional swarming described by the noisy Kuramoto model

The unit vector $\hat{\boldsymbol{\sigma}}$ in the three-dimensional noisy Kuramoto model (5.13) can either be a vector about the position or the velocity. If interpreting the vector σ as the position vector of agents diffusing on the surface of a three-dimensional sphere, the model can be potentially used to describe the dynamics of N interacting magnetic moments [Rit98], where each unit has a natural precession vector $\hat{\boldsymbol{\omega}}_i (i = 1, \cdots, N)$. Also, the model could potentially be used to describe the coupling of the active surface of the cell cortex [Mie+19], displaying interesting pattern formation via dynamic instability. Therein the polar instability determined by the first spherical harmonics and nematic instability determined by the second spherical harmonics in Ref. [Mie+19] are very similar to the instability of the incoherent state in the case of first-order coupling and second-order coupling respectively in Kuramoto model. This kind of instability determination is also seen in a mean-field version of the Vicsek model [PDB08], where the ferromagnetic and liquid-crystal alignment are the counterparts of the first-order and second-order coupling in the Kuramoto model. More deep connections among these models need to be unveiled in future research.

If considering $\hat{\boldsymbol{\sigma}}$ as the unit velocity vector of a particle, i.e., $\hat{\boldsymbol{v}} = \hat{\boldsymbol{\sigma}}$, the three-dimensional Kuramoto model can be used to describe the swarming phenomenon of microswimmers with flagella. The helical motion is induced by a non-zero rotational frequency ω. In this case, all the analysis is the same as the above sections, just replacing $\hat{\boldsymbol{\sigma}}$ with $\hat{\boldsymbol{v}}$. Therefore, the nonzero mean field $\boldsymbol{\rho} = \frac{1}{N}\sum_{j=1}^{N}\hat{\boldsymbol{v}}_j$ represents the alignment of agents or particles, while $\boldsymbol{\rho} = 0$ means all the particles move in uniformly random directions in three-dimensional space.

In this case, the equation describing the alignment dynamics of N particles with the same speed amplitude v_0 but in various directions $\hat{\boldsymbol{v}}_i(t)$ $(i = 1, \cdots, N)$ is as
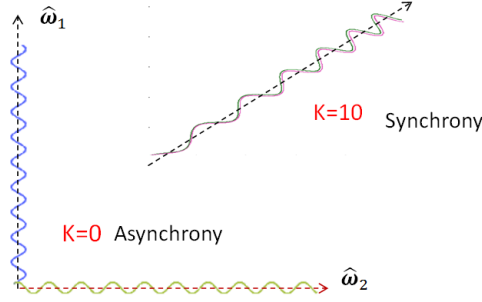
FIGURE 5.9: Schematic description of two particles's helical motion with the direction of rotation frequency $\hat{\boldsymbol{\omega}}_1$ and $\hat{\boldsymbol{\omega}}_2$ respectively. Synchronization occurs when the coupling strength is large enough.

follows:

$$\dot{\boldsymbol{x}}_i = v_0\hat{\boldsymbol{v}}_i$$
$$\frac{d\hat{\boldsymbol{v}}_i}{dt} = K(\boldsymbol{\rho} - (\boldsymbol{\rho} \cdot \hat{\boldsymbol{v}}_i)\hat{\boldsymbol{v}}_i) + (\omega_i\hat{\boldsymbol{\omega}}_i + \boldsymbol{\xi}_i(t)) \times \hat{\boldsymbol{v}}_i, \tag{5.67}$$

or an alternative form:

$$\dot{\boldsymbol{x}}_i = v_0\hat{\boldsymbol{v}}_i$$
$$\dot{\hat{\boldsymbol{v}}}_i = \boldsymbol{\mu}_i \times \hat{\boldsymbol{v}}_i, \tag{5.68}$$
$$\boldsymbol{\mu}_i = \omega_i\hat{\boldsymbol{\omega}}_i + K\left(\hat{\boldsymbol{v}}_i \times \boldsymbol{\rho}\right) + \boldsymbol{\xi}_i,$$

In writing the expression in the third line of Eq. (5.68), we have used the triple product expansion

$$(\hat{\boldsymbol{v}} \times \boldsymbol{\rho}) \times \hat{\boldsymbol{v}} = \boldsymbol{\rho}(\hat{\boldsymbol{v}} \cdot \hat{\boldsymbol{v}}) - \hat{\boldsymbol{v}}(\hat{\boldsymbol{v}} \cdot \boldsymbol{\rho}). \tag{5.69}$$

The torque $\boldsymbol{\mu}_i$ can be any time-dependent global or individual forcing. Here we assume it is the summation of a constant rotation bias of amplitude ω around an axis in the direction $\hat{\boldsymbol{\omega}}$, an alignment force rotating $\hat{\boldsymbol{v}}$ towards a vector $\boldsymbol{\rho}$ and a noise component $\boldsymbol{\xi}_i$, which is Gaussian white noise as in the model (5.13).

When there is rotational frequency $\boldsymbol{\omega}_i = \omega_i\hat{\boldsymbol{\omega}}_i$ for each oscillator $i (i = 1, \cdots, N)$, similar to the charged particle in magnetic field, a nonzero frequency in Eq. (5.68) will make the particles move in a helical way. To better understand the synchronization in the model, we consider two particles move in random directions, here we choose two orthogonal vectors, and see how a large positive coupling strength K will align or synchronize these two particles (see Fig. 5.9).

5.3.1 Connection to a mean-field version of the Vicsek model

In the case where there is no natural frequency, i.e., $\omega_i = 0$ $(i = 1, \cdots, N)$, the model is actually a mean-field version of the Vicsek model [Vic+95] where the velocity of each particle is aligned by the mean field $\boldsymbol{\rho}$.

The Vicsek model is a model to study the collective motion in terms of velocity alignment, observed in a wide range of scales in nature, from flocking of birds and fish schools to bacteria colonies. It describes a collection of N particles moving with the same constant speed and aligning their direction of motion with their local neighbours. The Vicsek model is originally proposed in two dimensions, but for the generalization for higher dimensions we adopt the following discrete equation for the updates of the position of the i-th particle [Cha+08]:

$$\boldsymbol{x}_i(t + \Delta t) = \boldsymbol{x}_i(t) + v_0\hat{\boldsymbol{v}}_i(t)\Delta t, \tag{5.70}$$
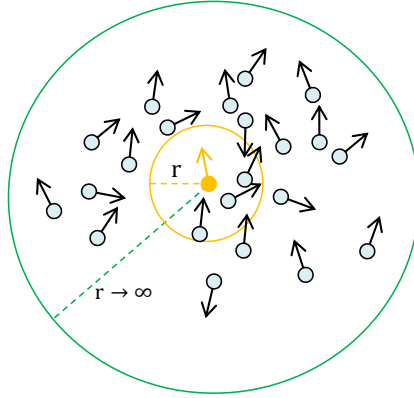
FIGURE 5.10: Schematic description of the Vicsek model. Each particle (an example marked yellow) interact locally with the neighbours within the distance r. In the long-range limit $(r \to \infty)$, the dynamics of the particles can be described by the mean-field approach.

with v_0 being the speed amplitude of the particles, and the discrete equation describing the orientation dynamics:

$$\hat{\boldsymbol{v}}_i(t + \Delta t) = (R_\eta \circ \vartheta) \left[\sum_{|\boldsymbol{x_i} - \boldsymbol{x}_j| < r} \hat{\boldsymbol{v}}_j(t) \right], \tag{5.71}$$

where $\hat{\boldsymbol{v}}_i$ is the unit vector for the direction of the i-th particle and the aligning regime is a ball of radius r (circle in 2 dimensions). Here ϑ is a normalization operator to ensure $\vartheta(\boldsymbol{c}) = \boldsymbol{c}/|\boldsymbol{c}|$ and R_η executes a random rotation uniformly distributed around the argument vector. There are generally two versions of the time-continuous and globally coupled Vicsek model, of which the schematic figure can be represented by Fig. 5.10. One version is applied to the cases of ferromagnetic and liquid-crystal alignment [PDB08], corresponding to the first-order and second-order coupling in the Kuramoto model. Therefore, the linear stability of the disordered state is similar to its counterpart, i.e., the linear stability of the incoherent state, in the Kuramoto model. The stability in the case of ferromagnetic alignment (first-order coupling) is determined by the first harmonic function, while in the case of liquid-crystal alignment (second-order coupling) it is determined by the second harmonic function. The other version is proposed by Degond and Motsch [DM08], where a projection matrix is used to describe the coupling of neighbor particles. These two versions are both based on the Fokker-Planck formalism but the former version is limited to two dimensions while the latter one is straightforward to extend to the higher-dimensional case.

Instead, we formulate the alignment of velocities of the coupled particles in a vector form, which not only is more convenient for the generalization to higher-dimensional versions but also shows a direct connection to the Kuramoto model.

In Fig. 5.11 we show the order parameter (mean velocity) as a function of the relative noise strength D/K for an isotropic distribution of rotation axes $G(\hat{\boldsymbol{\omega}}) = 1/(4\pi)$ for the direction of the frequency and Lorentzian distributions $g(\omega) = \frac{\gamma}{\pi}(\omega^2 + \gamma^2)^{-1}$ with mean frequency zero for the amplitude. Depending on the ratio γ/K a stationary mean field bifurcates from the incoherent state ($\rho = 0$) at a critical value of $(D/K)_{cr}$, which the linear stability analysis in Sec. 5.2.2 can predict.

This bifurcation point on the horizontal axis is connected to a point on the vertical axis in the noise-free limit discussed in[CGO19b]. The existence of a critical ratio $(D/K)_{cr}$ for the transition from incoherence to coherence means that the noise-free
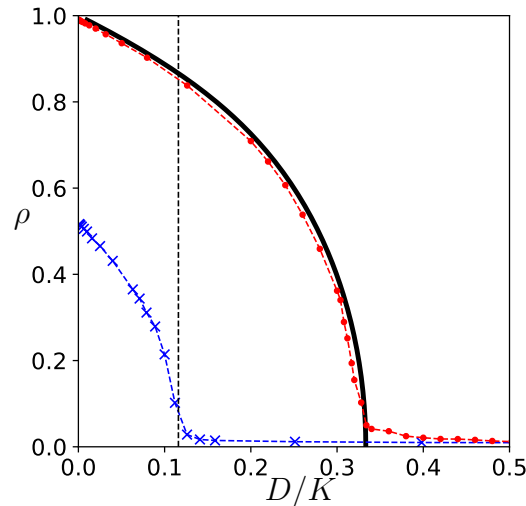
FIGURE 5.11: Amplitude of the (stationary) mean velocity as a function of the ratio D/K. Shown are the experimentally measured mean velocity in simulations for $\gamma/K = 0.02$(red circles) and for $\gamma/K = 10$ (blue crosses) of $N = 4 \times 10^4$ velocity vectors, the parametric analytic solution of the globally coupled Vicsek model (solid line) and the critical ratio $(D/K)_{cr}$ for the example with $\gamma/K = 10$ (dashed vertical line). Figure reprinted with permission from Ref. [ZTP20].

limit $D \to 0$ is singular as the critical coupling strength also goes to zero. In Fig. 5.11 we show two examples, a very homogeneous frequency distribution with $\gamma/K = 0.02$, very close to the rotation free case of the globally coupled Vicsek model, and a very heterogeneous frequency distribution with $\gamma/K = 10$. Here the incoherent state, where the mean velocity is zero, is stable for even lower ratios of D/K. For $D = 0$ the mean velocity in the limit $\gamma/K \to \infty$ is $\rho = 0.5$, corresponding to the limit $K \to 0^+$ as predicted in [CGO19b]. Therefore, the noise makes the dynamics much richer in terms of bifurcation from the incoherent state, compared with the deterministic case where the critical coupling strength is always zero regardless of the frequency distribution.

In the two, or generally speaking, even-dimensional Kuramoto model [CGO19b], when $D \to 0$, ρ will not approach 0.5 as in the three-dimensional case. Instead, there always exists a critical coupling determined by the frequency distribution. However, the role of noise would still be the same, i.e., it always stabilizes the incoherent state and inhibits the synchronous state. For instance, in the classical two-dimensional case [SM91], noise shifts the discrete spectrum of the linear operator to the left-half plane.

5.3.2 Swarming with helical trajectories

Helical motion is a common form of movement in active particles, e.g micro swimmers using flagella for propulsion [LP09; Bec+16]. It facilitates chemotaxis even for small particles. Oscillating in circles much larger than the body size, biological swarmers can detect chemical gradients and adapt their translational motion accordingly. When such self-propelled particles interact their velocities can align resulting in a directed collective motion. In the swarming model described by Eq. 5.68, the rotational bias $\omega\hat{\omega}$ results in the helical trajectories of the individual particle, while the distribution of the amplitude and direction of it generally influences the swarming as a whole. Here we mainly describe two cases:
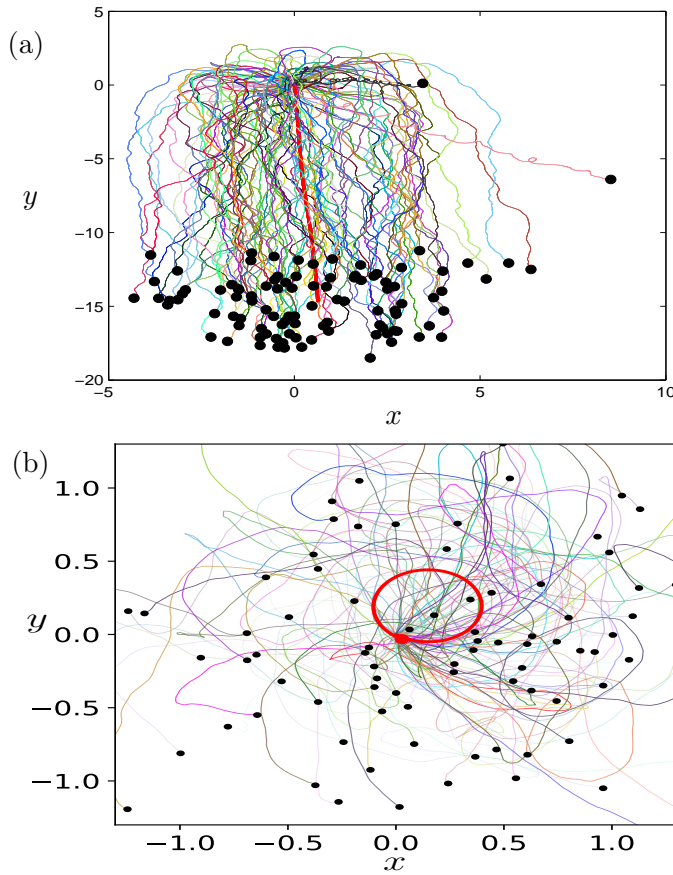
FIGURE 5.12: Trajectories of 100 particles (final position marked with black circles) in an ensemble of 4×10^4 particles with synchronized helical motion. (a) The mean field (bold red line) is a constant vector. (b) The mean field (bold red line) is rotating while the particles diffuse away from the center. Fig. (b) reprinted with permission from Ref. [ZTP20].

1), the individual particles diffusing in the same direction as that of the mean field $\boldsymbol{\rho} = \frac{1}{N} \sum_{j=1}^{N} \hat{\boldsymbol{v}}_j$, as shown in Fig. 5.12 (a). This phenomenon is widely expected in the collective motion of microswimmers, e.g., sperm suspensions in which each swimmer is propelled by rotating flagella [SK18].

2), each particle is diffusing and moving helically, while the center of mass of the particles rotates in the $x - y$ plane, as shown in Fig. 5.12 (b). The collective oscillations here are nontrivial and are induced by a Hopf bifurcation from the disordered state. The analysis of the linear stability of the disordered state is in Sec. 5.2.2. Collective oscillations are ubiquitous in physical and biological systems. One prominent example in experiments is reported recently in Ref. [Che+17], where motile cells in dense bacterial suspensions undergo collective oscillations by self-organization while individual cells move in an erratic manner, corresponding to the diffusing behavior of individuals in our noisy kuramoto model. In their model, a locally coupled version of the Kuramoto-type (or Vicsek-type) model is adopted. It is hopeful that the mean-field theory and the stability analysis in the noisy Kuramoto model will shed a light on the analytical solution to explain the experiment results.

5.4   Summary

In summary, firstly we introduce the generalization from the classical (2d) Kuramoto model to the deterministic high-dimensional versions, of which we focus on the version with vector model proposed by Chandra and coauthors [CGO19b]. Secondly, we extend it to the three-dimensional noisy case that captures more realistic features in nature, since the noise is ubiquitous and usually can not be ignored in the collective motion of microswimmers.

We want to state that the vector $\boldsymbol{\sigma}$ can be either a position vector or a velocity vector, depending on the considered context. On one hand, imagining the 3d sphere as a cell, the model can be potentially used to describe the synchronization of the active surface. On the other hand, considering $\boldsymbol{\sigma}$ as a velocity vector $\boldsymbol{v}$, the model can be used to describe synchronization in a swarming model with velocity alignment. In this sense, the case with no bias ($\boldsymbol{\omega} = 0$) can be connected to a mean-field version of the Vicsek model, while the case with bias ($\boldsymbol{\omega} \neq 0$) can be used to describe the swarming with helical trajectories. The bias (frequency) $\boldsymbol{\omega}$ makes the particles rotate helically while the noise makes them diffusing, and hence the general paths of the particles are rotating, diffusing and meanwhile are subject to a mean field $\boldsymbol{\rho}$.

Our main results are boiled down to the following:

(a), in the case of no frequency, the self-consistent solution of the order parameter is derived and a continuous transition with a square-root relation at the vicinity of the criticality is demonstrated. By explaining $\boldsymbol{\sigma}$ as the velocity vector of a particle moving in 3d space, the 3d Kuramoto model is connected to the 3d globally coupled Vicsek model, which is widely used to describe the collective motion and swarming with velocity alignment.

(b), the critical coupling strength K_c for the incoherent state ($\rho = 0$) to lose stability for a general frequency distribution, i.e., $g_d(\hat{\boldsymbol{\omega}})$ for the direction and $g_{(\omega)}$ for the amplitude, is derived in 3d by the linear stability analysis, where the spherical harmonics serve as the orthogonal basis instead of Fourier series in classical (2d) Kuramoto model.

(c), due to the influence of noise, the transition to synchrony is continuous (the second order), rather than discontinuous (the first order) in the deterministic case reported in [CGO19b], where the noise intensity $D = 0$ is a singular point by our analysis. In general, the noise, by which we mean the individual noise instead of the common noise [Gon+19], always stabilizes the incoherent state and therefore inhibits synchronization.

(d), the noisy three-dimensional Kuramoto model simplifies an equivalent random-top model proposed by Ritort [Rit98], where the amplitudes of frequency are limited to a constant, i.e., $g(\omega) = \delta(\omega - \omega_0)$. However, the analysis in the present thesis is more general for different kinds of distribution both in the direction $g_d(\hat{\boldsymbol{\omega}})$ and in the amplitude $g(\omega)$.

(d), the swarming model with helical trajectories described by the noisy Kuramoto model is hopefully to explain the collective motion of active particles, e.g., microswimmers with flagella such as *C. reinhardtii* cells [GPT09] and sperm cells [Jik+15].

Chapter 6

Conclusions and Outlook

In conclusion, we investigated two problems in this thesis: a coherent spiking phenomenon which we call *stochastic bursting* in excitable noisy systems with time-delay feedback and a three-dimensional noisy Kuramoto model, which can be used to describe the synchronization of a swarming model with helical trajectories. The common feature these two phenomena share is that they occur in the oscillatory systems with noise. The conclusions of the thesis can be drawn as the following two main parts:

(A) We have investigated the *stochastic bursting* phenomenon in a single excitable system with delayed feedback (Chap. 2), in unidirectionally delay-coupled systems (Chap. 3) and in a chain of delay-coupled units (Chap. 4). The combined effects of both time delay and noise result in complex statistics of the spike train, which is hard to describe analytically due to its non-Markovian nature. However, the *stochastic bursting* in our model is well described by a point process of a leader-follower relationship under the assumption of time-scale separation, which is based on the weak noise and the large time delay. The leaders correspond to the spontaneous spikes in excitable systems induced purely by noise, leading to Poisson statistics approximately. The followers correspond to the induced spikes by the combined effect of noise and delay, leading to random bursts. In a single excitable noisy system described in Chap. 2, the stochastic bursting is determined mainly by two essential parameters: the spontaneous spiking rate λ, which is easy to obtain analytically by the Fokker-Planck formalism, and the probability p to induce a spike, which is obtained by a high-precision numerical method.

The stochastic bursting phenomenon is not limited to a single system, but also can be observed in networks of coupled systems. In Chap. 3 we consider unidirectionally coupled ring networks of excitable systems that interact with each other by delayed pulse coupling. The highlight in this chapter is that we describe the pairwise correlation in terms of the conditional probability of a joint event that there is an induced spike at time $t + \tau$ given that there is a spike at time t. In other words, we consider the correlation function, which is usually seen as the second-order statistics, as the first-order statistics of a joint event. Surprisingly, the correlation function of the spike train in each unit and the cross-correlation function of the spikes between any two units in the ring networks share a general formalism.

In Chap. 4, we investigate the stochastic bursting in a chain of three delay-coupled excitable units, which serves as a minimum model of star-network coupled systems. We use a lattice model that is similar to the branching process in probability theory to represent the probabilities to induce spikes in each unit of the chain approximately. By virtue of the method to describe the statistics of the spikes in each unit and that

between any pair of units, the correlation function and hence the power spectrum are derived straightforwardly.

One promising direction of the future study would be applying the model developed here to the real data from the experiments in neural labs. Moreover, the analytical result in our model is not limited to the excitable neural system but can be also be potentially applied to optical systems such as vertical-cavity surface-emitting lasers [Sci+03] and semiconductor lasers [FS07].

However, a question remains open as to whether the point process with a leader-follower relationship can be applied to more complex networks, e.g., the globally delay-coupled excitable systems.

(B) We investigate a noisy version of the three-dimensional Kuramoto model and connect it to two other models, i.e., the globally coupled Vicsek model [Vic+95], in the case without frequency and a random top model [Rit98] potentially used to describe strongly coupled magnetic systems. Compared with the classical (2d) Kuramoto model, the dynamics in the 3d version are much richer in terms of the following aspects:

- From the deterministic case to the noisy case, the transition from the incoherent state to partial synchrony differs fundamentally in the 3d version. In the deterministic case, the transition is discontinuous (the first-order) and happens at an infinitely small coupling strength ($K_c \to 0^+$) [CGO19b] while it's mostly continuous (the second-order) in the case with noise. However, in the 2d Kuramoto model, noise usually just stabilizes the incoherent state and leads to a larger critical coupling strength K_c, but doesn't change the type of the transition [SM91].

- The frequency not only has the distribution of the amplitude $g(\omega)$ but also has the distribution of the direction $g_d(\hat{\boldsymbol{\omega}})$ in 3d version, while it has only the distribution of the amplitude. Our linear stability analysis in Sec. 5.2.2 shows that the critical coupling strength K_c for the incoherent state to lose stability is highly dependent on the frequency distribution of both the amplitude and the direction. For instance, the most commonly considered distribution of the frequency direction is the uniform distribution [CGO19b; ZTP20], i.e., the vectors are isotropically located. It would be interesting to consider more complex but realistic distribution in future work.

- In the classical (2d) Kuramoto model, there always exists a co-rotating reference frame and therefore one can simply set the frequency distribution as $g(\omega)$ instead of $g(\omega - \omega_0)$, with a zero mean. However, there is no such co-rotating reference frame in the three-dimensional version, due to the influence of an additional dimension. There exists not only limit cycle but also torus for the motion of the agents moving on the spherical surface.

In the case without natural frequency for each oscillator, a self-consistent equation of the mean field was derived in q-dimensional ($q \geq 2$) space, with all the oscillators diffusing on a $q - 1$ dimensional sphere. Actually similar generalization to the case with natural frequency is also possible, provided that the cross product term is replaced by the product of a $q \times q$ antisymmetric matrix including noisy elements and the unit vector in higher-dimensional space. However, in this thesis, we mainly focus on the three-dimensional case, where the physical meaning is straightforward, e.g.,

the microswimmers with flagella [LP09] in the living systems show collective motion with velocity alignment.

Here we also list some future topics regarding the three-dimensional Kuramoto model:

1) Further connections between the Kuramoto model and the Vicsek model should be revealed, while in the present thesis we restrict the discussion to the globally coupled case with all the unit vectors subject to a global mean field. However, in many real living systems, such as the flocking, the fish school etc., a local coupling with only some nearest neighbors are involved is believed to play an important role in the collective motion. It would be interesting to see how the three-dimensional Kuramoto model with local coupling describes the collective motion in real physical systems. Is there also a hydrodynamic description in this case, as in the Vicsek model or in more general flocking phenomenon [TT98; TTR05]? Or is there a more general model that can connect these two models? These are some interesting questions yet to be answered.

2) We have analyzed the linear stability of the incoherent state and calculated the critical coupling strength above which the incoherent state loses stability. To uncover the bifurcation of order parameter at the vicinity of the coupling strength explicitly, one needs to derive the amplitude equations up to the third order, promisingly by a multi-scale perturbation method, as done in the classical Kuramoto model [Ace+05].

3) What is the stationary probability density of the oscillators with general frequency distribution? The analytical solution of the corresponding Fokker-Planck equation (5.34) is not easy to derive because the probability current is related to both the polar angle and the azimuthal angle of the three-dimensional sphere.

Finally, we would like to say some words about some general aspects about the role noise plays in the oscillatory systems because the bursting and the synchronization discussed in this thesis are basically due to noise. The stochastic bursting in excitable systems is induced by the combined effects of delay and noise, while the synchronization in the Kuramoto model is influenced by the competing effects of the coupling strength (or matrix), the heterogeneous frequency and the noise. More about the topics about the combined effects of delay and noise especially in neuro systems, we refer the readers to [Sch+09; Lin+04] for further references. The influence of noise on synchronization differs for the individual noise studied in this thesis and for the common noise, which always promotes synchrony [Pim+16; Gol+17]. In the field of collective motion, noise due to the finite-size effect is recently demonstrated to induce schooling of fish [Jha+20], where the larger the noise is, the more alignment it introduces. Let us look forward to seeing more and more interesting phenomena induced by noise.

Acknowledgements

Appendix A

Derivation of the fixed points in the three-dimensional Kuramoto model

The 3 dimensional Kuramoto model in the deterministic case is described by the equation (5.3) For simplicity we write all the vectors without i. The fixed points are subject to the following equation:

$$K[\boldsymbol{\rho} - (\boldsymbol{\rho} \cdot \hat{\boldsymbol{v}})\hat{\boldsymbol{v}}] + \boldsymbol{\omega} \times \hat{\boldsymbol{v}} = 0. \tag{A.1}$$

Defining $\beta = \frac{\omega}{K\rho}$, Eq. (A.1) is reformulated as follows,

$$\hat{\boldsymbol{\rho}} - (\hat{\boldsymbol{\rho}} \cdot \hat{\boldsymbol{v}})\hat{\boldsymbol{v}} + \beta\hat{\boldsymbol{\omega}} \times \hat{\boldsymbol{v}} = 0, \tag{A.2}$$

which leads to

$$\hat{\boldsymbol{\omega}} \times \hat{\boldsymbol{v}} = -\frac{1}{\beta}[\hat{\boldsymbol{\rho}} - (\hat{\boldsymbol{\rho}} \cdot \hat{\boldsymbol{v}})\hat{\boldsymbol{v}}]. \tag{A.3}$$

Since the solution to the equation $A \times B = C$ is $B = C \times A/|A|^2 + aA$, the solution to Eq. (A.3) is

$$\begin{aligned}
\hat{\boldsymbol{v}} &= -\frac{1}{\beta}[\hat{\boldsymbol{\rho}} - (\hat{\boldsymbol{\rho}} \cdot \hat{\boldsymbol{v}})\hat{\boldsymbol{v}}] \times \hat{\boldsymbol{\omega}} + a\hat{\boldsymbol{\omega}} \\
&= -\frac{1}{\beta}\hat{\boldsymbol{\rho}} \times \hat{\boldsymbol{\omega}} + \frac{1}{\beta}(\hat{\boldsymbol{\rho}} \cdot \hat{\boldsymbol{v}})\hat{\boldsymbol{v}} \times \hat{\boldsymbol{\omega}} + a\hat{\boldsymbol{\omega}}.
\end{aligned} \tag{A.4}$$

Multiplying $\hat{\boldsymbol{\omega}}$ to the Eq. (A.4) to get $a = \hat{\boldsymbol{\omega}} \cdot \hat{\boldsymbol{v}}$ and substituting Eq. (A.3) into Eq. (A.4), leading to

$$\hat{\boldsymbol{v}} = \frac{1}{\beta}\hat{\boldsymbol{\rho}} \times \hat{\boldsymbol{\omega}} + \frac{\hat{\boldsymbol{\rho}} \cdot \hat{\boldsymbol{v}}}{\beta^2}\hat{\boldsymbol{\rho}} - \frac{(\hat{\boldsymbol{\rho}} \cdot \hat{\boldsymbol{v}})^2}{\beta^2}\hat{\boldsymbol{v}} + a\hat{\boldsymbol{\omega}}. \tag{A.5}$$

Putting the third term of the r.h.s to the l.h.s and after some simplification, we obtain the fixed points solution:

$$\hat{\boldsymbol{v}} = \frac{1}{\beta^2 + b^2}(\beta\hat{\boldsymbol{\omega}} \times \hat{\boldsymbol{\rho}} + b\hat{\boldsymbol{\rho}} + a\beta^2\hat{\boldsymbol{\omega}}), \tag{A.6}$$

where $\beta = \frac{\omega}{K\rho}$, $b = \hat{\boldsymbol{\rho}} \cdot \hat{\boldsymbol{v}}$ and $a = \hat{\boldsymbol{\omega}} \cdot \hat{\boldsymbol{v}}$. since multiplying Eq. (A.2) by $\hat{\boldsymbol{\omega}}$ leads to

$$\hat{\boldsymbol{\omega}} \cdot \hat{\boldsymbol{v}} = \frac{\hat{\boldsymbol{\rho}} \cdot \hat{\boldsymbol{\omega}}}{\hat{\boldsymbol{\rho}} \cdot \hat{\boldsymbol{v}}} \quad or \quad a = \frac{\hat{\boldsymbol{\rho}} \cdot \hat{\boldsymbol{\omega}}}{b}, \tag{A.7}$$

then multiplying Eq. (A.6) with $\hat{\boldsymbol{\rho}}$ and substituting Eq. (A.7) into it, we obtain a quadratic equation in b^2 with the solution

$$b = \hat{\boldsymbol{\rho}} \cdot \hat{\boldsymbol{v}} = \pm \sqrt{\frac{1 - \beta^2 + \sqrt{(1 - \beta^2)^2 + 4\beta^2(\hat{\boldsymbol{\rho}} \cdot \hat{\boldsymbol{\omega}})^2}}{2}}. \qquad (A.8)$$

The plus and minus signs correspond to the stable and unstable fixed points respectively, by linearizing the equation (5.3) with a small perturbation $\hat{\boldsymbol{\epsilon}}(t)$:

$$\frac{d\boldsymbol{\epsilon}}{dt} = -K(\boldsymbol{\rho} \cdot \hat{\boldsymbol{v}})\boldsymbol{\epsilon}. \qquad (A.9)$$

Appendix B

Derivation of the self-consistent equation (5.29) of the mean field ρ in general q dimensions

The self-consistent equation of the mean field in the linear order, according to Eq. (5.29), is

$$
\begin{aligned}
\rho &= \frac{\int_0^\pi \cos\theta \, e^{\epsilon\cos\theta} \sin^{q-2}\theta \, d\theta}{\int_0^\pi e^{\epsilon\cos\theta} \sin^{q-2}\theta \, d\theta} \\
&\approx \frac{\int_0^\pi \cos\theta (1 + \epsilon\cos\theta + \frac{1}{2}\epsilon^2\cos^2\theta + \frac{1}{6}\epsilon^3\cos^3\theta) \sin^{q-2}\theta \, d\theta}{\int_0^\pi (1 + \epsilon\cos\theta + \frac{1}{2}\epsilon^2\cos^2\theta) \sin^{q-2}\theta \, d\theta} \\
&\approx \frac{\epsilon B(\frac{3}{2}, \frac{q-1}{2}) + \frac{1}{6}\epsilon^3 B(\frac{5}{2}, \frac{q-1}{2})}{B(\frac{1}{2}, \frac{q-1}{2}) + \frac{1}{2}\epsilon^2 B(\frac{3}{2}, \frac{q-1}{2})},
\end{aligned}
\tag{B.1}
$$

where $B(x,y)$ is Beta function defined as

$$
B(x,y) = \int_0^1 t^{x-1}(1-t)^{y-1} dt
\tag{B.2}
$$

for Re x>0, Re y>0. Due to the property of the Beta function:

$$
B(x+1, y) = B(x,y) \cdot \frac{x}{x+y},
\tag{B.3}
$$

Eq. (B.1) can be further expanded to the third order of ϵ, i.e.,

$$
\begin{aligned}
\rho &\approx \frac{\epsilon B(\frac{3}{2}, \frac{q-1}{2}) + \frac{1}{6}\epsilon^3 B(\frac{5}{2}, \frac{q-1}{2})}{B(\frac{1}{2}, \frac{q-1}{2}) + \frac{1}{2}\epsilon^2 B(\frac{3}{2}, \frac{q-1}{2})} \\
&\approx [B(\frac{3}{2}, \frac{q-1}{2}) + \frac{1}{6}\epsilon^3 B(\frac{5}{2}, \frac{q-1}{2})] \frac{1}{B(\frac{1}{2}, \frac{q-1}{2})}[1 - \frac{\epsilon^2 B(\frac{3}{2}, \frac{q-1}{2})}{2B(\frac{1}{2}, \frac{q-1}{2})}] \\
&\approx \frac{\epsilon}{q} - \frac{\epsilon^3}{2}(\frac{1}{q^2} - \frac{1}{q(q+2)}).
\end{aligned}
\tag{B.4}
$$

Substituting $\epsilon = \frac{K\rho}{D}$ to Eq. (B.4), we obtain Eq. (5.29), i.e.,

$$
\rho \approx \frac{K\rho}{qD} - \frac{K^3\rho^3}{2D^3}(\frac{1}{q^2} - \frac{1}{q(q+2)}).
\tag{B.5}
$$

Appendix C

Derivation of the Fokker-Planck equation (5.34)

We first extend the unit vector $\boldsymbol{\sigma}$ to a general vector $\boldsymbol{\sigma} = r\hat{\boldsymbol{\sigma}}$, with r being the amplitude and $\hat{\boldsymbol{\sigma}}$ being the unit vector. Therefore, the velocity can be rewritten as follows,

$$
\begin{aligned}
\boldsymbol{v} &= K(\boldsymbol{\rho} - (\boldsymbol{\rho} \cdot \hat{\boldsymbol{\sigma}})\hat{\boldsymbol{\sigma}}) + \boldsymbol{\omega} \times \hat{\boldsymbol{\sigma}} \\
&= K(\boldsymbol{\rho} - \frac{(\boldsymbol{\rho} \cdot \boldsymbol{\sigma})\boldsymbol{\sigma}}{r^2}) + \frac{1}{r}\boldsymbol{\omega} \times \boldsymbol{\sigma},
\end{aligned}
\tag{C.1}
$$

and hence

$$
\begin{aligned}
\boldsymbol{\nabla} \cdot (f\boldsymbol{v}) &= f\boldsymbol{\nabla} \cdot \boldsymbol{v} + \boldsymbol{v} \cdot \boldsymbol{\nabla} f \\
&= f\boldsymbol{\nabla} \cdot [\boldsymbol{\rho} - \frac{(\boldsymbol{\rho} \cdot \hat{\boldsymbol{\sigma}})\hat{\boldsymbol{\sigma}}}{r^2}] + \boldsymbol{v} \cdot (\frac{1}{r}\boldsymbol{\nabla}_s f + \hat{\boldsymbol{\sigma}}\frac{\partial f}{\partial r}) \\
&= -(q-1)\frac{\boldsymbol{\rho} \cdot \boldsymbol{\sigma}}{r^2} + \frac{1}{r}[\frac{\boldsymbol{\omega} \times \boldsymbol{\sigma}}{r} + K(\boldsymbol{\rho} - \frac{(\boldsymbol{\rho} \cdot \boldsymbol{\sigma})\boldsymbol{\sigma}}{r^2})] \cdot \boldsymbol{\nabla}_s f \\
&= -(q-1)\frac{\boldsymbol{\rho} \cdot \hat{\boldsymbol{\sigma}}}{r} + \frac{1}{r}[\boldsymbol{\omega} \times \hat{\boldsymbol{\sigma}} + K\boldsymbol{\rho}] \cdot \boldsymbol{\nabla}_s f.
\end{aligned}
\tag{C.2}
$$

In deriving Eq. (C.2), we have used the fact that $\boldsymbol{v} \cdot \boldsymbol{\sigma} = 0$, $\boldsymbol{\sigma} \cdot \boldsymbol{\nabla}_s f = 0$. Then substituting Eq. (C.2) to the Fokker-Planck equation (5.14), and integrating the equation over r from $1 - \delta$ to $1 + \delta$ with δ being a small number and we obtain the rewritten Fokker-Planck equation (5.34).

Appendix D

Integrals of the Lorentzian function in the complex plane

Here we derive the integrals about a Lorentzian function $g(\omega) = \frac{1}{\pi} \frac{\gamma}{(\omega - \omega_0)^2 + \gamma^2}$ in the complex plane, i.e.,

$$
\begin{aligned}
h_1 &= \int_{-\infty}^{\infty} \frac{\lambda}{\lambda^2 + \omega^2} g(\omega) d\omega \\
&= \frac{1}{4\pi} \int_{-\infty}^{\infty} \left(\frac{1}{\lambda + i\omega} + \frac{1}{\lambda - i\omega} \right) \left[\frac{1}{\gamma + i(\omega - \omega_0)} + \frac{1}{\gamma - i(\omega - \omega_0)} \right] d\omega.
\end{aligned}
\tag{D.1}
$$

For a complex value $\lambda = a + ib$, due to the cancelation of the two residues $-b + ia$ and $\omega_0 + i\gamma$ in the upper complex plane of the corresponding complex function, it's easy to check that

$$
\int_{-\infty}^{\infty} \frac{1}{a + i(b + \omega)} \frac{1}{\gamma + i(\omega - \omega_0)} d\omega = 0.
\tag{D.2}
$$

Also, the term with respect to

$$
\int_{-\infty}^{\infty} \frac{1}{a + i(b - \omega)} \frac{1}{\gamma - i(\omega - \omega_0)} d\omega
\tag{D.3}
$$

vanishes since there is no singular points in the upper complex plane. The other two terms in Eq. (D.1) can be calculated in terms of the residues at $\omega = -b + ia$ and $\omega = \omega_0 + i\gamma$, leading to

$$
\begin{aligned}
h_1 &= \frac{1}{2} \left(\frac{1}{\lambda + \gamma + i\omega_0} + \frac{1}{\lambda + \gamma - i\omega_0} \right) \\
&= \frac{\lambda + \gamma}{(\lambda + \gamma)^2 + \omega_0^2}.
\end{aligned}
\tag{D.4}
$$

Bibliography

[Abb+08]   D. Abbott, M. D. McDonnell, C. E. M. Pearce, and N. G. Stocks, eds. *Stochastic Resonance*. Cambridge: CUP, 2008.

[AS04]   Daniel M Abrams and Steven H Strogatz. "Chimera states for coupled oscillators". In: *Physical review letters* 93.17 (2004), p. 174102.

[Ace+05]   Juan A Acebrón, Luis L Bonilla, Conrad J Pérez Vicente, Félix Ritort, and Renato Spigler. "The Kuramoto model: A simple paradigm for synchronization phenomena". In: *Reviews of modern physics* 77.1 (2005), p. 137.

[Ath06]   Krishna B Athreya. "Branching process". In: *Encyclopedia of Environmetrics* 1 (2006).

[BJS04]   Alexander G Balanov, Natalia B Janson, and E Schöll. "Control of noise-induced oscillations by delayed feedback". In: *Physica D: Nonlinear Phenomena* 199.1-2 (2004), pp. 1–12.

[Bec+16]   Clemens Bechinger, Roberto Di Leonardo, Hartmut Löwen, Charles Reichhardt, Giorgio Volpe, and Giovanni Volpe. "Active particles in complex and crowded environments". In: *Reviews of Modern Physics* 88.4 (2016), p. 045006.

[BSV81]   Roberto Benzi, Alfonso Sutera, and Angelo Vulpiani. "The mechanism of stochastic resonance". In: *Journal of Physics A: mathematical and general* 14.11 (1981), p. L453.

[BSS20]   Rico Berner, Jakub Sawicki, and Eckehard Schöll. "Birth and stabilization of phase clusters by multiplexing of adaptive networks". In: *Physical Review Letters* 124.8 (2020), p. 088301.

[BNS92]   Luis L Bonilla, John C Neu, and Renato Spigler. "Nonlinear stability of incoherence and collective synchronization in a population of coupled oscillators". In: *Journal of statistical physics* 67.1-2 (1992), pp. 313–330.

[BK05]   Christoph Börgers and Nancy Kopell. "Effects of noisy drive on rhythms in networks of excitatory and inhibitory neurons". In: *Neural computation* 17.3 (2005), pp. 557–608.

[Bre14]   Paul C Bressloff. *Stochastic processes in cell biology*. Vol. 41. Springer, 2014.

[BB68]   John Buck and Elisabeth Buck. "Mechanism of Rhythmic Synchronous Flashing of Fireflies: Fireflies of Southeast Asia may use anticipatory time-measuring in synchronizing their flashing". In: *Science* 159.3821 (1968), pp. 1319–1327.

[CGO19a]   Sarthak Chandra, Michelle Girvan, and Edward Ott. "Complexity reduction ansatz for systems of interacting orientable agents: Beyond the Kuramoto model". In: *Chaos: An Interdisciplinary Journal of Nonlinear Science* 29.5 (2019), p. 053107.

[CGO19b]   Sarthak Chandra, Michelle Girvan, and Edward Ott. "Continuous versus discontinuous transitions in the d-dimensional generalized Kuramoto model: Odd d is different". In: *Physical Review X* 9.1 (2019), p. 011002.

[Cha+08]   Hugues Chaté, Francesco Ginelli, Guillaume Grégoire, Fernando Peruani, and Franck Raynaud. "Modeling collective motion: variations on the Vicsek model". In: *The European Physical Journal B* 64.3 (2008), pp. 451–456.

[Che+17]   Chong Chen, Song Liu, Xia-qing Shi, Hugues Chaté, and Yilin Wu. "Weak synchronization and large-scale collective oscillation in dense bacterial suspensions". In: *Nature* 542.7640 (2017), pp. 210–214.

[CN11]   Hayato Chiba and Isao Nishikawa. "Center manifold reduction for large populations of globally coupled phase oscillators". In: *Chaos: An Interdisciplinary Journal of Nonlinear Science* 21.4 (2011), p. 043103.

[Cox67]   David Roxbee Cox. *Renewal theory*. Vol. 1. Methuen London, 1967.

[DLR+07]   Jaime De La Rocha, Brent Doiron, Eric Shea-Brown, Krešimir Josić, and Alex Reyes. "Correlation between neural spike trains increases with firing rate". In: *Nature* 448.7155 (2007), p. 802.

[DDM14]   Pierre Degond, Giacomo Dimarco, and Thi Bich Ngoc Mac. "Hydrodynamics of the Kuramoto–Vicsek model of rotating self-propelled particles". In: *Mathematical Models and Methods in Applied Sciences* 24.02 (2014), pp. 277–325.

[DM08]   Pierre Degond and Sébastien Motsch. "Continuum limit of self-driven particles with orientation interaction". In: *Mathematical Models and Methods in Applied Sciences* 18.supp01 (2008), pp. 1193–1215.

[Doi+16]   Brent Doiron, Ashok Litwin-Kumar, Robert Rosenbaum, Gabriel K Ocker, and Krešimir Josić. "The mechanics of state-dependent neural correlations". In: *Nature neuroscience* 19.3 (2016), p. 383.

[DB14]   Florian Dörfler and Francesco Bullo. "Synchronization in complex networks of phase oscillators: A survey". In: *Automatica* 50.6 (2014), pp. 1539–1564.

[EM20]   Jan R Engelbrecht and Renato Mirollo. "Is the Ott-Antonsen manifold attracting?" In: *Physical Review Research* 2.2 (2020), p. 023057.

[EK86]   G Bard Ermentrout and Nancy Kopell. "Parabolic bursting in an excitable system coupled with a slow oscillation". In: *SIAM Journal on Applied Mathematics* 46.2 (1986), pp. 233–253.

[FS07]   Valentin Flunkert and Eckehard Schöll. "Suppressing noise-induced intensity pulsations in semiconductor lasers by means of time-delayed feedback". In: *Physical Review E* 76.6 (2007), p. 066202.

[Fra05]   TD Frank. "Delay Fokker-Planck equations, perturbation theory, and data analysis for nonlinear stochastic systems with time delays". In: *Physical Review E* 71.3 (2005), p. 031106.

[Gam+98]   Luca Gammaitoni, Peter Hänggi, Peter Jung, and Fabio Marchesoni. "Stochastic resonance". In: *Reviews of modern physics* 70.1 (1998), p. 223.

[Gan+93]   Hu Gang, T Ditzinger, Cun-Zheng Ning, and H Haken. "Stochastic resonance without external periodic force". In: *Physical Review Letters* 71.6 (1993), p. 807.

[Gar09]   Crispin Gardiner. *Stochastic methods.* springer Berlin, 2009.

[Ger+14]   Wulfram Gerstner, Werner M Kistler, Richard Naud, and Liam Panin-
             ski. *Neuronal dynamics: From single neurons to networks and models of
             cognition.* Cambridge University Press, 2014.

[GRP03a]   D. Goldobin, M. Rosenblum, and A. Pikovsky. "Coherence of noisy os-
             cillators with delayed feedback". In: *Physica A* 327 (2003), pp. 124–128.

[GRP03b]   D. Goldobin, M. Rosenblum, and A. Pikovsky. "Controlling oscillator
             coherence by delayed feedback". In: *Phys. Rev. E* 67.6 (2003), p. 061119.

[Gol+17]   Denis S Goldobin, Anastasiya V Pimenova, Michael Rosenblum, and
             Arkady Pikovsky. "Competing influence of common noise and desyn-
             chronizing coupling on synchronization in the Kuramoto-Sakaguchi en-
             semble". In: *The European Physical Journal Special Topics* 226.9 (2017),
             pp. 1921–1937.

[GPT09]   Raymond E Goldstein, Marco Polin, and Idan Tuval. "Noise and syn-
             chronization in pairs of beating eukaryotic flagella". In: *Physical review
             letters* 103.16 (2009), p. 168103.

[Gon+19]   Chen Chris Gong, Chunming Zheng, Ralf Toenjes, and Arkady Pikovsky.
             "Repulsively coupled Kuramoto-Sakaguchi phase oscillators ensemble sub-
             ject to common noise". In: *Chaos: An Interdisciplinary Journal of Non-
             linear Science* 29.3 (2019), p. 033127.

[GG15]   I. Goychuk and A. Goychuk. "Stochastic Wilson Cowan models of neu-
             ronal network dynamics with memory and delay". In: *New J. Phys.* 17
             (2015), p. 045029.

[Hau+06]   B Hauschildt, NB Janson, A Balanov, and E Schöll. "Noise-induced coop-
             erative dynamics and its control in coupled neuron models". In: *Physical
             Review E* 74.5 (2006), p. 051906.

[Hod48]   Alan L Hodgkin. "The local electric changes associated with repetitive
             action in a non-medullated axon". In: *The Journal of physiology* 107.2
             (1948), p. 165.

[Izh00]   Eugene M Izhikevich. "Neural excitability, spiking and bursting". In: *In-
             ternational journal of bifurcation and chaos* 10.06 (2000), pp. 1171–1266.

[Izh06]   Eugene M. Izhikevich. "Polychronization: Computation with spikes". In:
             Neural Computation 18.2 (2006), pp. 245–282.

[JBS04]   Natalia B Janson, Alexander G Balanov, and E Schöll. "Delayed feedback
             as a means of control of noise-induced motion". In: *Physical review letters*
             93.1 (2004), p. 010601.

[Jha+20]   Jitesh Jhawar, Richard G Morris, UR Amith-Kumar, M Danny Raj, Tim
             Rogers, Harikrishnan Rajendran, and Vishwesha Guttal. "Noise-induced
             schooling of fish". In: *Nature Physics* 16.4 (2020), pp. 488–493.

[Jik+15]   Jan F Jikeli, Luis Alvarez, Benjamin M Friedrich, Laurence G Wil-
             son, René Pascal, Remy Colin, Magdalena Pichlo, Andreas Rennhack,
             Christoph Brenker, and U Benjamin Kaupp. "Sperm navigation along
             helical paths in 3D chemoattractant landscapes". In: *Nature communica-
             tions* 6.1 (2015), pp. 1–10.

[JR16]   Stojan Jovanović and Stefan Rotter. "Interplay between graph topology
             and correlations of third order in spiking neuronal networks". In: *PLoS
             computational biology* 12.6 (2016), e1004963.

[KMSG10]   N. Kouvaris, F. Mueller, and L. Schimansky-Geier. "Ensembles of excitable two-state units with delayed feedback". In: *Phys. Rev. E* 82 (2010), p. 061124.

[Kro+14]   Justus A Kromer, Reynaldo D Pinto, Benjamin Lindner, and Lutz Schimansky-Geier. "Noise-controlled bistability in an excitable system with positive feedback". In: *EPL (Europhysics Letters)* 108.2 (2014), p. 20007.

[Kur75]   Yoshiki Kuramoto. "Self-entrainment of a population of coupled non-linear oscillators". In: *International symposium on mathematical problems in theoretical physics*. Springer. 1975, pp. 420–422.

[Kur84]   Yoshiki Kuramoto. "Chemical oscillations, waves, and turbulence". In: (1984).

[KB02]   Yoshiki Kuramoto and Dorjsuren Battogtokh. "Coexistence of coherence and incoherence in nonlocally coupled phase oscillators". In: *arXiv preprint cond-mat/0210694* (2002).

[LP09]   Eric Lauga and Thomas R Powers. "The hydrodynamics of swimming microorganisms". In: *Reports on Progress in Physics* 72.9 (2009), p. 096601.

[Li+10]   Yunyun Li, Gerhard Schmid, Peter Hänggi, and Lutz Schimansky-Geier. "Spontaneous spiking in an autaptic Hodgkin-Huxley setup". In: *Physical Review E* 82.6 (2010), p. 061907.

[LCL05]   Benjamin Lindner, Maurice J Chacron, and André Longtin. "Integrate-and-fire neurons with threshold noise: A tractable model of how interspike interval correlations affect neuronal signal transmission". In: *Physical Review E* 72.2 (2005), p. 021911.

[LDL05]   Benjamin Lindner, Brent Doiron, and André Longtin. "Theory of oscillatory firing induced by spatially correlated noise and delayed inhibitory feedback". In: *Physical Review E* 72.6 (2005), p. 061919.

[Lin+04]   Benjamin Lindner, Jordi Garcıa-Ojalvo, Alexander Neiman, and Lutz Schimansky-Geier. "Effects of noise in excitable systems". In: *Physics reports* 392.6 (2004), pp. 321–424.

[LMS19]   Max Lipton, Renato Mirollo, and Steven H Strogatz. "On Higher Dimensional Generalized Kuramoto Oscillator Systems". In: *arXiv preprint arXiv:1907.07150* (2019).

[Loh09]   MA Lohe. "Non-Abelian Kuramoto models and synchronization". In: *Journal of Physics A: Mathematical and Theoretical* 42.39 (2009), p. 395101.

[Loh18]   MA Lohe. "Higher-dimensional generalizations of the Watanabe–Strogatz transform for vector models of synchronization". In: *Journal of Physics A: Mathematical and Theoretical* 51.22 (2018), p. 225101.

[Lon13]   A. Longtin. "Neuronal noise". In: *Scholarpedia* 8.9 (2013). revision #137114, p. 1618.

[MD78]   Peter F Major and Lawrence M Dill. "The three-dimensional structure of airborne bird flocks". In: *Behavioral Ecology and Sociobiology* 4.2 (1978), pp. 111–122.

[MJ99]   Kantilal Varichand Mardia and Peter E Jupp. "Directional statistics". In: (1999).

[MMS09]   Seth A Marvel, Renato E Mirollo, and Steven H Strogatz. "Identical phase oscillators with global sinusoidal coupling evolve by Möbius group action". In: *Chaos: An Interdisciplinary Journal of Nonlinear Science* 19.4 (2009), p. 043104.

[Mas03]   Cristina Masoller. "Distribution of residence times of time-delayed bistable systems driven by noise". In: *Physical Review Letters* 90.2 (2003), p. 020601.

[Mie+19]   Alexander Mietke, V Jemseena, K Vijay Kumar, Ivo F Sbalzarini, and Frank Jülicher. "Minimal model of cellular symmetry breaking". In: *Physical review letters* 123.18 (2019), p. 188101.

[MS07]   Renato Mirollo and Steven H Strogatz. "The spectrum of the partially locked state for the Kuramoto model". In: *Journal of Nonlinear Science* 17.4 (2007), pp. 309–347.

[MS90]   Renato E Mirollo and Steven H Strogatz. "Amplitude death in an array of limit-cycle oscillators". In: *Journal of Statistical Physics* 60.1-2 (1990), pp. 245–262.

[MPR15]   Ernest Montbrió, Diego Pazó, and Alex Roxin. "Macroscopic description for networks of spiking neurons". In: *Physical Review X* 5.2 (2015), p. 021028.

[NK10]   Ken H Nagai and Hiroshi Kori. "Noise-induced synchronization of a large population of globally coupled nonidentical oscillators". In: *Physical Review E* 81.6 (2010), p. 065202.

[Nei07]   A. Neiman. "Coherence resonance". In: *Scholarpedia* 2.11 (2007). revision #91135, p. 1442.

[NL03]   Sheila Nirenberg and Peter E Latham. "Decoding neuronal spike trains: How important are correlations?" In: *Proceedings of the National Academy of Sciences* 100.12 (2003), pp. 7348–7353.

[OY00]   Toru Ohira and Toshiyuki Yamane. "Delayed stochastic systems". In: *Physical Review E* 61.2 (2000), p. 1247.

[OS06]   Reza Olfati-Saber. "Swarms on sphere: A programmable swarm with synchronous behaviors like oscillator networks". In: *Proceedings of the 45th IEEE Conference on Decision and Control*. IEEE. 2006, pp. 5060–5066.

[Ome18]   Oleh E Omel'chenko. "The mathematics behind chimera states". In: *Nonlinearity* 31.5 (2018), R121.

[OBH09]   Srdjan Ostojic, Nicolas Brunel, and Vincent Hakim. "How Connectivity, Background Activity, and Synaptic Properties Shape the Cross-Correlation between Spike Trains". In: *The Journal of Neuroscience* 29.33 (2009), pp. 10234–10253.

[OA08]   Edward Ott and Thomas M Antonsen. "Low dimensional behavior of large systems of globally coupled oscillators". In: *Chaos: An Interdisciplinary Journal of Nonlinear Science* 18.3 (2008), p. 037113.

[OA09]   Edward Ott and Thomas M Antonsen. "Long time evolution of phase oscillator systems". In: *Chaos: An interdisciplinary journal of nonlinear science* 19.2 (2009), p. 023117.

[PK96]   Seon Hee Park and Seunghwan Kim. "Noise-induced phase transitions in globally coupled active rotators". In: *Physical Review E* 53.4 (1996), p. 3425.

[Par+80]   Brian L Partridge, Tony Pitcher, J Michael Cullen, and John Wilson. "The three-dimensional structure of fish schools". In: *Behavioral Ecology and Sociobiology* 6.4 (1980), pp. 277–288.

[Per+11]   Volker Pernice, Benjamin Staude, Stefano Cardanobile, and Stefan Rotter. "How structure determines correlations in neuronal networks". In: *PLoS computational biology* 7.5 (2011), e1002059.

[PDB08]   Fernando Peruani, Andreas Deutsch, and Markus Bär. "A mean-field theory for self-propelled particles interacting by velocity alignment mechanisms". In: *The European Physical Journal Special Topics* 157.1 (2008), pp. 111–122.

[PR08]   Arkady Pikovsky and Michael Rosenblum. "Partially integrable dynamics of hierarchical populations of coupled oscillators". In: *Physical review letters* 101.26 (2008), p. 264103.

[Pik+03]   Arkady Pikovsky, Jurgen Kurths, Michael Rosenblum, and Jürgen Kurths. *Synchronization: a universal concept in nonlinear sciences*. Vol. 12. Cambridge university press, 2003.

[PK97]   Arkady S Pikovsky and Jürgen Kurths. "Coherence resonance in a noise-driven excitable system". In: *Physical Review Letters* 78.5 (1997), p. 775.

[Pim+16]   Anastasiya V Pimenova, Denis S Goldobin, Michael Rosenblum, and Arkady Pikovsky. "Interplay of coupling and common noise at the transition to synchrony in oscillator populations". In: *Scientific reports* 6 (2016), p. 38518.

[PJ08]   A. Pototsky and N. Janson. "Excitable systems with noise and delay, with applications to control: Renewal theory approach". In: *Phys. Rev. E* 77 (2008), p. 031113.

[Pra+07]   T. Prager, H.-P. Lerch, L. Schimansky-Geier, and E. Schoell. "Increase of coherence in excitable systems by delayed feedback". In: *J. Phys. A: Math. Theor.* 40 (2007), pp. 11045–11055.

[Ris96]   Hannes Risken. *Fokker-planck equation*. Springer, 1996.

[Rit98]   Felix Ritort. "Solvable dynamics in a system of interacting random tops". In: *Physical review letters* 80.1 (1998), p. 6.

[Rod+16]   Francisco A Rodrigues, Thomas K DM Peron, Peng Ji, and Jürgen Kurths. "The Kuramoto model in complex networks". In: *Physics Reports* 610 (2016), pp. 1–98.

[Sak88]   Hidetsugu Sakaguchi. "Cooperative phenomena in coupled oscillator systems under external fields". In: *Progress of theoretical physics* 79.1 (1988), pp. 39–46.

[SK18]   Simon F Schoeller and Eric E Keaveny. "From flagellar undulations to collective motion: predicting the dynamics of sperm suspensions". In: *Journal of The Royal Society Interface* 15.140 (2018), p. 20170834.

[Sch+09]   Eckehard Schöll, Gerald Hiller, Philipp Hövel, and Markus A Dahlem. "Time-delayed feedback in neurosystems". In: *Philosophical Transactions of the Royal Society A: Mathematical, Physical and Engineering Sciences* 367.1891 (2009), pp. 1079–1096.

[SP10]   Justus TC Schwabedal and Arkady Pikovsky. "Effective phase description of noise-perturbed and noise-induced oscillations". In: *The European Physical Journal Special Topics* 187.1 (2010), pp. 63–76.

[Sci+03]   Marc Sciamanna, Krassimir Panajotov, H Thienpont, I Veretennicoff, P Mégret, and M Blondel. "Optical feedback induces polarization mode hopping in vertical-cavity surface-emitting lasers". In: *Optics Letters* 28.17 (2003), pp. 1543–1545.

[SK86]   Shigeru Shinomoto and Yoshiki Kuramoto. "Phase transitions in active rotator systems". In: *Progress of Theoretical Physics* 75.5 (1986), pp. 1105–1110.

[Son+13]   Bernard Sonnenschein, Michael A Zaks, Alexander B Neiman, and Lutz Schimansky-Geier. "Excitable elements controlled by noise and network structure". In: *The European Physical Journal Special Topics* 222.10 (2013), pp. 2517–2529.

[Str67]   Rouslan L Stratonovich. *Topics in the theory of random noise*. CRC Press, 1967.

[SM91]   Steven H Strogatz and Renato E Mirollo. "Stability of incoherence in a population of coupled oscillators". In: *Journal of Statistical Physics* 63.3-4 (1991), pp. 613–635.

[SW12]   H. A. Swadlow and S. G. Waxman. "Axonal conduction delays". In: *Scholarpedia* 7.6 (2012). revision #125736, p. 1451.

[SSW92]   James W Swift, Steven H Strogatz, and Kurt Wiesenfeld. "Averaging of globally coupled oscillators". In: *Physica D: Nonlinear Phenomena* 55.3-4 (1992), pp. 239–250.

[Tan14]   Takuma Tanaka. "Solvable model of the collective motion of heterogeneous particles interacting on a sphere". In: *New Journal of Physics* 16.2 (2014), p. 023016.

[Tes+07]   Claudio J Tessone, Alessandro Scire, Raúl Toral, and Pere Colet. "Theory of collective firing induced by noise or diversity in excitable media". In: *Physical Review E* 75.1 (2007), p. 016203.

[TT98]   John Toner and Yuhai Tu. "Flocks, herds, and schools: A quantitative theory of flocking". In: *Physical review E* 58.4 (1998), p. 4828.

[TTR05]   John Toner, Yuhai Tu, and Sriram Ramaswamy. "Hydrodynamics and phases of flocks". In: *Annals of Physics* 318.1 (2005), pp. 170–244.

[Tro+12]   James Trousdale, Yu Hu, Eric Shea-Brown, and Krešimir Josić. "Impact of network structure and cellular response on spike time correlations". In: *PLoS computational biology* 8.3 (2012), e1002408.

[Tsi14]   Lev S Tsimring. "Noise in biology". In: *Reports on Progress in Physics* 77.2 (2014), p. 026601.

[TP01]   LS Tsimring and A Pikovsky. "Noise-induced dynamics in bistable systems with delay". In: *Physical Review Letters* 87.25 (2001), p. 250602.

[Tyu+18]   Irina V Tyulkina, Denis S Goldobin, Lyudmila S Klimenko, and Arkady Pikovsky. "Dynamics of noisy oscillator populations beyond the Ott-Antonsen ansatz". In: *Physical review letters* 120.26 (2018), p. 264101.

[VDLG72]   Hendrik Van Der Loos and Edmund M Glaser. "Autapses in neocortex cerebri: synapses between a pyramidal cell's axon and its own dendrites". In: *Brain research* 48 (1972), pp. 355–360.

[Vic+95]   Tamás Vicsek, András Czirók, Eshel Ben-Jacob, Inon Cohen, and Ofer Shochet. "Novel type of phase transition in a system of self-driven particles". In: *Physical review letters* 75.6 (1995), p. 1226.

[VSL14]   Andrea Vüllings, Eckehard Schöll, and Benjamin Lindner. "Spectra of delay-coupled heterogeneous noisy nonlinear oscillators". In: *The European Physical Journal B* 87.2 (2014), p. 31.

[War+19]   Mya R Warren, Hui Sun, Yue Yan, Jonas Cremer, Bo Li, and Terence Hwa. "Spatiotemporal establishment of dense bacterial colonies growing on hard agar". In: *Elife* 8 (2019), e41093.

[WS94]   Shinya Watanabe and Steven H Strogatz. "Constants of motion for superconducting Josephson arrays". In: *Physica D: Nonlinear Phenomena* 74.3-4 (1994), pp. 197–253.

[Win67]   Arthur T Winfree. "Biological rhythms and the behavior of populations of coupled oscillators". In: *Journal of theoretical biology* 16.1 (1967), pp. 15–42.

[Yam+03]   Shun Yamaguchi, Hiromi Isejima, Takuya Matsuo, Ryusuke Okura, Kazuhiro Yagita, Masaki Kobayashi, and Hitoshi Okamura. "Synchronization of cellular clocks in the suprachiasmatic nucleus". In: *Science* 302.5649 (2003), pp. 1408–1412.

[Zak+03]   MA Zaks, AB Neiman, S Feistel, and L Schimansky-Geier. "Noise-controlled oscillations and their bifurcations in coupled phase oscillators". In: *Physical Review E* 68.6 (2003), p. 066206.

[ZP18]   Chunming Zheng and Arkady Pikovsky. "Delay-induced stochastic bursting in excitable noisy systems". In: *Physical Review E* 98.4 (2018), p. 042148.

[ZP19]   Chunming Zheng and Arkady Pikovsky. "Stochastic bursting in unidirectionally delay-coupled noisy excitable systems". In: *Chaos: An Interdisciplinary Journal of Nonlinear Science* 29.4 (2019), p. 041103.

[ZPnu]   Chunming Zheng and Arkady Pikovsky. "Stochastic bursting in networks of excitable units with delayed coupling". In: (manuscript to be submitted).

[ZTP20]   Chunming Zheng, Ralf Toenjes, and Arkady Pikovsky. "Tansition to synchrony in a three dimensional swarming model of helical trajectory". In: *arXiv:2007.07612* (2020).